Hot Embossing Process Parameters: Simulation and Experimental Studies

A thesis
Submitted to Cardiff University
For the degree of

Doctor of Philosophy

By

Fuad Omar

Institute of Mechanical and Manufacturing Engineering
Cardiff School of Engineering
Cardiff University

Cardiff, Wales
United Kingdom

2013

ABSTRACT

Fabrication processes for the high volume production of parts with micro and nano scale features are very important in the global research and industry efforts to meet the increasing needs for device miniaturisation in numerous application areas. Processes for the replication of surface geometries are promising technologies that are capable to meet the demand of manufacturing products at a low cost and in high volume. Among these technologies, hot embossing is a process which relies on raising the temperature of a sheet of polymer up to its melting range and on pressing a heated master plate into the polymer for triggering a local flow of the material to fill the cavities to be replicated. This technique has attracted increased attention in recent years in particular due to the relatively simple set-up and low cost associated with its implementation in comparison to other replication techniques.

The present work is concerned with investigating the process factors that influence hot embossing outcomes. In particularly, a detailed study of the process parameters' effect on the cavity pressure, demoulding force and uniformity of the residual layer for different materials is conducted to analyse the further potential of this process. A review of the current state of the art on these topics reported in Chapter 2, is also used to assess the capability of this replication technology.

Chapter 3 presents an experimental study on the effects of process parameters on pressure conditions in cavities when replicating parts in PMMA and ABS. To measure the pressure state of a polymer inside mould cavities, a condition monitoring system was implemented. Then, by employing a design of experiment approach, the

pressure behaviour was studied as a function of different process conditions. In particular, the effects of three process parameters, embossing temperature and force and holding time, on the mould cavity pressure and the pressure distribution were investigated. In addition, using a simple analytical model, the minimum required embossing force to fill the cavities across the mould surface was calculated. The theoretical value obtained was then used to inform the design of the experiments. It was shown that cavity pressure and pressure distribution were dependent on both materials and processing conditions. The obtained results indicate that an increase in temperature and holding time reduced the pressure in the central and edge cavities of the mould and the pressure distribution while the opposite effect takes place when considering the embossing force. Also, it was observed that an increase of the embossing force has a positive effect on cavity filling but a negative influence for homogenous filling.

In Chapter 4, a theoretical model was proposed to predict demoulding forces in hot embossing by providing a unified treatment of adhesion, friction and deformation phenomena that take place during demoulding of polymer microstructures. The close agreement between the predicted results and those measured experimentally suggests that the model successfully captures the relationship between mould design, feature sidewall, applied pressure, material properties, demoulding temperature and the resulting demoulding force. The theoretical results have been confirmed through comparisons with the demoulding experiments. The temperature at which the demoulding force is minimised depends on the geometry of the mould features along with the material properties of the mould and replica. The applied pressure has an important influence on the demoulding force

as the increase in pressure augments the adhesion force due to changes in material dimensions and reduces the friction force due to resulting decrease in the thermal stress.

Furthermore, the relationship between the residual layer uniformity and three process parameters was investigated in Chapter 5, using simulation and experimental studies when processing PMMA sheets. In particular, the characteristics of the residual layer thickness of embossed parts were analysed as a function of the moulding temperature, the embossing force and the holding time. Increasing the moulding temperature resulted in a reduction on the average residual layer thickness and on its non-uniformity. An increase in the embossing force led to a decrease in the homogeneity of the residual layer. Also, an improvement of the residual layer thickness uniformity was also observed when embossing with a longer holding time. The results of the conducted experimental and simulation studies were analysed to identify potential ways for improving the hot embossing process.

Finally, in Chapter 6 the results and main findings from each of the investigations are summarised and further research directions are proposed.

ACKNOWLEDGEMENTS

First, I would like to give thanks to Allah the almighty, the all great without whom I could not have completed this educational endeavour.

I wish to express my sincere thanks to Cardiff University, especially the Manufacturing Engineering Centre (MEC) for the use of the facilities to pursue this research.

I would like to extend special thanks and gratitude to my supervisor Dr E. Brousseau. Thanks for all the inspiring and wonderful discussions, encouragement and patience he provided throughout my study at Cardiff University. Also, I am deeply grateful to my advisor Professor S. S. Dimov, for all his direction and expert insight which he has shared with me and supported me during my study.

In addition, I would like to express my gratitude to Dr H. Hirshy and Dr A. Elkaseer. I am deeply grateful to them for their consistent encouragement, invaluable guidance and strong support during the course of this study. Also, I am highly indebted to Professor D. T. Pham. I must appreciate his ever-ready helping attitude, which was a constant motivating factor for me to complete this thesis.

However, the support provided by my senior colleagues Dr Kolew, Dr Bigot, Dr Yuce, Dr Popov, Dr Petkov, Dr Lacan, Dr Lalev and Dr Scholz from the MEC is more than appreciated. I am also very grateful to all the members of the Manufacturing Engineering Centre for their friendship and help. Special thanks go to Mr Imanguliyev, Dr Packianather, Mrs Rees, Miss Whyte and Dr Matthews for their sincere help and support.

I would also like to acknowledge to my home country Azerbaijan and the Ministry of Education of Azerbaijan Republic due to the funding and support. Also, my sincere thanks go to Azerbaijan Embassy in London for their support.

My most sincere gratitude and appreciation go to my dear wife Mrs Narmin Omar for her patience, continuous encouragement and support over the past difficult years. Thanks as well to Allah for his gift; my beloved daughter Ayan.

I am deeply indebted to my parents and all the members of my family who gave me continuous support and encouragement throughout my life.

DECLARATION

This work has not previously been accepted in substance for any degree and is not concurrently submitted in candidature for any degree.

Signed …… (candidate) Date ……

STATEMENT 1

This thesis is being submitted in partial fulfillment of the requirements for the degree of ……(insert MCh, MD, MPhil, PhD etc, as appropriate).

Signed …… (candidate) Date ……

STATEMENT 2

This thesis is the result of my own independent work/investigation, except where otherwise stated. Other sources are acknowledged by explicit references. The views expressed are my own.

Signed …… (candidate) Date ……

STATEMENT 3

I hereby give consent for my thesis, if accepted, to be available for photocopying and for inter-library loan, and for the title and summary to be made available to outside organisations.

Signed …… (candidate) Date ……

CONTENTS

LIST OF FIGURES

LIST OF TABLES

NOMENCLATURE

$\dot{\gamma}$	shear strain rate
A	total surface area of contact between the polymer and the mould
A_s	area of a given mould structure
A_w	area of contact on the sidewalls of the cavities
dl	value of the RLT variation
dr	elementary thickness of a segment of a cylinder
dz	differential height of a segment of a cylinder
E	Young's modulus
F	embossing force
F_{ad}	adhesion force
F_{bd}	force generated by σ_{bd}
F_d	demoulding force
F_{def}	deformation force
F_{fr}	friction force
f	feed rate
K	bulk modulus
L	tooth load
N	number of teeth of the micro drill
n	material constant
P	Pressure
P_c	pressure in the center
P_e	pressure in the edge
P_{max}	maximum pressure

q	flow rate
r	radius
r_c	tool nose radius
T_d	demoulding temperature
T_g	glass transition temperature
T_m	embossing temperature
t_h	holding time
t_p	thickness of the polymer
v	spindle speed
V_d	demoulding velocity
V_m	embossing velocity
v_r	flow velocity in the radial direction
W_{ad}	work of adhesion
α_m	coefficients of thermal expansion for the mould material
α_p	coefficients of thermal expansion for the polymer
γ	adhesive energy
γ_a, γ_β	surface energies of the two solids
$\gamma_{\alpha\beta}$	interfacial energy between the two materials
δ	maximum peak to valley distance generated with the micro drill
ΔP	P_c - P_e
ε	thermal shrinkage strain
η	viscosity
η_0	viscosity at zero rate of shear
μ	coefficient of friction
ν	Poisson ratio

σ_1	contact stress upon demoulding on the mould feature
σ_2	contact stress acting on the adjacent structure
σ_{ad}	adhesion strength
σ_{bd}	contact stress before demoulding
σ_d	contact stress on the sidewalls of the mould structures upon demoulding
σ_T	thermally-induced residual stress
σ_f	flow-induced residual stress
τ	shear stress

CHAPTER 1

INTRODUCTION

1.1 Motivation and Background

Over the last few decades there has been a continuing trend for compact, integrated and smaller products and this trend requires miniaturisation of components that integrate functional features from meso- to micro- and nano-scales (Koc, 2011). Meeting such demands led to development of MEMS-based and micro-machining processes (Elkaseer, 2011). However, these processes are not adequate for high-volume and low-cost production. Thus, fabrication techniques for the high volume production of parts with micro and nano scale features are very important in the global research and industry efforts to meet the increasing needs for device miniaturisation in numerous application areas (Hansen *et al.* 2011). Consequently, micro and nano replication technologies have been developed rapidly and a large number of research studies have been published on this topic in the last decade. Some of the current micro and nano replication methods include micro injection moulding (µIM) (Griffiths *et al.* 2011), hot embossing (HE) (Worgull, 2009) and UV-imprint lithography (Chou *et al.* 1995). These three methods are applicable for large series production as they enable the replication of polymers parts with micro and nano scale structures from a master mould. Thus, the replication of surface geometries is a promising method for micro and nano manufacturing which is capable to meet the

demand of producing products at a low cost and in high volume.

Among these moulding techniques, hot embossing is a process which relies on raising the temperature of a sheet of polymer up to its melting range and on pressing a heated master plate into the polymer for triggering a local flow of the material to fill the cavities to be replicated. This technique has attracted increased attention in recent years in particular due to the relatively simple set-up and low cost associated with its implementation in comparison to other replication techniques (Heckele and Schomburg, 2004; He *et al.* 2007 and Becker and Heim, 2000). HE enables relatively high aspect ratio features to be replicated while their sizes can vary from several hundred micrometres down to several nanometres (Cui and Veres, 2006 and Heckele *et al*. 2001)

The main objective of any replication technique is to enable a complete filling of the mould structures. It is obvious that process parameters influence the quality of moulded parts, particularly, their dimensional accuracy. Thus, the minimum required filling pressure, *P*, within the mould cavities is an important parameter in HE to completely fill the structures to be replicated and thus ensure that the functionality of the moulded features can be fulfilled. At the same time, the applied embossing force induces a pressure distribution which causes non-uniform filling. Thus, monitoring the evolution of the cavity pressure can provide valuable information about the process dynamics and also about the filling behaviour of different polymers. In spite of the limited publications in this field, it is suggested that pressure is one of the critical parameters to determine the outcome of the process at different embossing conditions (Worgull, 2009; He *et al.* 2007 and Lin *et al.* 2002). Therefore, it is

essential to understand and systematically to analyse the relationship between pressure in the mould cavities and the hot embossing process parameters.

In addition, although polymer replication techniques are suitable for the production of parts with micro and nano structures, one of the most challenging issues to overcome when implementing them is to prevent the formation of structural defects that can occur during demoulding. In the case of hot embossing, such problems have been reported by a number of researchers (Worgull and Heckele, 2004; He *et al.* 2005; Dirckx *et al.* 2007; Guo *et al.* 2007a and Dirckx and Hardt, 2011). Demoulding-related defects can include overdrawn or damaged edges due to thermal stresses associated with differences in the shrinkage behaviour of replicas and the mould during cooling, and overstretched and separated structures, due to high adhesion and friction forces. For instance, overdrawn or damaged edges are problematic for the production of microfluidic systems as they can affect the sealing between cover plates and channels of the HE replicas, and also can compromise the functionality of the fabricated devices. In addition, broken or overstretched features can render the HE replicas unusable and can also result in polymer material residue in the mould cavities, which is detrimental in batch production of parts. Another costly defect, which is sometimes reported in the literature, consists of broken mould structures/features (Dirckx, 2010). The state-of-the-art review conducted in this research reveals that there is still a need to develop more comprehensive simulation models for investigating the combined effects of material properties, demoulding temperatures, polymer pressure histories, locations and geometry of the mould structures and the adhesion on the demoulding forces.

Due to the principle on which the process relies, hot embossed parts are characterised by the existence of a residual layer underneath the replicated structures. For some applications, the existence of a residual layer is beneficial and it can be used for housing purposes. This is the case when replicating micro-fluidic channels for instance (Mathur *et al.* 2009). This layer can also be removed or etched which is typical for thermal nanoimprint lithography, a process that shares similarities with hot embossing (Guo, 2007). The uniformity of the residual layer thickness (RLT) is an important issue for both processes as variations in its distribution may affect the functionality or further processing of replicated parts (Lazzarino *et al.* 2004 and Sirotkin *et al.* 2007). For example, an inconsistent RLT will result in adjacent micro or nano structures being oriented at different angles. This can be detrimental for optical applications for instance as it could affect the functionality of devices such as benches or wave guides. Also, it could cause problems during the sealing of microfluidic devices where flat bonding will be difficult and defects can result in leakages. The influence of the machine, the mould, the polymer and the process parameters on the uniformity of the RLT in HE is complex and has to be investigated systematically.

In summary, the main barrier for further improvement to the quality of the embossed parts for different conditions, designs and materials, is the lack of more advanced scientific understanding and systematic analysis of the process. Particularly, although, the scientific community working in the field of HE agrees that process parameters have a significant effect on the quality of the moulded parts, so far, there has been no detailed study of their influences on the cavity pressure, demoulding force and uniformity of the residual layer for different materials. As discussed, low

cavity pressure could cause incomplete filling, high demoulding force could damage or separate the replicated structures and non-uniform residual layers could be a cause of functional failure for final applications. Thus, the understanding of the process parameters influence on these outcomes is a challenging research issues that should be addressed. Therefore, there is a real need to examine systematically such parameters and to investigate their influence on the process, especially, on the quality of the part for optimising the process and thus, achieve consistently the required quality.

1.2 Research Objectives

The overall aim of this research was to investigate and to gain a deeper understanding of the factors affecting the quality of hot embossed parts. Due to the large number of input and output factors only a selection of them was studied applying empirical and analytical methods and tools.

To achieve the overall aim of the research, the following objectives were set:

- To investigate the process parameters effect on cavity pressure behaviour during the filling of microstructures by conducting experimental studies. Also, to develop a special condition monitoring technique to read and quantify the pressure distribution during the embossing process.

- To develop and validate an analytical model for predicting the demoulding force in hot embossing of polymer materials. This model should consider the effects of material properties, the demoulding temperature, the polymer

pressure history, the design of the mould structures and the adhesion phenomenon.

- To investigate the process factors influence on the residual layer homogeneity achieved on embossed parts by conducting experimental and simulation studies. Based on this, to provide an in-depth analysis of the phenomena that affect the part uniformity.

1.3 Thesis Organisation

The remainder of the thesis is organised as follows:

Chapter 2 contains a review and analysis of the current state of the art in hot embossing. This chapter discuses different replication processes for micro and nano fabrication. The factors affecting the replication quality in hot embossing are also reviewed. Next, previous research studies covering the topics of cavity filling, pressure behaviour, demoulding force and the residual layer uniformity in hot embossed are reported. Finally, the chapter is concluded with a summary of some of the key research issues in the HE research areas discussed in this chapter.

Chapter 3 presents an experimental investigation of the effect of process parameters on cavity pressure in hot embossing. First, the chapter describes the experimental set-up used which includes the hot embossing machine employed, the test mould and materials along with the condition monitoring technique adopted to

investigate the effects of the process parameters on cavity pressure. Next, the conducted design of experiments is presented together with the analytical approach utilised to estimate the minimum embossing force and pressure for performing the trials. Finally, the experimental results are reported and the effects of the different parameters are investigated.

Chapter 4 describes a new model to simulate the demoulding force during hot embossing and reports an experimental study conducted to validate it. First, the developed model is presented taking into account the contribution from the adhesion, deformation and friction forces. Next, the test material, mould design, plan of experiments and the method used to measure the demoulding force are explained. Finally, the comparison between the simulation and the experimental results is discussed focusing on the effect of demoulding temperature, applied force and structure layout on the achieved demoulding force.

Chapter 5 reports a study on the process factors influence on the homogeneity of the RLT for embossed parts. Initially, the experimental and simulation set-up, the mould, the selected material and the RLT measurement technique used in this research are described. The design of experiments together with the approach adopted to perform the trials and analyse the data are also presented. Finally, the results obtained are reported and the relationship between the process settings and the RLT achieved in hot embossing are discussed.

Finally, **chapter 6** summarises the contributions and conclusions of the thesis and proposes directions for further research.

CHAPTER 2

LITERATURE REVIEW

2.1 Overview

In this chapter, a review and analysis of the current state of the art in hot embossing is presented. The chapter is organised as follows. The first section discuses different replication processes for micro and nano fabrication, especially, hot embossing, micro injection moulding and UV-imprint lithography. In addition, comparison of these techniques is described. Then, the factors affecting the replication quality in hot embossing are reviewed. Next, previous research covering the topic of cavity filling and pressure behaviour in hot embossing is presented. The fourth section focuses on investigations studying the demoulding force in hot embossing. Following this, published research on the residual layer uniformity in hot embossed part is reported. Finally, the chapter is concluded with a summary of some of the key research issues in the hot embossing research areas discussed in this chapter.

2.2 Replication of micro and nano structures

Replication of surface geometries is an established method in micro and nano manufacturing technologies and it satisfies the demand of producing products at a low cost and at high volume. The replication processes can be divided in three stages: master/mould preparation, replication and separation (Figure 2.1). Typically, the mould/master is in direct contact with the substrate material with exceptions for the deposition methods. Also, the replicated part can be used as a mould/master for a subsequent replication technique which is sometimes the case when producing electroplated nickel or casted polydimethylsiloxane (PDMS) tools (Narasimhan and Papautsky, 2003; Bogdanski *et al.* 2004 and Guo *et al.* 2007b). In a replication process, micro and nano structures of the master/mould is transferred to a substrate by inversely copying the geometry. This transfer can be accomplished with the action of one or several physical phenomena such as heat, force, chemical activation and deposition (Hansen *et al.* 2011). The last step of a replication process is the separation of the master and the substrate. The type of transfer and states of the substrate material (solid, solid/viscous and liquid/viscous) characterises the replication techniques as shown in Figure 2.2. Among the techniques that are presented in Figure 2.2, polymer replication processes include:

- Micro Injection Moulding. It is characterised by the injection of polymer melt into a structured mould (Giboz *et al.* 2007). Further description of this process is given in Chapter 2.

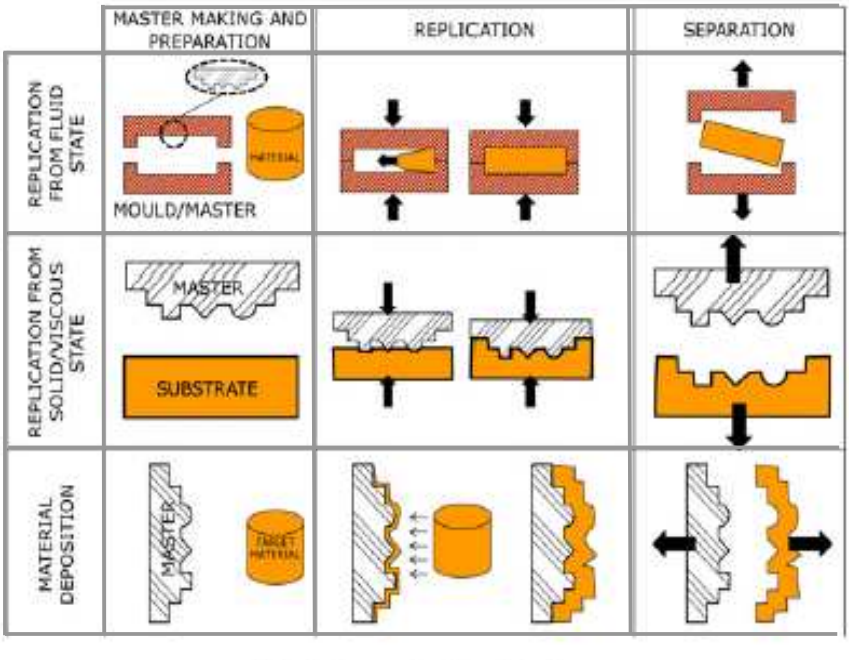

Figure 2.1 Concepts of replication process (Hansen *et al.* 2011).

	Liquid	**Viscous**	**Solid**
Force or Heat	- Micro Injection Moulding - Casting Reaction Injection Moulding	- Hot Embossing - Roll-to-Roll Embossing - Thermal Nano Imprint Lithography - Injection compression moulding - Thermoforming	- Metal forming
Chemical activation or deposition	- UV-Embossing		- Electroplating

Figure 2.2 Mechanisms of the different replication processes.

- Micro Reaction Injection Moulding. The process relies on the injection and mixing of two or more components of polymer liquid and polymerisation of these components in the mould. The schematic view of this process is provided in Figure 2.3 (Heckele and Schomburg, 2004).

- Injection Compression Moulding. The process works by injecting and compressing a low viscosity polymer melt into the mould. Figure 2.4 describes the different steps for this process (Guan *et al.* 2012).

- Hot Embossing. In this case, a heated mould and polymer sheet are pressed against each other (Heckele and Schomburg, 2003). Chapter 2 provides an in-depth description of this process.

- Thermal Nano Imprint Lithography (NIL). This process shares similarities with hot embossing. In particular, heating and pressing are the fundamental steps for both processes. However, thermal nanoimprint lithography is typically conducted for moulding nano scale structures on thin spin-coated polymer films, which are then further used as etching masks (Guo, 2007).

- UV-Imprinting. It is characterised by solidifying a UV-curable polymer resist by UV-radiation through the transparent mould (Guo, 2007). Further description of this process is given in Chapter 2.

- Roll-to-Roll Embossing. In this process, a highly viscous polymer is deformed using structured rolls instead of plates. The overview of this technology is presented in Figure 2.5 (Yeo *et al.* 2010).

- Micro Thermoforming. This process relies on forming a thin polymer film by applying gas pressure against the film and mould. This is illustrated in Figure 2.6 (Focke *et al.* 2011).

- Casting. This process is concerned with the filling of the mould using thermosetting polymers or elastomers and then polymerising them by heat, light or chemicals (Adithyavairavan and Subbiah, 2011).

The following sub-sections give an overview on three different micro and nano replication processes: 1) hot embossing, 2) micro injection moulding and 3) UV-imprinting and finally, a comparison between these techniques is presented.

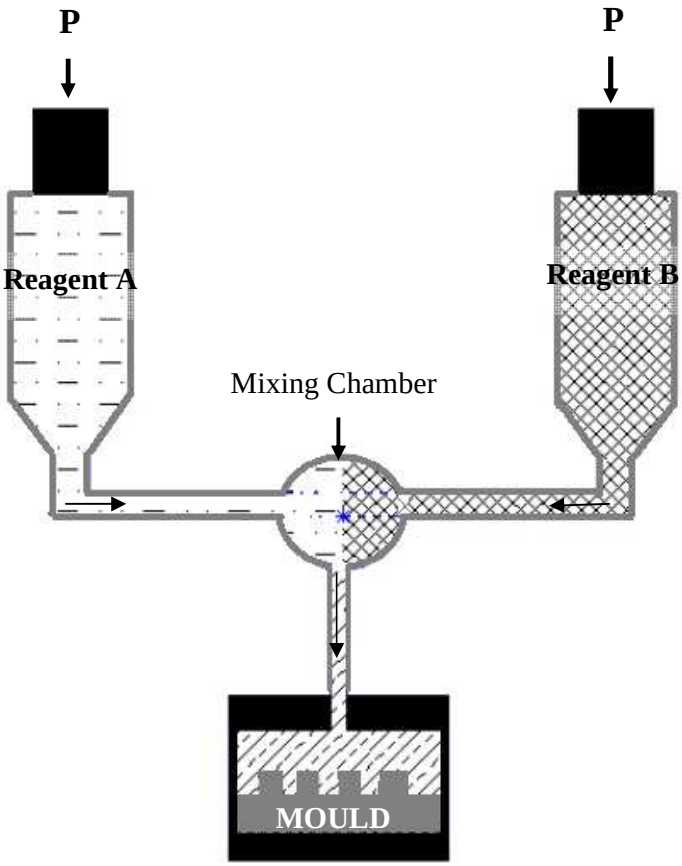

Figure 2.3 Schematic description of Reaction Injection Moulding.

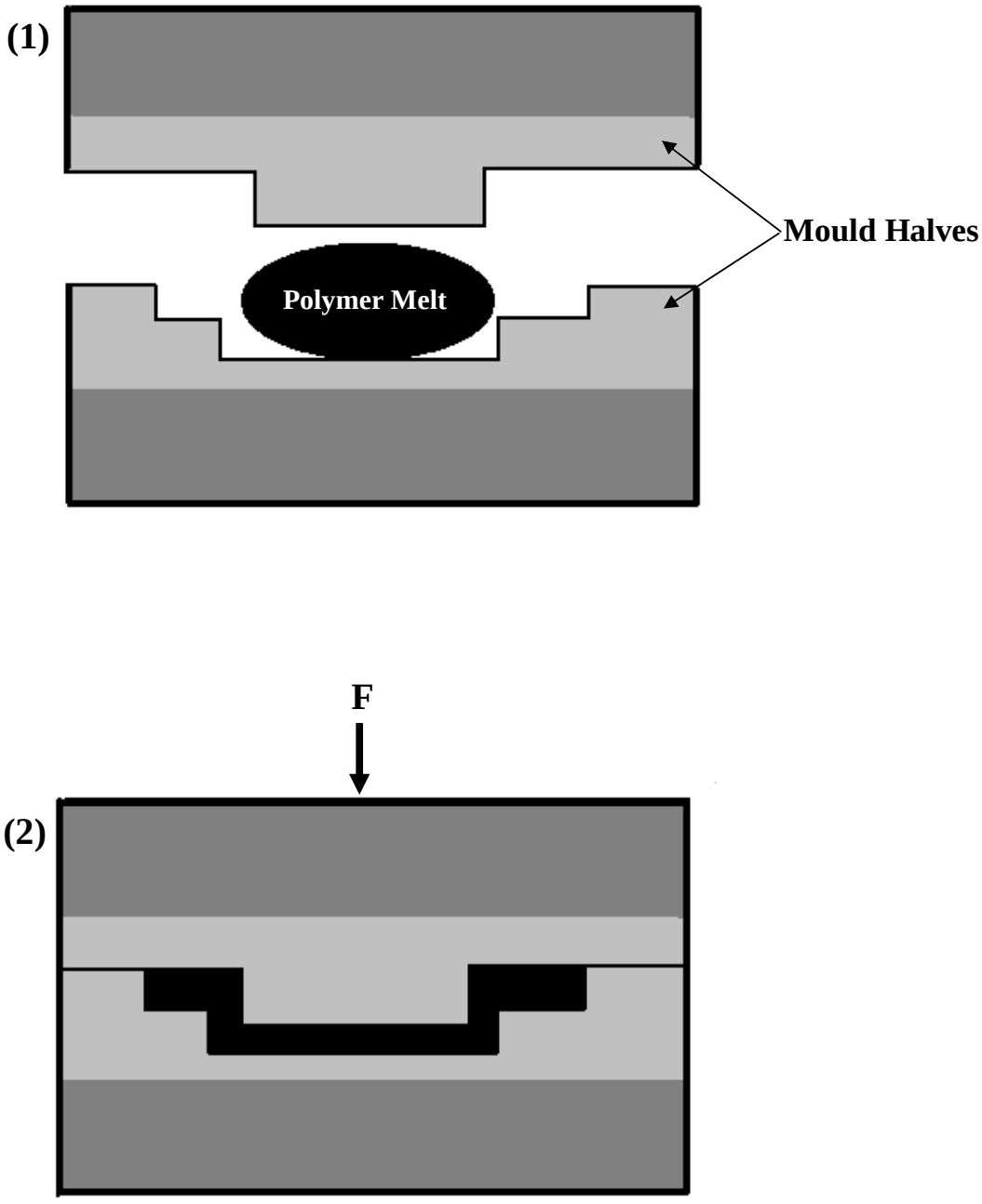

Figure 2.4 Schematic view of Compression Injection Moulding.

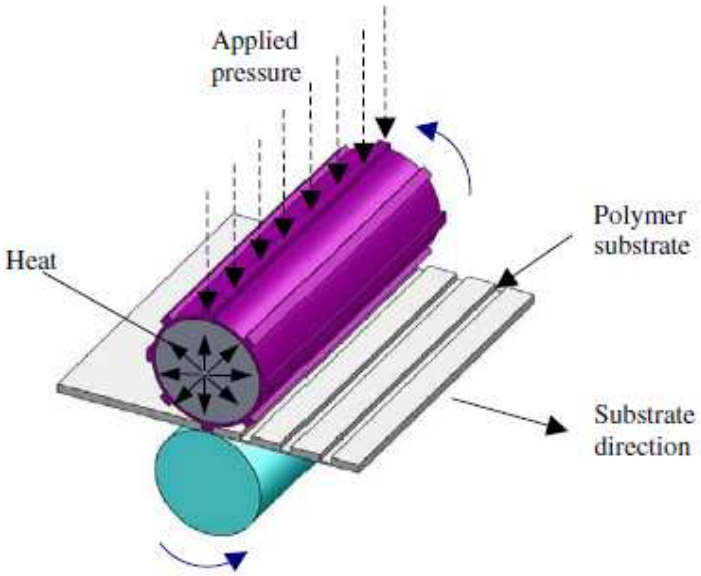

Figure 2.5 Schematic view of Roll-to-Roll embossing (Yeo *et al.* 2010).

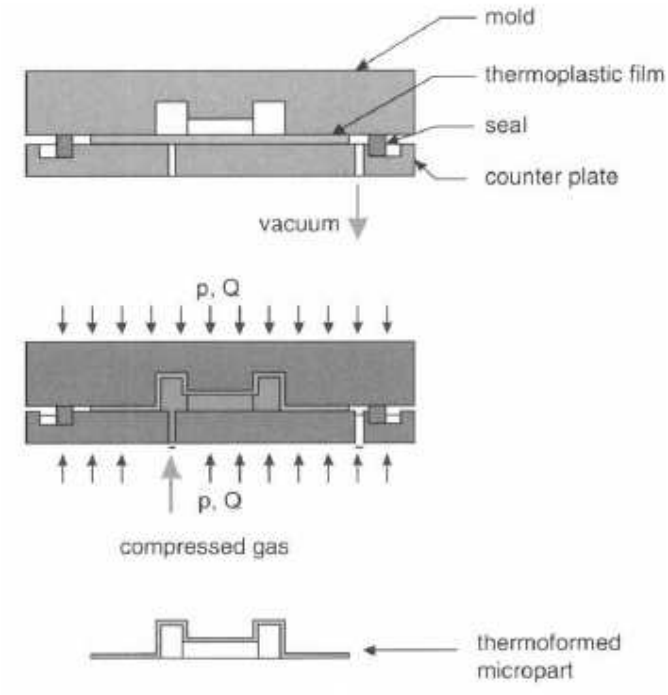

Figure 2.6 Schematic description of Thermoforming process (Worgull, 2009).

2.2.1 Hot Embossing

HE is a process which relies on increasing the temperature of a polymer sheet up to its melting range and then on pressing a heated mould into the polymer for generating a pressure to fill the surface structures. This technology has attracted a significant interest among micro and nano replication processes due to the relatively simple set-ups and short lead times associated with its implementation. HE enables relatively high aspect ratio features to be replicated while their sizes can vary from several hundred micrometres down to several nanometres. The hot embossing process is also characterised by short flow distances, low shear stress and the capability of replicating a variety of materials. On the other hand, the HE cycle time is relatively long if compared with injection moulding due to the low cooling and heating rate of the bottom and top plates. This process could take up to 30 mins depending on the mould design and the replicated materials where the complex and high aspect ratio structures will prolong the process. Also the material viscoelastic behaviour under embossing conditions which determines the replicability of the polymer will directly effect the processing time.

A typical HE cycle is composed of the following steps:

a) A micro-nano structured mould and the polymer sheet are inserted into the HE machine.

b) The mould and polymer are heated to the embossing temperature.

c) Then, the mould is pressed into the softened polymer film.

d) A few minutes of holding time is applied in order to ensure full replication.

e) The embossed part is cooled down to the demoulding temperature (for amorphous polymers demoulding temperature is below the glass transition temperature (T_g)).

f) The mould and the part are separated by moving them away from each other.

A schematic diagram of the HE process is given in Figure 2.7.

Compared with other replication technologies, a wide variety of materials can be structured by hot embossing. However, the most suitable embossing materials are thermoplastic polymers. Although amorphous and semicrystalline thermoplastic polymer sheets can be utilised, it is easier to emboss amorphous polymers due to the flexibility in applying a range of embossing temperature. As shown in Figure 2.8, the embossing window of amorphous polymers typically starts in the flow range and ends in the melt temperature range, while this window is narrower and within the melting range for semicrystalline polymers (Worgull *et al.* 2011). In addition to polymers, glasses like Pyrex and Borosilicate (Schubert *et al*. 2006) and metals such as lead, aluminium and bulk metallic glasses (Cao *et al.* 2004 and Pan *et al.* 2008) can be structured using hot embossing.

The applications of hot embossing can be found in the area of optical devices such as compact discs, lenses, mirrors, optical benches, wave guides and switches. Especially, this technology can be used to produce low cost micro-fluidic devices such as lab-on-chip analysis systems, pumps, valves, pressure sensors and flow sensors. Also, it can be used as an intermediate step for the fabrication of electrical devices like acceleration sensors, electrical switches and comb drives.

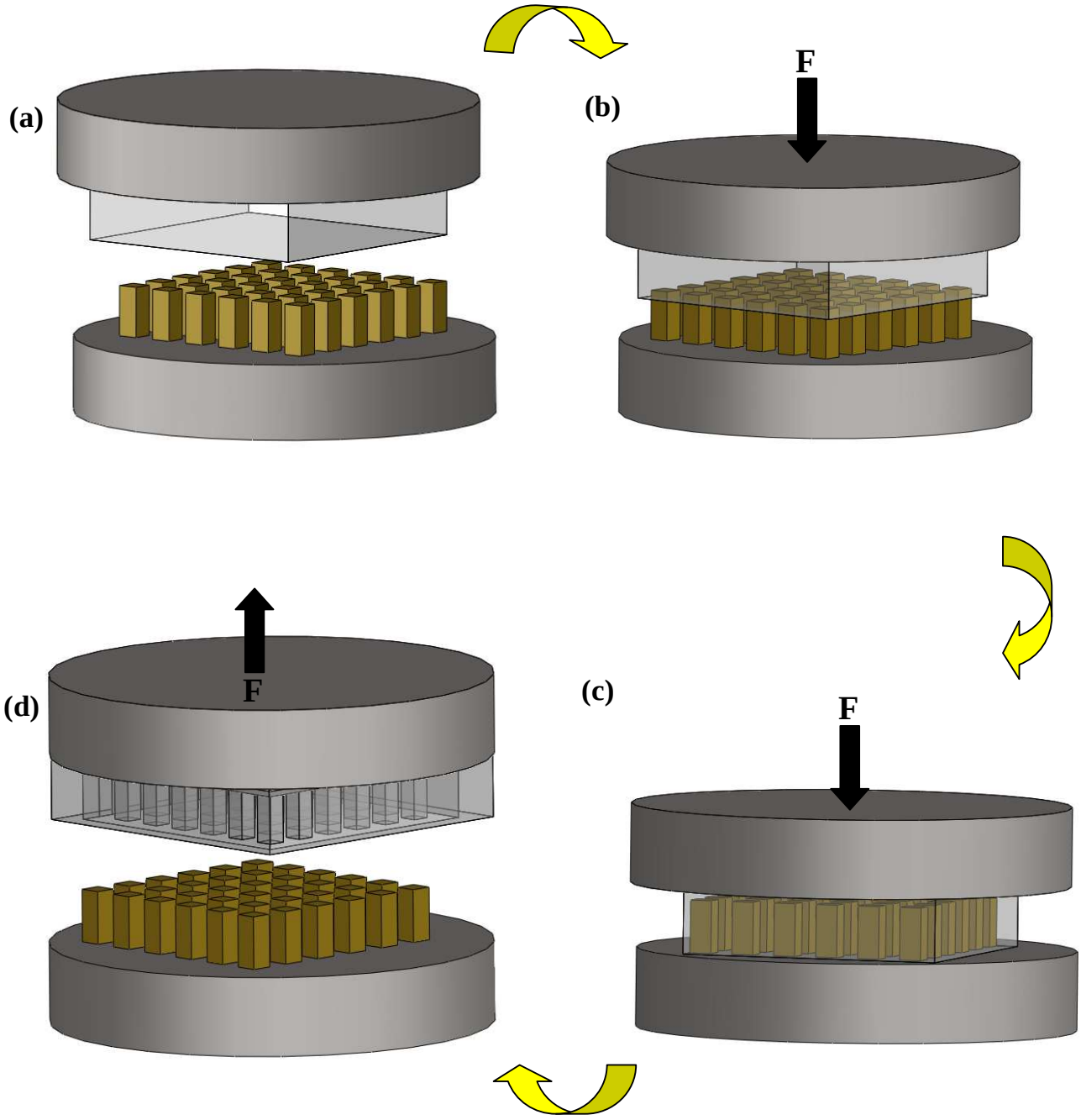

Figure 2.7 Schematic diagrams of the HE process steps: a) Mould and polymer material inserted, b) Touch force created by bringing mould and polymer in contact with each other and then heating up to the embossing temperature, c) Embossing force applied to replicate the structures via penetration of the polymer and letting the viscous material to completely fill the cavities while holding it for a few mins and d) Separating the polymer from the mould surface by moving the plates away from each other.

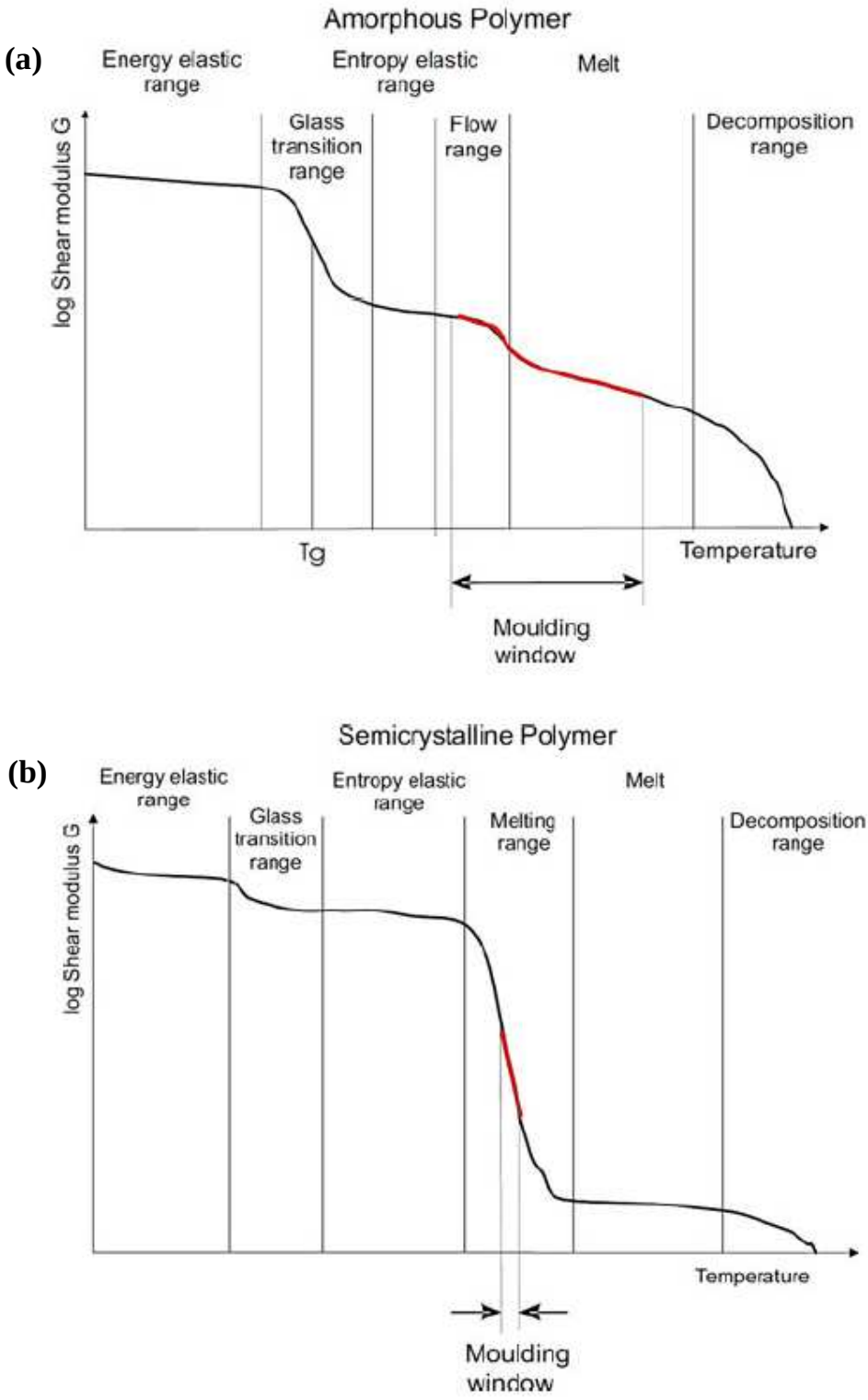

Figure 2.8 Moulding windows of a) amorphous and b) semicrystalline polymers (Worgull *et al.* 2011).

2.2.2 Micro Injection Moulding

A general and simple definition of micro injection moulding describes the process as the production of polymeric parts with structure dimensions in the micrometre or sub-micrometre range via the injection of the polymer melt into the mould (Piotter *et al.* 2002). Injection moulding is a well-established process, which is also used in industry for the replication of large series. Compared with other replication techniques, injection moulding is characterised by short cycle times, down to a few seconds. It should be noted that high injection speeds increase the internal stresses of replicated parts and thus the process is not well-suited for the production of optical devices. Also, it is difficult to fill sub-micrometre structures with high aspect ratio due to long flow distances.

The generic steps of the micro injection moulding process occur successively as follows:

a) A micro structured mould and polymer granules are inserted into the machine.
b) The granules are heated up in the plastifying unit to a temperature above the melting range.
c) The polymer melt is injected by a palstifying screw through a nozzle and a runner system into the cavities of the mould.
d) The injected polymer cools below T_g or melting temperature.
e) The cooled is part separated from the mould via ejector pins.

The injection unit of a Battenfeld Microsystem 50 machine is shown in Figure

2.9. Amorphous and semicrystalline thermoplastic polymers are well suited for this process. Also, metal and ceramic powders can be moulded by using the concept of powder injection moulding. A wide range of applications can be found for this process in the areas of micro mechanical, medical and electronic devices.

2.2.3 UV-imprinting

UV-imprint lithography is one of the emerging technologies for the manufacturing of future devices. This process is based on the low pressure applied by a transparent mould to curable liquid resists which are deposited or spin-coated on a substrate. The UV-imprint technique does not require heating and cooling steps, which reduces the cycle time and also, the low pressure applied minimises the stress and distortions. This process is capable of replicating structures down to 5 nm (Austin *et al.* 2004). However, it is limited to materials and moulds that are UV- curable and transparent, respectively.

The generic steps of UV-imprint lithography can be presented as follows:

a) A UV-transparent mould (eg. glass, fused silica) is inserted into the machine and a UV-curable resist is spin coated or dispensed on a substrate.
b) A low pressure is applied to the resist by pressing the mould onto it.
c) The resist is cured by UV-irradiation at ambient temperature.
d) The mould is separated from the resist during a demoulding step.
e) Finally, depending on the application, the residual layer left can be etched away.

The schematic diagram of the process is presented in Figure 2.10. This process

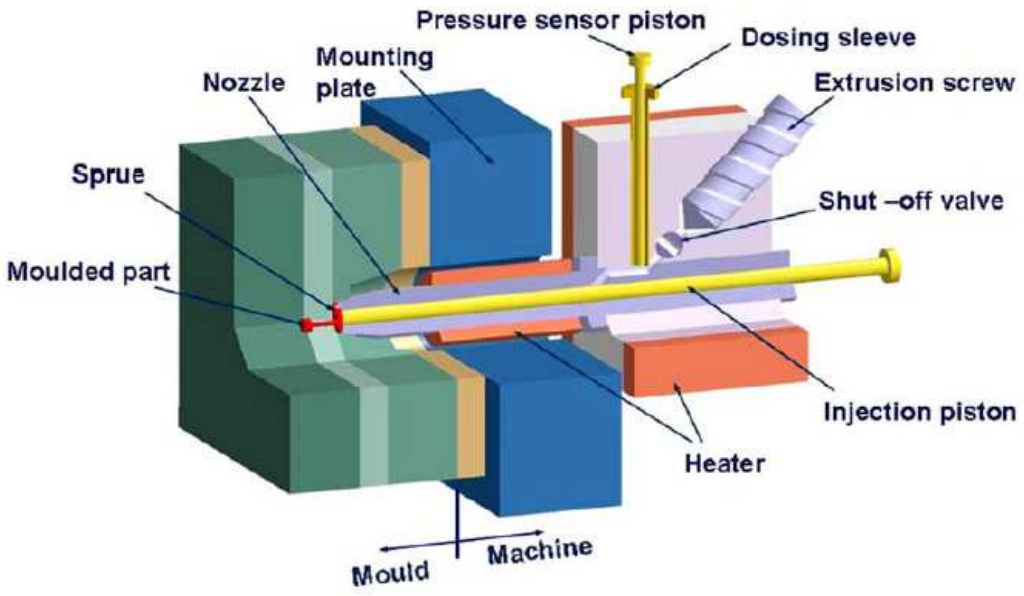

Figure 2.9 Battenfeld Microsystem 50 Injection units (Tosello, 2008).

can be used for producing etch masks for pattern transfer process (wet or dry etching), nano-optical components, micro and nano fluidics or microelectronic devices.

2.2.4 Comparison of processes

Overall, the main clear difference between the three replication processes described in the previous sections is the range of processing temperature (see Figure 2.11). A more detailed comparison of micro injection moulding, hot embossing and UV-imprint lithography is given in Table 2.1. Generally, it can be concluded that UV-imprinting is limited with respect to the replica and mould materials can be used. However it can replicate feature size down to 5 nm and can produce replicated parts with very low residual stress. Typically, this process is faster than hot processes due to the lack of heating and cooling units, but it is still slower than micro injection moulding (Hocheng and Wen, 2010). Micro injection moulding is a well-established technology for replicating large series of components. The suppliers of such machines are numerous and the commercialised systems are generally less expensive than those implementing other replication techniques. However, the principle of injection moulds, the concepts of separate plastifying units, injection and compression systems give complexity to the machine and increase the set-up time. Compared to other replication techniques, very short cycle times can be achieved, which makes it suitable for mass fabrication. Other disadvantages that should be noted are the higher residual stress and longer flow paths compared to hot embossing and UV-imprinting. Hot embossing is suited for medium or small series productions and still under development with respect to its transition to industry. It is generally less complex to implement in comparison with other processes. Regarding the achievable minimum

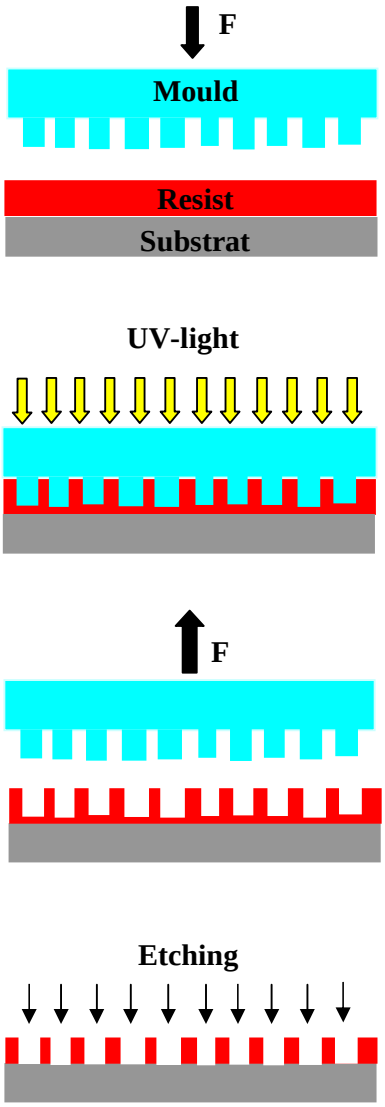

Figure 2.10 Schematic diagram of UV-imprint lithography.

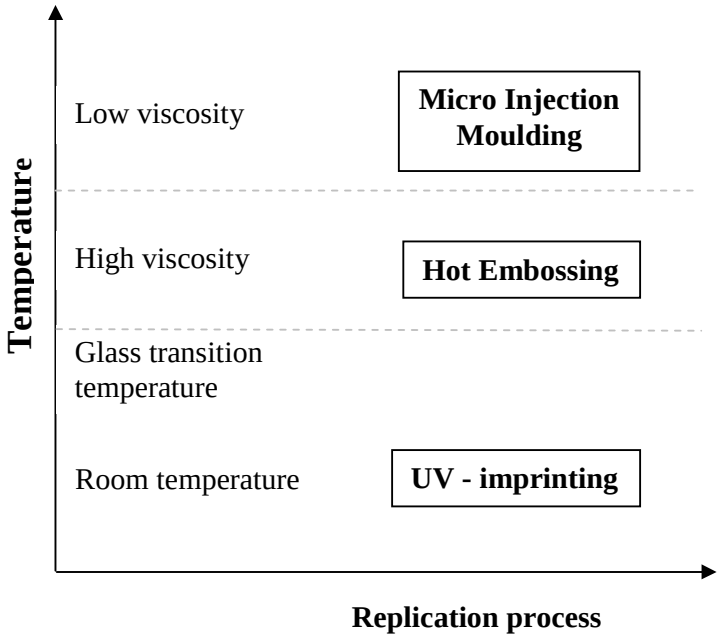

Figure 2.11 Processing temperature ranges between different replication techniques.

Table 2.1 Comparison of replication processes.

Criteria	Injection Moulding	Hot Embossing	UV-imprinting
Cycle time	Few seconds	5 – 30 min.	10 - 30 sec.
Flow length	Length of runner system	Height of cavity	Height of cavity
Raw material	Granules	Sheets	Thin film
Materials	Thermoplastic polymers, Ceramics and metals (Powder injection moulding)	Thermoplastics, glass and metals.	UV-curable resists
Residual stress	High	Medium	Low
Moulding window	Above melting temperature	Above T_g or in the melting range	Room temperature
Serial production	Large	Medium	Medium

feature size and the residual stress, it is difficult to report specific data given that a wide range of different results have been reported in the literature. However, it can generally be said that the minimum feature size achievable with hot embossing is in between micro injection moulding and UV-imprinting. Although the process is slower than the other two technologies, it can be applied for producing parts in a wide range of materials with high aspect ratio and high quality micro-nano structures.

2.3 Factors affecting the replication and part quality in hot embossing

As mentioned earlier, the principle of the HE process is based on heating and pressing the mould and a polymer sheet to fill the cavities to be replicated. The overall factors affecting the control of the process and the quality of the embossed parts can be classified into the following five groups, which are also illustrated in Figure 2.12:

- Embossing machine
- Embossing plates
- Polymer material
- Mould insert
- Process parameters

Together, these five categories of factors influence the quality of the final part. Therefore, their understanding and characterisation is important to avoid defects or

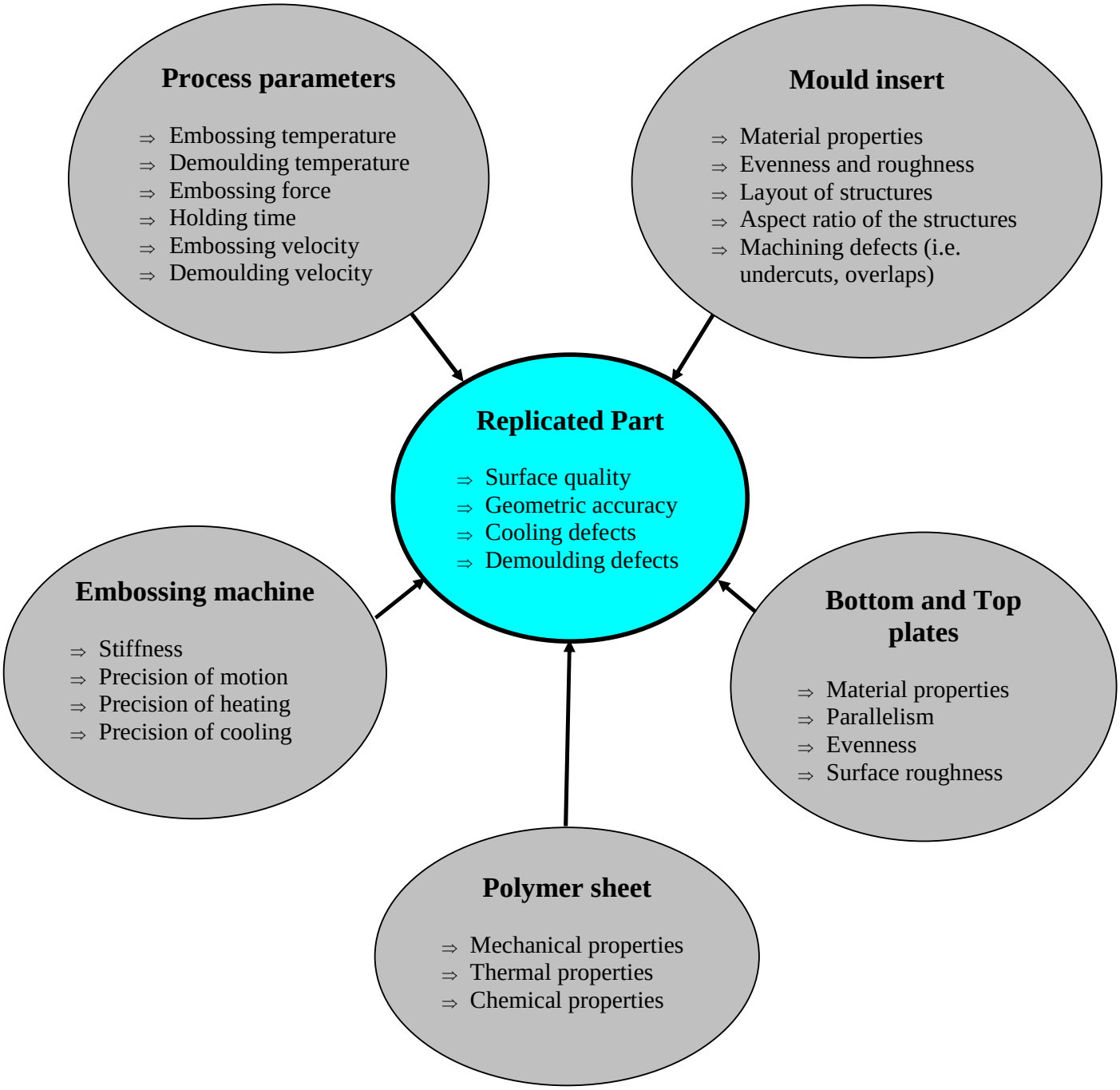

Figure 2.12 Schematic diagram of the factors influencing the quality of the embossed parts.

failures on the embossed samples.

The HE machine has to be as stiff as possible in order to prevent the bending of the plates under the embossing load. The accuracy of the plate displacement through the motion of the crossbars is responsible for the required parallel movement of the mould and substrate material, which in turn influences the quality of the part. Another important factor is the homogeneous temperature distribution during heating and cooling. In particular, non-homogeneous temperature distribution during the heating stage could cause a non-uniform flow of the polymer melt and also, can contribute to variations in the thickness of the residual layer. A non-homogenous temperature distribution during the cooling stage could be more problematic as it can result in anisotropic shrinkage which can lead to warping of the produced replica.

The bottom and top plates have to be parallel in order to prevent the occurrence of a non-uniform residual layer, non uniform filling and the generation of high stress in one area which can cause damage to the mould. Furthermore, the evenness and surface roughness of the plates will affect final the uniformity of the embossed part (see section 2.5).

The thermal properties of the polymer material are very important to control the embossing process, specifically the moulding and demoulding temperatures which are crucial parameters for achieving high quality replicated products. Also, the material chemical properties will affect the shrinkage behaviour whereas amorphous polymers are typically characterised by isotropic shrinkage which is not the case for semicrystalline materials. Furthermore, the molecular weight of the material will

affect the cavity filling as higher molecular weight materials are beneficial to support successful imprint at reduced temperatures by utilising shear rate effects (Schulz *et al*. 2005 and 2006).

The material properties of the mould are responsible for its deformation behaviour when it is under load. For instance, silicon moulds can be broken easily under a small applied force and other moulds made of relatively soft materials can be bent easily which will cause failures or defects on the final product. Evenness and parallelism of the mould is also of high importance to achieve a uniform filling and flat residual layers. A very important factor is concerned with mould machining defects like overlaps or the roughness of the vertical walls as such surface features could damage or separate the polymer structures during the demoulding step. In addition, the layout and the aspect ratio of the structures could cause filling problems during embossing and high forces during the demoulding step.

Probably, the most important category of factors which affect the replication quality and accuracy is concerned with the controllable process parameters. Most of the publications in the area of HE part quality are focused on the process parameters influence by using systematic experimental and simulation techniques to optimise the process (Chien, 2006; Datta and Goettert, 2006; Veres *et al.* 2006; Yao *et al.* 2008; He *et al.* 2008 and Luo *et al*. 2006). During the setting up of a replication operation on a hot embossing machine, the following process parameters can be controlled by the user:

- Embossing temperature

- Demoulding temperature
- Embossing force
- Holding time
- Embossing velocity
- Demoulding velocity

An embossing cycle starts by bringing the plates closer to each other until an initial contact between the polymer and the mould generates a force of around 100 N to 300 N. Then, the material to be replicated and the mould are heated above the glass transition temperature in the case of amorphous polymers or up to the melting range of semi-crystalline polymers. Following this step, the polymer and mould are pressed together which a stage referred to as velocity-controlled moulding until a set force is attained. Then the process switches to a force-controlled moulding mode during which the embossing force is kept constant for a duration determined by the holding time. Next, the cooling cycle starts. This cycle is characterised by the reduction of the embossing temperature until a set demoulding temperature is reached. Finally, the embossed polymer is separated from the mould by moving the plates away from each other. This separation can be accomplished by utilising different techniques which are discussed in section 2.4. The schematic diagram of a typical hot embossing cycle including the evolution of characteristic process parameters is shown in Figure 2.13. The relative motion between the mould and the substrate can provide some insight into the material behaviour under various process parameters. In particular, measuring the crossbar movement in the direction of the embossing force can give approximate compression strain and stress curves which are especially helpful if such material parameters for a polymer are not available in the literature.

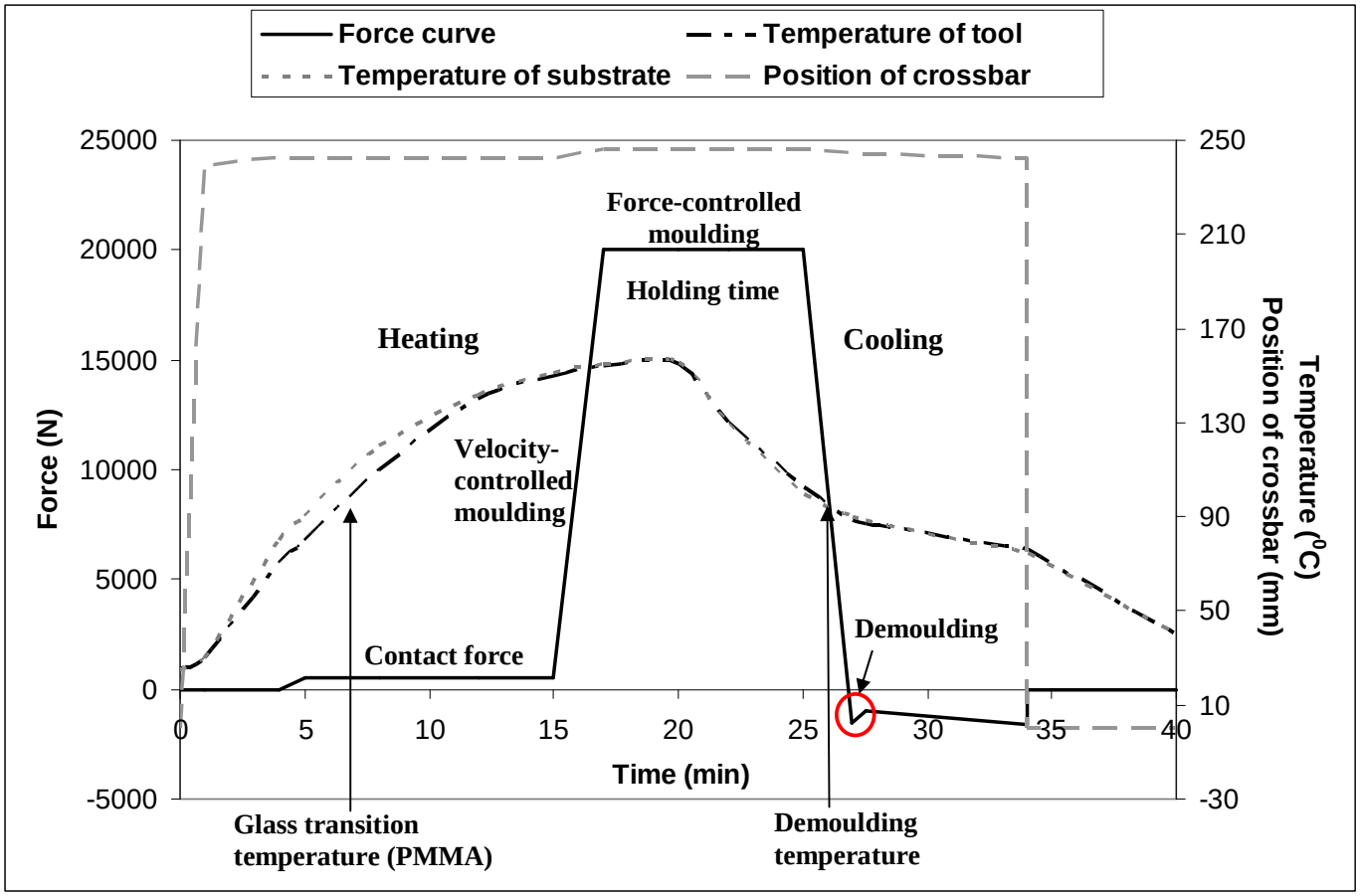

Figure 2.13 Temperature, force and position curve trajectory of a typical hot embossing cycle.

Defects can occur during the main process stages as follows:

1) Filling stage. The main objective of the replication process is a complete filling of the structures as an incomplete filling leads to the geometric inaccuracy of the replicated structures. Defects during this stage could happen due to the lack of required pressure to fill the cavities at a given temperature.

2) Cooling stage. Sink marks can occur during this stage if the applied pressure is not enough to prevent part shrinkage as it will induce poor contact pressure between the mould and the polymer. Also, the differences in shrinkage during cooling could cause a warpage of structures or of the whole part. Furthermore, a short cooling time will increase the internal stress of the part as there will not be enough time for the relaxation of the shear stress during embossing and the orientation of the polymer molecules will be frozen too rapidly.

3) Demoulding stage. This is the most sensitive stage which tends to cause the worst failures. Overstretched and separated structures and damaged edges could happen during this step as a result of high adhesion and friction forces between mould structures and the polymer.

Thus, process parameters have a significant effect on the quality of the replicated parts. These effects need to be studied and analysed comprehensively for the further development of the hot embossing technology. More specifically, there is a lack of detailed studies on factors influencing the cavity pressure, the demoulding force and the uniformity of the residual layer. As mentioned, low cavity pressure

could cause incomplete cavity filling, high demoulding forces could damage or separate the replicated structures and a non-uniform residual layer could be problematic for final applications. Thus, these particular process characteristics are challenging issues that need addressing. The following sub-sections are present a review on each of these research topics.

2.4 Mould cavity filling and pressure behaviour

Existing studies generally agree that the main process parameters affecting the filling stage of the HE process are the embossing temperature (T_m), the embossing force (F) and the holding time (t_h). A number of researchers investigated the effects of these factors and the generic conclusions from these investigations are that an increase of these three process parameters leads to improvements of the process performance (Chien, 2006; Ng *et al*. 2006a and Li *et al.* 2008). In particular, T_m was found to be of major importance for achieving better replication results (Li *et al.* 2008; Lan *et al.* 2009 and Shen *et al.* 2002). Thus, such findings indicate that high values of process parameters can be used to ensure the complete filling of microcavities. However, it should be noted that such settings may also lead to some negative effects such as an increased cycle time. Therefore, it is also important to consider the consequences of using given process settings in order to assess the overall performance of an embossing operation.

To achieve a consistent replication quality, one proven method is to monitor the influence of varying factors during the process. It is obvious that process

parameters influence the quality of moulded parts, particularly, their dimensional accuracy, mechanical behaviour, and surface quality. For example, T_m, F and t_h are such factors that can have a direct impact on dimensional accuracy. The filling of microcavities via the hot embossing process is characterised by short flow lengths determined by the depth of the mould cavities. Typical flow distances are comprised between a few tens of nanometres and typically a few tens of micrometres, although lengths of approximately 1 mm can be reached in special cases. The lateral dimensions of the mould features can vary from the nano scale range up to widths of several hundreds of micrometres.

The minimum required filling pressure, P, within the mould cavities is an important parameter in order to completely fill the structures to be replicated. However, this is not a process parameter which can be directly controlled by the user in a typical HE machine. Therefore, by measuring P in mould cavities during an embossing cycle, it is possible to assess the overall behaviour of the process when varying some controllable parameters. Subsequently, by monitoring P as an output signal, it is possible to ensure a consistent replication and uniform product quality across repeated embossing cycles.

A relatively small number of studies in HE focused on the description of the cavity filling behaviour. Heyderman *et al.* (2000), Schift *et al*. (2001), Ressier *et al.* (2004) and Macintyre and Tomas (2005) assessed experimentally the different filling states of replicated structures by optical microscopy and Atomic Force Microscopy (AFM) measurements. Also, it was observed that there are two mechanisms involved in the filling of micro and nano scale structures, namely the simple flow of the

polymer from along the sides of a mould cavity and the formation of mounds within the cavity. In both cases, there is evidence of compression causing buckling of the polymer and also capillary action drawing the polymer up to the top of a mould cavity.

Hirai *et al.* (2004) studied the polymer deformation process by numerical simulations and experiments during the filling of groove structures. These authors noticed that the required embossing pressure increases when the initial thickness of the part decreases to less than about twice the groove depth of the mould insert.

Rowland *et al.* (2004 and 2007) analysed and simulated polymer flow during the imprinting process with a particular focus on the filling of micro and nano scale structures. The profile of the polymer flow during filling was characterized by two different modes: single peak and dual peak as described in Figure 2.14. This experimental investigation considered the effects of embossing time, temperature and master cavity width and various stages of the initial deformation of polymer during HE were analysed. The dual peak profile was detected in larger structures while single peak formation was characteristic of feature widths below 30 µm. Also, the dual peak profile was observed when embossing at a temperature below T_g due to the high viscosity of the polymer. In this case, the flow is restricted and longer loading times at the same temperature increase the overall height of the deformation while the peaks move slowly and closer together. The increase in embossing temperature to the T_g of the polymer resulted in both polymer peaks merging into one at the feature centreline. The simulation results also indicated that large differences in cavity size lead to non-uniform filling and non-local polymer flow.

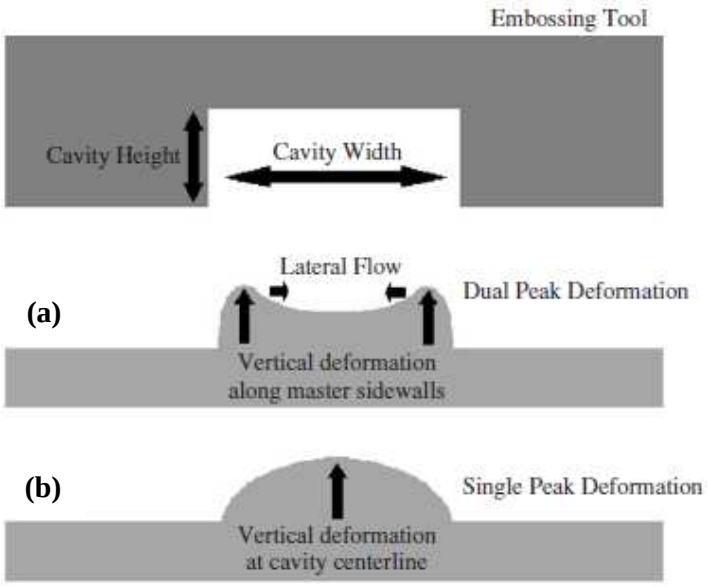

Figure 2.14 Polymer deformation within mould cavity (a) dual peak deformation and (b) single peak deformation (Rowland and King, 2004).

Scheer *et al.* (2001) also analysed the polymer flow via experimental and simulation studies. Investigation of the polymer profile around protruding mould features revealed that, during penetration of the mould into the film, a polymer front starts moving away from the edge of each protruding feature, filling the recessed area. Furthermore, Scheer *et al.* (2006) investigated the recovery effects of polymers under embossing conditions by performing simulations of the elastic behaviour of the material. The results obtained indicate that initially, the mould intrusion into the polymer melt is fast due to shear thinning at the periphery of the features.

Li *et al.* (2008) investigated the effect of process parameters on polymer flow via online observation with stereo vision microscopy. The results showed that the embossing temperature has a significant role in the replication accuracy of the width and shape of the structures, followed by the embossing force and the embossing time.

Figure 2.15 depicts the theoretical pressure behaviour for circular cavities which are 100 µm in height and which have different diameters as a function of the embossing temperature (Worgull, 2009). Due to the viscoelastic behaviour of the polymer melt, the pressure reduction observed between different temperature settings does not evolve linearly with the increase in the structure diameter. A significant influence is exerted by the moulding temperature. In this example, an increase in temperature of about 20°C reduces the pressure needed for filling a cavity by about 50%. Hence, it is recommended to fill cavities, especially cavities with high aspect ratios, at a higher temperature, supported by low moulding velocities.

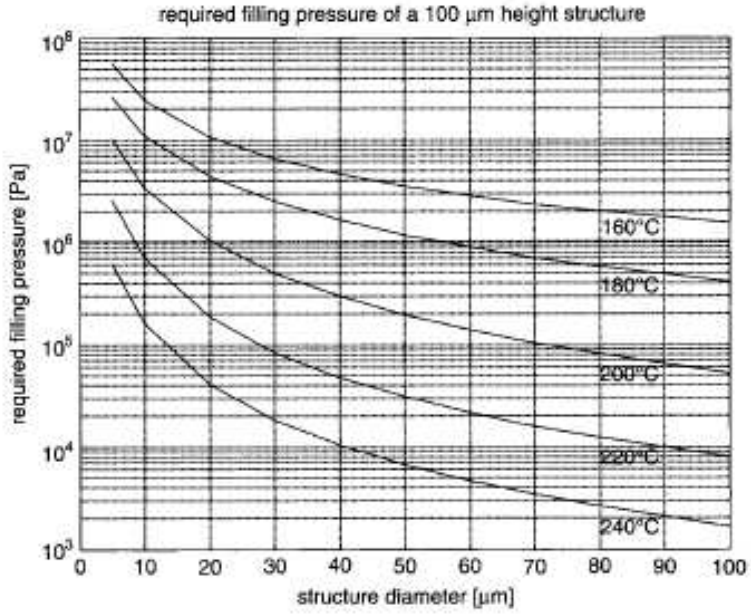

Figure 2.15 Estimated pressure drops in cavities as a function of embossing temperature for PMMA (Worgull, 2009).

During the moulding of a polymer above its glass transition temperature, the compression force induced by pressing the mould plate onto the polymer sheet causes a non uniform pressure distribution in the melt. It was reported that the typical pressure distribution is parabolic during embossing, with the maximum in the centre of the mould (He *et al.* 2007 and Lin *et al.* 2002). Such a pressure variation can lead to the non uniform filling of the structures and the bending of thin moulds. Thus, the knowledge of the pressure distribution during moulding can enable the estimation of the filling behaviour of microcavities.

The simulation of the pressure behaviour in hot embossing conducted by Worgull (2009) also showed that, during the velocity-controlled moulding stage, the pressure increases and reaches a maximum value at the end of this moulding step. After switching to the force-controlled moulding stage, the pressure gradient gradually decreases with time, as the moulded area become larger due to the creeping behaviour of the polymer under constant load. The pressure behaviour during the force-controlled moulding step is described in Figure 2.16. The simulation results presented show that a higher moulding velocity results in a higher pressure in the center of the mould at the end of the velocity-controlled moulding step (i.e at $t=0$). After a holding time of 248 seconds, however, the pressure difference between both profiles is minimal. Thus, the pressure profile at the end of the holding time can be considered independent of the moulding velocity.

In spite of the limited publications on the effect of the process factors on cavity pressure during HE, the review of related studies suggest that polymer pressure within mould cavities is one of the critical parameter that can provide some insight

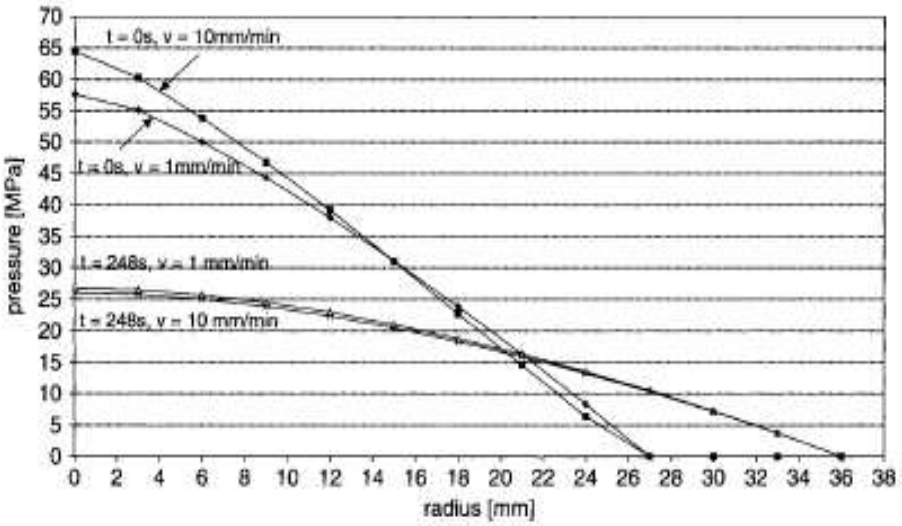

Figure 2.12 Characteristic pressure profile of a circular disk during the force-controlled moulding stage (Worgull, 2009).

into the process at different embossing conditions. Unfortunately, studies aiming at analysing the relationship between pressure in mould cavities and the HE process parameters are scarce. For this reason, one of the objectives of this research is to understand and systematically analyse such relationship using a specific condition monitoring set-up for measuring cavity pressure during HE.

2.5 Demoulding

2.5.1 Factors affecting the demoulding force

A comprehensive understanding of the mechanisms involved in the demoulding of polymer parts is a complex task as several factors of different nature influence this process. More specifically, the required separation force is dependent on chemical, physical and mechanical interactions between replicas and plates as illustrated in Figure 2.17.

The physical and chemical interactions are responsible for the adhesion of replicas to the plates. In particular, adhesion is the result of molecular attraction that holds the surfaces of two dissimilar substances together (Gerberich and Cordill, 2006). Chemical interactions comprise covalent bonds, ionic or electrostatic bonds, and metallic bonds. Physical interactions include hydrogen and van der Waals bonds as a result of intermolecular forces. Hydrogen and van der Waals bonds are much weaker than the chemical interactions as they do not involve electron exchange. Van der Waals forces are always present when two asperities are in close proximity.

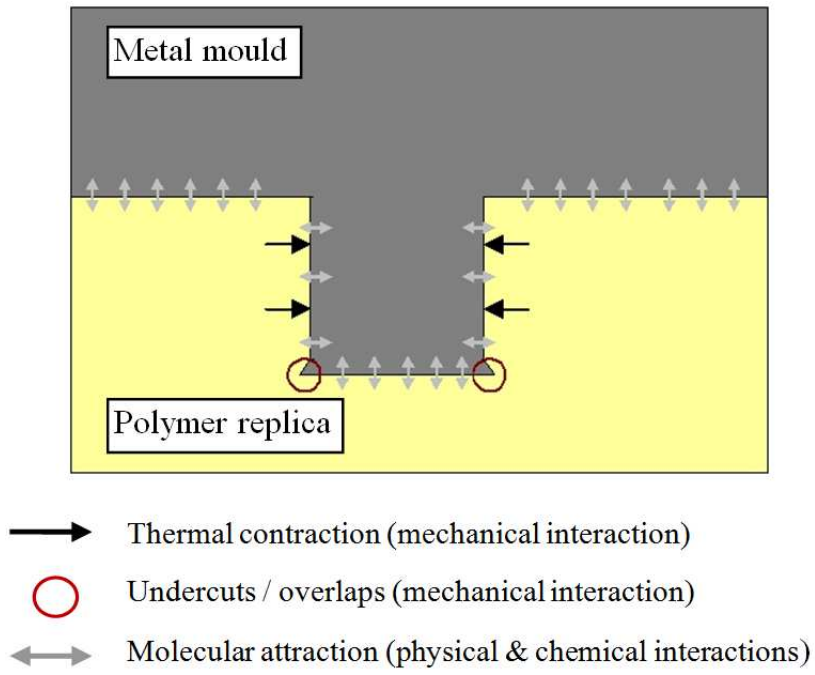

Figure 2.17 Schematic of mechanisms affecting demoulding.

Metals, which have relatively little attraction for their valence electrons, tend to form ionic bonds when they interact with non-metals. If a polymer is brought into contact with a metal, there is a large separation of charge at the interface. This results in an electrostatic attraction between them in addition to the van der Waals interaction (Bhushan, 2003). Moreover, adhesion affects friction forces; the so-called adhesive friction is the effort required to break the cold-welded junctions between asperity pairs on contiguous surfaces (Prokopovich *et al.* 2010).

As illustrated in Figure 2.18, it was observed by Dirckx *et al.* (2011) that a decrease of the demoulding temperature reduces the contribution of the adhesion force significantly until a point where the demoulding force becomes dominated by friction. Other studies also showed that mould and polymer materials have an effect on the adhesion phenomena (Guo *et al.* 2007a and 2007b; Saha *et al*. 2010; Jaszewski *et al*. 1999 and Park *et al.* 2004). For instance, the application of coatings on the mould surface can improve the demoulding in HE as it reduces the influence of the chemical and physical interactions.

The contribution of mechanical interactions to the demoulding force manifests itself on the sidewalls of the mould structures and it is a consequence of (1) friction and (2) interlocking of undercut features which can result from the roughness of the surface structures. This interaction is measured by the coefficient of friction which is the ratio of the friction force to the normal force acting on the contact area. In the case of HE, the normal force is caused by the difference in the shrinkage between the mould and the polymer material. In particular, as polymers have higher shrinkage rates than metals, this leads to a high contact stress between the mould and the

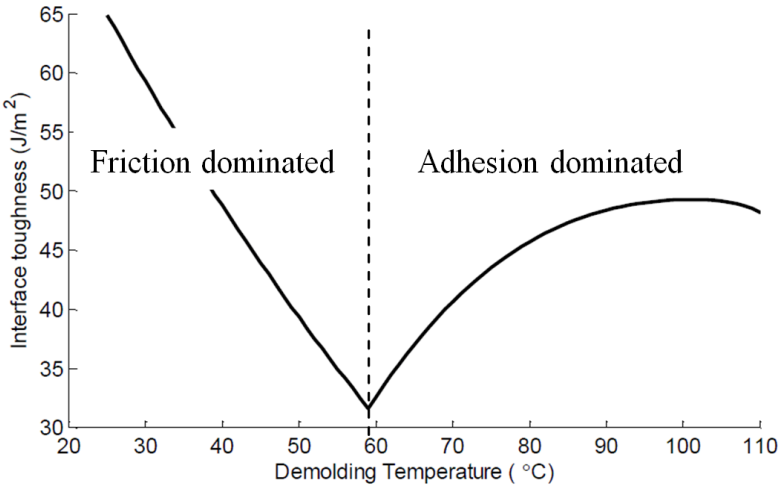

Figure 2.18 Combined effects of friction and adhesion on the required demoulding force for a given poly(methyl methacrylate) (PMMA) replica as a function of the demoulding temperature. Adapted from Dirckx (2010).

polymer on the sidewalls of the structures to be replicated (Dirckx *et al.* 2007; Guo *et al*. 2007c and Titomanlio and Jansen, 1996). Previous studies also suggested that undercuts or overlaps could restrain the material into the mould and cause further deformations or failures during demoulding. For example, investigations conducted by Pham and Colton (2002) and Delaney *et al*. (2010) showed that, for moulds with features fabricated by stereolithography or turning, the resulting surface roughness on the sidewalls of these structures increases the demoulding force as the generated surface asperities act as undercuts. It was also observed that moulds with structures that incorporate a draft angle such as silicon moulds produced by potassium hydroxide (KOH) etching could be demoulded more easily (Esch *et al.* 2003). This further suggests that the influence of such mechanical interactions should not be neglected during the demoulding process.

Reported experimental studies on demoulding in hot embossing refer to qualitative (Dirckx *et al.* 2007 and Hirai *et al.* 2003) and quantitative (Trabadelo *et al.* 2008 and Park *et al.* 2009) evaluations of the effect of the demoulding temperature or that of including additional mould structures. These studies generally reveal that the demoulding force initially decreases with the reduction of the demoulding temperature and then, when a given minimum value is reached, it starts increasing as the temperature is further decreased. However, limited demoulding temperature ranges are commonly considered and only a single type of HE mould design is generally tested in such studies. In one particular paper, Worgull *et al.* (2008a) described a specialised test apparatus used to characterize the friction between embossed polymers and mould materials. It was reported that variations of embossing temperatures and pressures influenced the static friction coefficient, while the

dynamic friction coefficient was affected by the mould material and its surface roughness.

The majority of the theoretical investigations of the demoulding stage in hot embossing polymer microstructures includes finite element (FE) simulations of demoulding forces that consider the effects of thermal stresses and sidewall friction between the replica and the mould (He *et al.* 2005; Worgull *et al.* 2005; Worgull *et al.* 2008b; Song *et al.* 2008 and Hsueh *et al.* 2006). In particular, these simulations were used to study the effect of sidewall friction on the stresses in the parts and mould or on the demoulding forces. In addition to the thermal stress and the sidewall friction, Guo *et al.* (2007a) and Dirckx and Hardt (2011) considered the contribution of the adhesion force between the replica and the mould in creating their FE models. The latter authors also implemented a special test method that was similar to the cantilever beam fracture technique in order to study the effect of feature geometry and demoulding temperature on the demoulding toughness. Although, the replica-plate separation method studied was not representative of the typical demoulding technique used in commercial HE machines, it provides valuable information about adhesion and friction dominated demoulding phenomena. The developed FE models contribute to a better understanding of the demoulding process mechanisms in HE. However, there is still a need to develop more comprehensive simulation models for investigating the combined effects of material properties, demoulding temperatures, polymer pressure histories, locations and geometry of the mould structures and the adhesion on the demoulding forces.

2.5.2 Demoulding techniques

Various methods have been developed in order to separate the embossed polymer from the mould in HE. One of the most common demoulding methods can be found in commercially available hot embossing machines and it relies on a clamping technique (Trabadelo *et al*. 2008). This technique is illustrated in Figure 2.19. It uses demoulding clamps which are placed on the edge of the polymer material and fixed to the plate. As the top plate moves up, these clamps keep the embossed sample fixed to the bottom plate. The disadvantage of this technique is that when the mould is released the deformation of the polymer in the center of the sheet is larger than that at the periphery. This can result in distorted structures as shown in Figure 2.19b.

An automatic pneumatic demoulding device is an advanced system, which can be found in some commercial embossing machines (Figure 2.20). When compressed gas (such as nitrogen) is injected through the gas inlet, the mould and the polymer are pushed away from each other. In this case, because of the uniform pressure in the demoulding device chamber, distortions similar to those that can occur with the clamping technique will not happen. During demoulding, the adhesion between the mould and the polymer can be decreased when the gas molecules start occupying the space between the mould and the polymer.

Another demoulding system using strips was developed by Hardt *et al*. (2010) and it is depicted in Figure 2.21. In this system, the metal strips which are located on the edges of the mould push off the part to separate it from the mould surface when the embossing load is released and the top plate moves up.

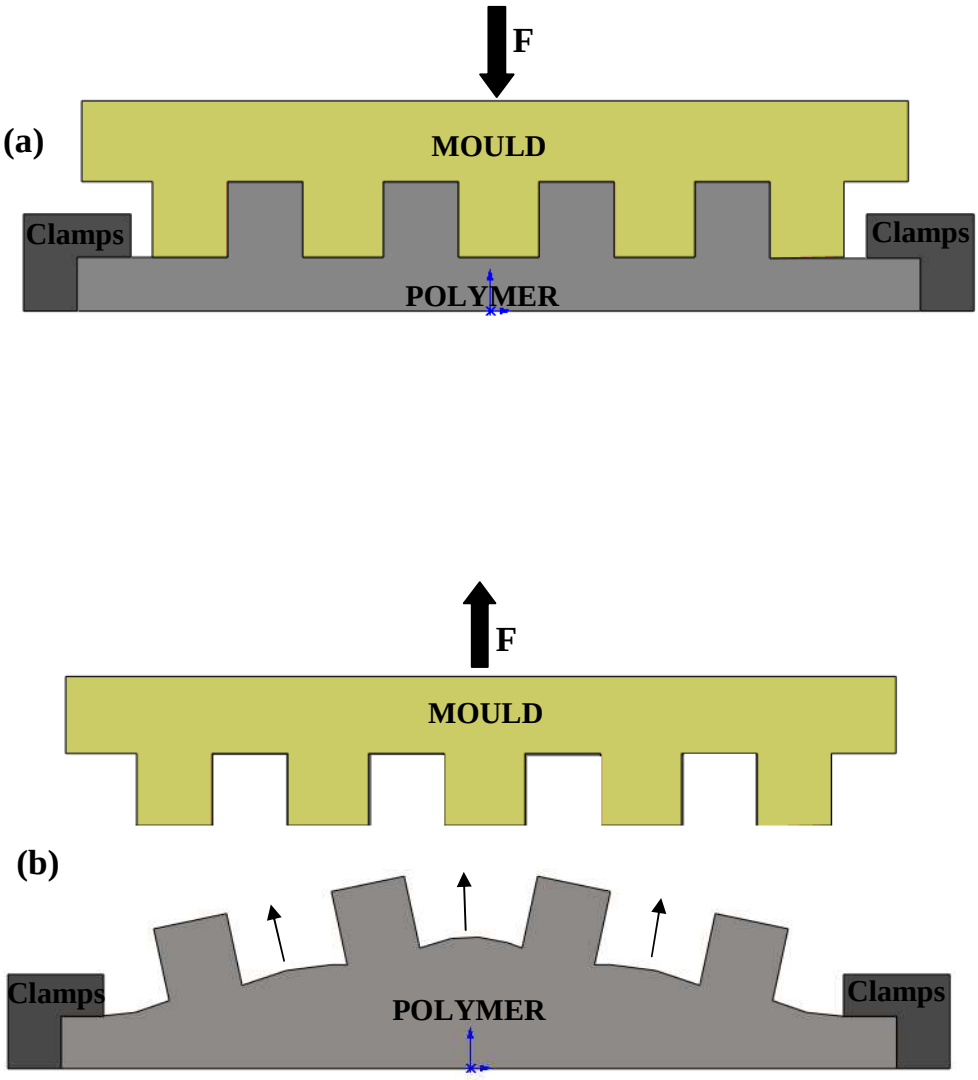

Figure 2.19 a) Moulding and b) demoulding by the clamping technique.

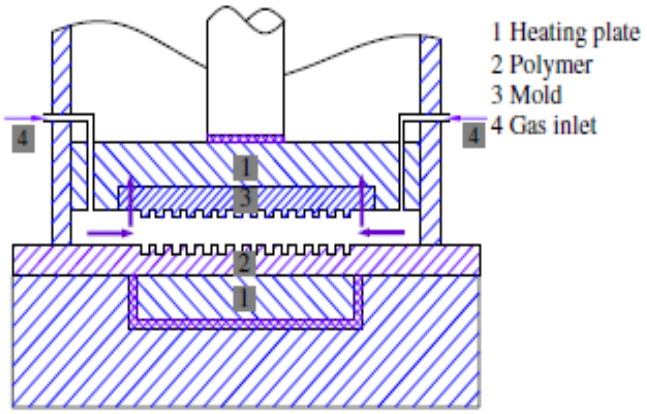

Figure 2.20 Demoulding via automatic pneumatic system (He *et al.* 2007).

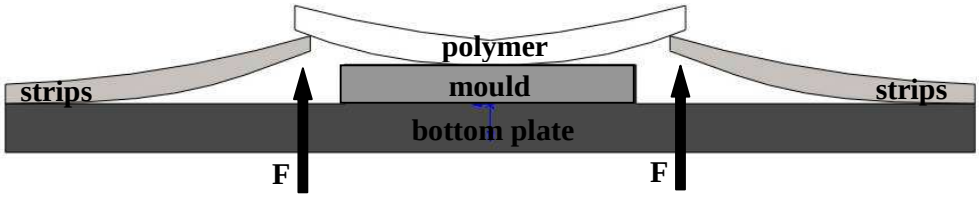

Figure 2.21 Demoulding using strips.

Ejector pins are well-established in the demoulding of macroscopic moulded parts, especially in the injection moulding process (Figure 2.22). This concept may be transferred to micro replication processes. Nevertheless, it has some limitations; for instance the thickness of the residual layer has to be large enough to transmit the ejection forces to avoid part breakage. Another undesirable situation can occur when the moulding area increases. In particular, if the ejector pins are located only on the edges of mould, bending during demoulding cannot be avoided and this can result in forces on the microstructures that are perpendicular to the demoulding direction.

A cantilever test method was developed by Dirckx (2010) in order to study the demoulding force in HE (see Figure 2.23). A demoulding bar which was placed on the end of the embossed part was used to separate it from the mould. The disadvantage of this technique is that the residual layer of the sample has to be thick enough for successful demoulding. Also, lifting the part from the side will bend the embossed replica and as a result will induce further forces on the walls of the structures.

A simple, but effective way for demoulding is to use a rough substrate plate. Such a plate with a rough surface having undercuts in the micro-nanometre range can be fabricated by sand blasting or lapping and will generate high adhesion force (Worgull, 2009). Thus, during isothermal demoulding where the top and bottom plate are set up at the same temperature, a high adhesion between the residual layer and the rough surface will occur. Typically, it is significantly higher than the demoulding forces required to separate the replica from the mould. Note that non-isothermal cooling could cause a warpage in the replica. Therefore it is commonly preferred to use isothermal conditions. This concept is recommended because of its simplicity and

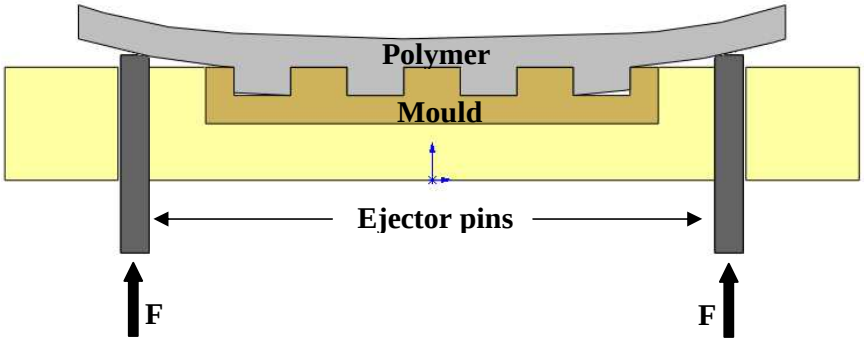

Figure 2.22 Demoulding with ejector pins.

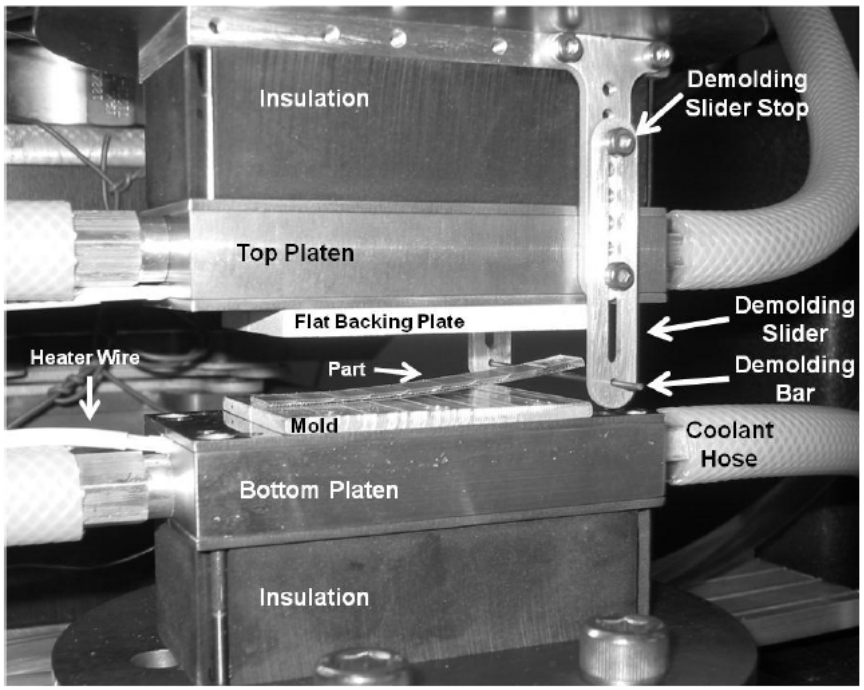

Figure 2.23 Demoulding with the cantilever method (Dirckx, 2010).

it is adopted for the present work. A minor limitation of this method is that adhesion decreases after a number of cycles and the substrate plate needs to be processed again. Additionally, it can be difficult to separate the part from the substrate plate depending on its roughness.

2.6 Factors affecting the residual layer uniformity

As mentioned previously due to the principle on which the process relies, hot embossed parts are characterised by the existence of a residual layer underneath the replicated structures. The residual layer is a carrier layer for the embossed structures and it can be also called a remaining layer. Figure 2.24 describes the residual layer for positive and negative structures. The next sections discuss the factors affecting the RLT.

2.6.1 Hot embossing machine

To achieve a high replication quality, stiff construction concepts for the axes and support elements of the HE machine have to be adopted. In particular, the stiffness of the construction should be large enough to prevent bending under embossing loads as elastic bending of the whole assembly may result in non-uniform embossed parts. In typical implementations of the process, the mould and the polymer are pressed against each other as a result of the relative vertical motion of the hot plates of the machine (see Figure 2.25).

(a) Positive structures (b) Negative structures

Figure 2.24 Schematic view of residual layer.

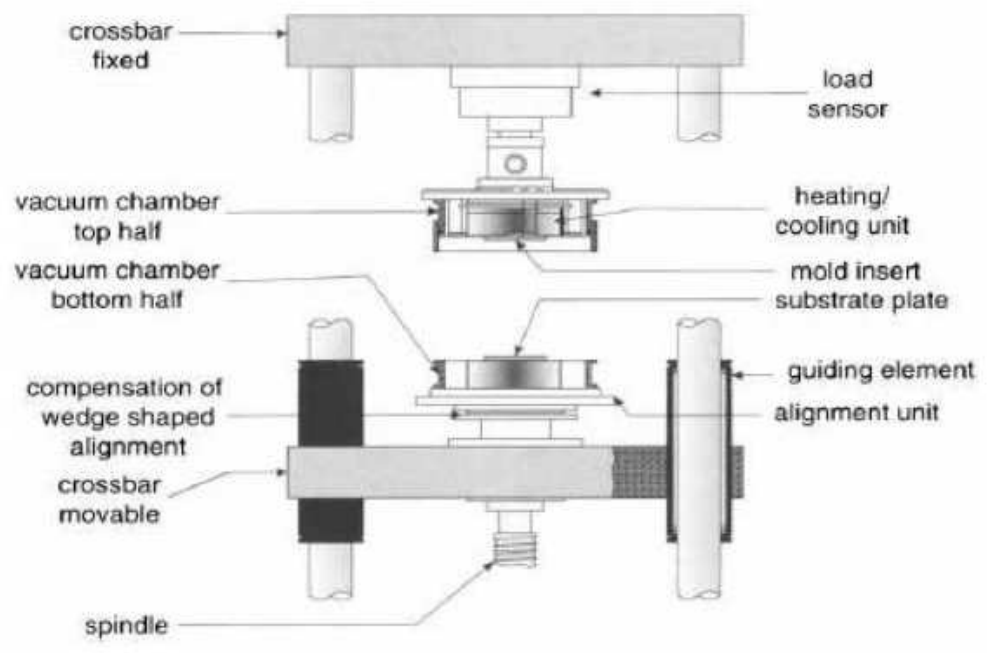

Figure 2.25 Schematic view of the main elements of a typical hot embossing machine (Worgull, 2009).

When manufacturing and assembling the plates and mould inserts, their roughness and flatness deviation should be minimised as these will be a source of RLT non-uniformity as illustrated in Figure 2.26a and 2.26b. Using grinding and lapping, the possible achievable roughness and flatness of the plates and the back side of the mould can be as low as 10 nm Ra and 500 nm respectively, depending on the processed thickness, surface area and material (McGeough, 2002). Another challenge is to achieve a high degree of parallelism between both plates as this will not only increase the non-uniformity of the residual layer but also, it could generate high pressure in small areas causing damages to the mould or the substrate (see Figure 2.26c). With some commercial hot embossing machines, it is possible to compensate the non-parallelism of the plates or the mould through the motion of two wedge-shaped disks that can be rotated relative to each other.

To improve the uniformity of the RLT, Chang and Yang (2003) conducted gas-assisted hot embossing where a polymer film is pressed against the mould by gas pressure rather than a solid plate, and reported that this technique significantly improved the uniformity of the applied pressure. Hocheng and Wen (2008) investigated a similar gas-assisted hot embossing set-up although it is questionable whether the reported results provide a suitable comparison between both traditional and gas-assisted hot embossing given that a clear gradient in one direction for the pressure distribution was observed for the solid plate set-up as shown in Figure 2.27a.

The major limitation of the investigations reported in these studies is that manual demoulding is required. A similar technique called the “air cushion press” has been implemented for thermal NIL where a gas (or fluid) is utilised when pressing

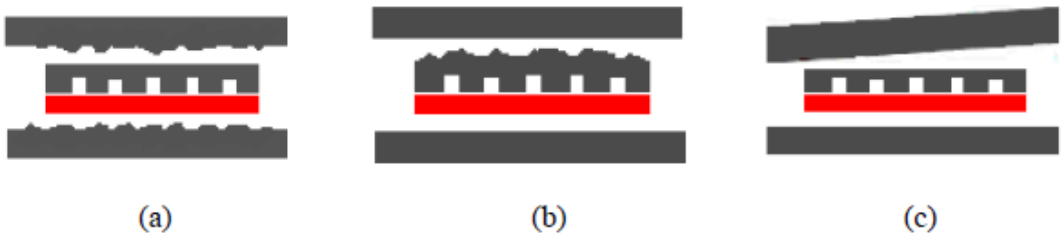

Figure 2.26 Schematics of possible issues affecting the parallelism of the hot plates: (a) imperfect plate surface; (b) uneven mould backside; (c) non-parallel plates.

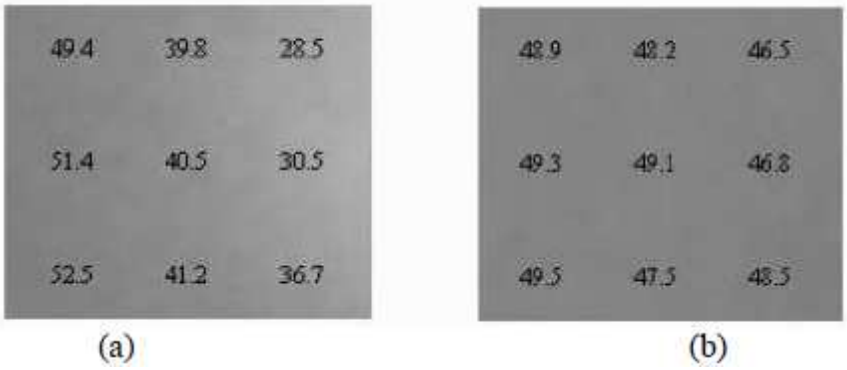

Figure 2.27 Pressure distributions in (a) solid plate embossing and (b) gas assisted embossing (kgf/cm2) (Hocheng and Wen, 2008).

both the mould and the substrate against each other. In particular, Gao *et al.* (2006) reported that this method leads to a more uniform pressure distribution over large mould areas. A possible drawback of gas or fluid assisted imprinting however is the bending of very thin moulds or stamps during the embossing step due to the uneven pressure distribution that can be generated by the polymer flow under compression. This bending is negligible when the mould or stamp is fully supported by thick plates which are a typical HE set-up.

Variations in the processing temperature directly impact on the polymer behaviour. Thus, ensuring a homogenous temperature distribution in the mould and substrate plate is also essential for successful replications, especially when large micro structured areas are processed. Hence, the heating system of the machine has to guarantee a homogenous and stable moulding and demoulding temperature over the replicated area. In particular, during heating, an inhomogeneous temperature distribution will lead to variations in the polymer viscosity which may result in a non-uniform melt flow into the cavities to be filled. In turn, this may induce variations in the thickness of the residual layer. During cooling, a uniform temperature distribution should also be ensured to prevent anisotropic shrinkage and inhomogeneous solidification of the polymer.

2.6.2 Mould insert and polymer material

During HE, the mould is subjected to mechanical stress in structured and non structured areas. This stress is a function of the mould design, the applied force on the backside of the mould and the opposing forces due to the viscoelastic

behaviour of polymers. This stress can result in undesirable deformations across the mould which will contribute to the non-uniformity of the residual layer. In addition, gaps left between the mould insert and the master plate during their integration can also contribute to the bending of the mould under load, which will result in a gradient in the RLT. Reported studies for thermal NIL provide experimental evidence that the density of the structures to be replicated also has an important influence on the residual layer uniformity (Lazzarino *et al.* 2004 and Sirotkin *et al.* 2007). In particular, the mould deformation was observed to be higher in areas where structures are denser as a result of higher opposite forces generated by the polymer melt. It was also reported that the RLT decreases towards the edges of the mould due to the abrupt decrease in structure density. In particular, mould deformation in such areas can be significant and lead to damaging thin structures at the periphery of the mould as demonstrated in Lazzarino *et al.* (2004). The importance of the mould thickness on the RLT was also investigated in the case of thermal NIL by Merino *et al.* (2008). These authors studied the influence of the thickness of silicon and nickel moulds, the filling factors and the patterned area sizes on the residual layer homogeneity. The imprinted parts were scratched using a mechanical profiler to measure the RLT. It was concluded that the thickness of Si moulds had an important influence on the RLT, while this effect was not so pronounced in the case of Ni. In addition, a larger bending was experienced by the thinner 400 µm thick Si mould utilised, which resulted in an increased flow of polymer to the non patterned area.

During the moulding of a polymer above its glass transition temperature, the compression force induced by pressing the mould plate onto the polymer sheet causes a non uniform pressure distribution in the melt. It was reported that the typical

pressure distribution is parabolic during embossing, with the maximum in the centre of the mould (He *et al.* 2008). Such a pressure variation can lead to the bending of thin moulds. However, this bending could be negligible if the mould is supported by a rigid plate as this is the case in commonly found HE implementations and thus, only localised mould deflections could be an issue. Once the polymer reaches its demoulding temperature, the mould plate is lifted up. Following this unloading, the polymer will expand to some extend due to its elastic behaviour (Worgull, 2009 and Schan *et al.* 2008). Polymer elastic or compression modulus at demoulding temperature may have an influence on the RLT uniformity. More specifically, a higher moulding pressure applied in the central area of the mould will induce larger changes in polymer expansion after the release of the embossing force compared to areas at the edges. The polymer macromolecular arrangement also has an effect on the uniformity of the residual layer as amorphous polymers are typically characterized by isotropic shrinkage, while semicrystalline polymers exhibit anisotropic behaviour. Non-uniform shrinkage over the whole moulded part will result in a non-uniform residual layer distribution (Lin *et al.* 2003).

Worgull (2009) presented a method relying on integrating additional structures in the margin region of the substrate plate or the mould as shown in Figure 2.28 in order to improve the homogeneity of the pressure distribution during moulding and thus, the uniformity of the RLT. The additional role of these structures was to absorb the majority of the stress and thus to protect the main features on the mould.

It can be said that in order to achieve a high level of RLT uniformity, different factors linked to the machine, the mould design and the process parameters should be

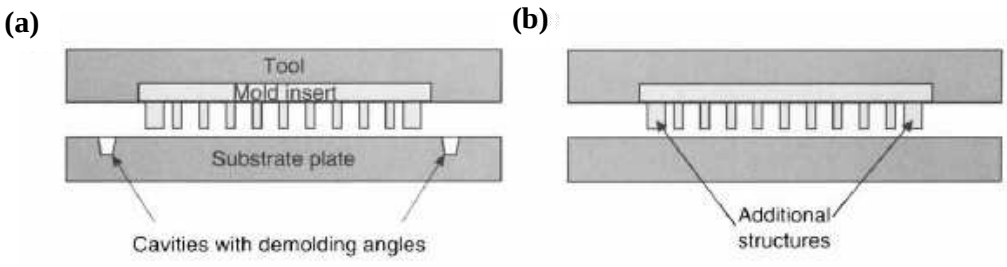

Figure 2.28 Additional structures for preventing the formation high contact stress at the boundary of the mould. (a) Circular cavities in the substrate plate; (b) circular structures in the mould insert (Worgull, 2009).

considered. Previous studies that investigated the homogeneity of the RLT mostly focused on the influence of factors linked to the hot embossing machine, the mould design and the polymer processed. None of the reported investigations studied whether the process parameters also had an effect on the RLT uniformity by employing a systematic design of experiments approach. Thus, one of the objectives of this research is to study the influence of process parameters on the RLT uniformity achieved with hot embossing.

2.7 Summary

This chapter reported a number of research studies in hot embossing. Although, the process cycle time is longer than most of other replication techniques, HE is characterised by the ability of producing high quality micro and nano structures over large areas. It can be seen from the conducted literature review that there is still a need for further improvement of the quality of embossed parts for different conditions, mould designs and materials, through scientific investigations and systematic analysis of the process. Particularly, although it has been revealed that process parameters have a significant effect on the quality of the moulded parts, a detailed study of their influences on the cavity pressure, demoulding force and uniformity of the residual layer for different materials is still required. As highlighted in this chapter, low cavity pressure could cause incomplete cavity filling, high demoulding forces could damage or separate the replicated structures and non-uniform residual layer could be problematic for final applications. Thus, such knowledge gaps are the focus of the remaining chapters of this thesis.

CHAPTER 3

Process Factors Influence on Cavity Pressure Behaviour in Hot Embossing

3.1 Overview

The measurement of the evolution of the pressure on the polymer front within mould cavities during HE can provide valuable information about the process dynamics and also about the cavity filling behaviour of different polymers. This can be achieved through the online monitoring of cavity pressure exerted by the polymer during embossing for different settings of process factors. As highlighted in Chapter 2, in spite of the limited number of publications in this particular area of HE research, it is suggested that pressure is one of the critical parameters to determine the outcome of the process for different embossing conditions. Therefore, it is very important to capture and analyse systematically the relationship between pressure in the mould cavities and the HE process parameters. In this context, this chapter presents an experimental study on the influence of three process parameters, namely the moulding temperature, the embossing force and the holding time, on the pressure in cavities located in the centre and the edge of a HE master when processing 2 mm thick PMMA and ABS sheets.

The chapter is organised as follows. The next section describes the experimental set-up used which includes the HE machine employed, the test mould and materials along with the condition monitoring technique adopted to investigate the effects of the process parameters on cavity pressure. Next, the conducted design of experiments is presented together with the approach utilised to estimate the minimum embossing force and pressure for performing the trials. Finally, the experimental results are reported and the effects of the different parameters are investigated.

3.2 Experimental set-up

3.2.1 Hot embossing machine

In this study, the experiments were conducted with the HEX03 machine from Jenoptik Mikrotechnik (Figure 3.1). Table 3.1 provides the technical specifications of this system as given by the manufacturer (Jenoptik Mikrotechnik 2002). Grinding and lapping was performed on the aluminium top plate and brass bottom plate prior to mounting them on the machine and through these process steps, the achieved values of roughness and flatness of the plates used were 0.5 µm Ra and 4 µm, respectively. PT100 temperature sensors were installed by the machine manufacturer, 7 mm and 20 mm behind the bottom and top plates' surfaces, respectively. In addition, five heating cartridges are installed to raise the temperature of the plates. It is generally suggested in the literature to bring the mould and polymer in contact with each other while heating by applying low pressure in order to increase the heat transfer rate. Oil is used to flow through the bottom and top plates during the cooling process. Data from the temperature, force and distance sensors are collected every second.

Figure 3.1 HEX03 Jenoptik Mikrotechnik.

Table 3.1 Technical data of the HEX03 Jenoptik hot embossing machine

Properties	Values
Press force, adjustable (kN)	200, 250
Press force, increment (N)	10
Temperature inside chamber (°C)	320, 500
Moulding velocities (mm/min)	0.01-600
Maximum substrate size (diameter, mm)	180
Maximum embossing area (diameter, mm)	150
Overlay accuracy alignment (µm)	2
Power consumption (kW)	16.5
Total weight (± 10%) (kg)	1.700

3.2.2 Mould design and manufacturing

A 4 mm thick brass mould with overall lateral dimensions of 40 mm x 40 mm was used. The structured area of this mould consisted of 11 channels, each of which with a depth of 600 µm and a width of 2.55 mm. Two pin holes, 2 mm in diameter, were also drilled in the middle and the edge of the mould, as shown in Figure 3.2, in order to insert pressure sensors and thus, to measure the pressure in these two locations. The fabrication of the mould structures was carried out with micro wire electro-discharge machining process by employing an Agiecut Vertex machine.

3.2.3 Test materials

Two millimetres thick injection moulded PMMA and acrylonitrile butadiene styrene (ABS) with lateral dimensions of 50 mm x 50 mm sheets were used for the experiments. PMMA and ABS are amorphous polymers and common choices for HE operations (Ng *et al.* 2006b; Toh *et al.* 2009; Ramani and Yao, 2009 and Malek *et al.* 2008). PMMA is one of the hardest polymers, glass clear with glossy finish and has good weather resistance. ABS has good impact resistance and toughness. They are both found in many applications such as in optics, automotive, electrical engineering, medicine and office equipment. The mechanical properties of PMMA and ABS are shown in Table 3.2 (Matbase, 2012).

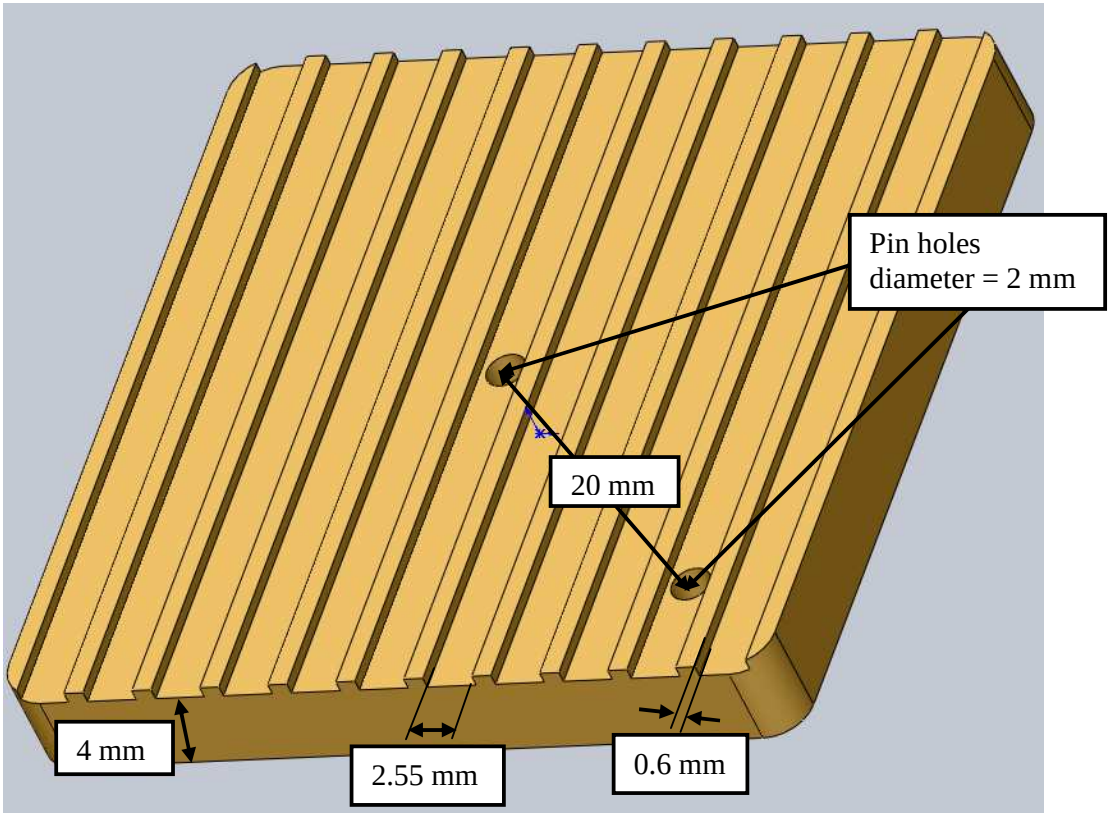

Figure 3.2 Mould design.

Table 3.2 Mechanical properties of PMMA and ABS

Properties	Values	
	PMMA	**ABS**
Tensile strength (MPa)	48 - 76	41 - 60
Young modulus (MPa)	1800 - 3100	2275 - 2900
Elongation at break (%)	< 10	< 25
Compressive strength (MPa)	83 - 124	60 - 86
Fatigue (MPa)	11 - 12	12 - 22
Impact strength (J/cm)	0.16 - 0.27	0.56 - 2.2
Glass transition temperature (^{0}C)	105	105
Coefficient of thermal expansion (/^{0}C)	5 - 10 x 10^{-5}	5 – 8.5 x 10^{-5}
Water absorption (%)	0.1 - 0.5	0.2 – 0.4
Transparency	Transparent	Transparent

3.2.4 Condition monitoring and cavity pressure behaviour

Condition monitoring techniques can be employed to quantify the pressure inside the mould during HE and thus, to indentify the correlation between the resulting pressure and the process parameters. In this study, an indirect measurement method was conducted to assess pressure variations in the selected cavity areas. In particular, two Kistler 9211b miniature piezoelectric force transducers were used in order to evaluate the pressure variations in cavities located in the middle and the edge of the mould. The upper working range of the Kistler sensors used was 3000 bar and 200^0C while their sensitivity was -4.4 pC/N.

The data acquisition was performed with a Kistler CoMo Injection Type 2869B system and the analysis of the sensor output signals was conducted by employing its online software (see Figure 3.3). The default set-up on the HEX03 machine was modified to accommodate an ejector assembly system previously used in a micro injection moulding machine and which enabled the integration of the condition monitoring system. This ejector assembly was mounted to the bottom plate of the hot embossing machine. Two pockets were milled in the ejector plate to accommodate the force transducers, which were located behind the 5 mm pins (see Figure 3.4). When the transducer is subjected to a mechanical load, the charge signal produced by the force sensor is converted into a proportional output voltage in a charge amplifier or a monitor.

The embossing cycle can be split into three consecutive stages: filling, holding, and cooling. During the polymer filling stage, the cavity pressure rises as a

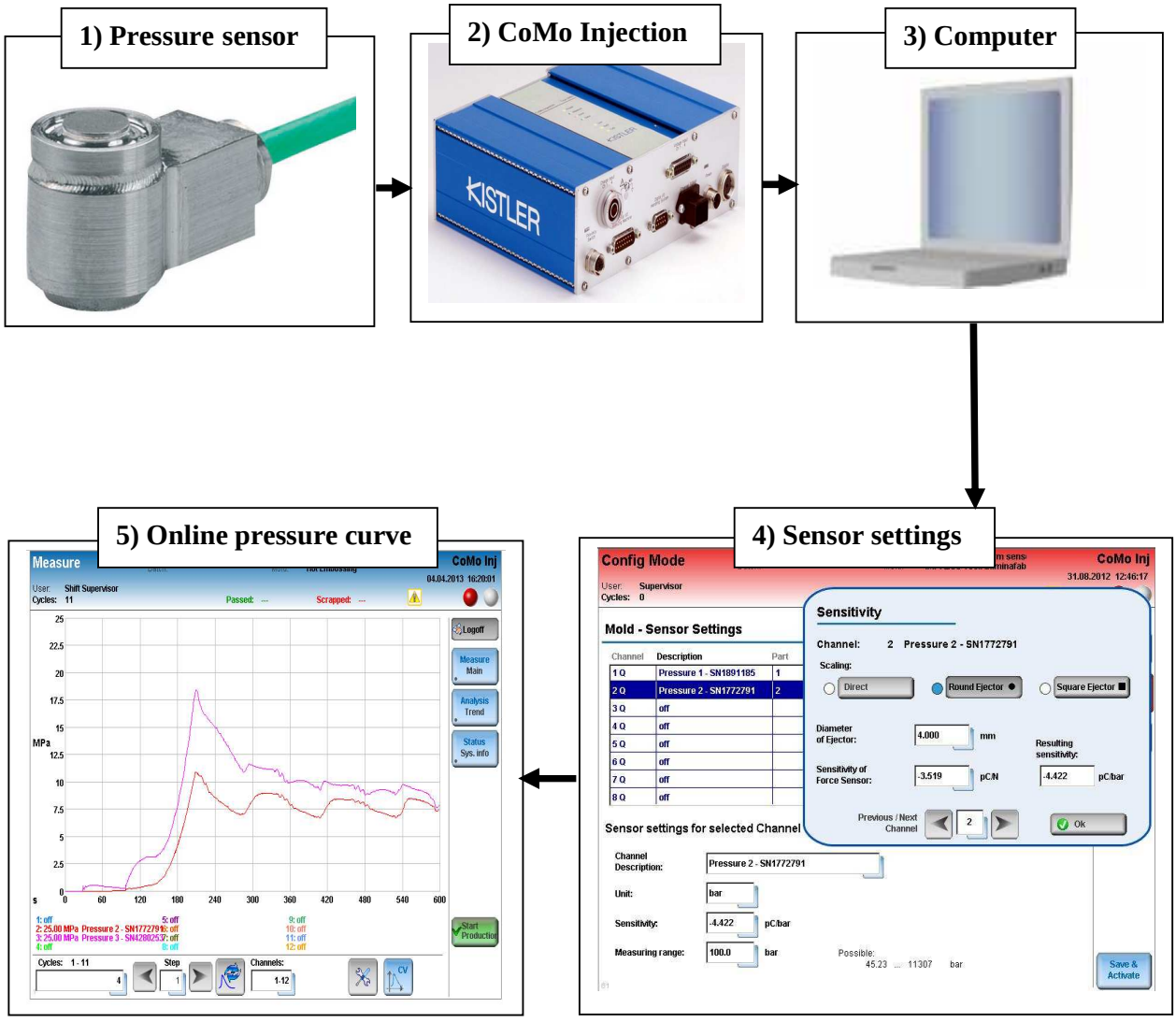

Figure 3.3 Schematic diagram of measurement system.

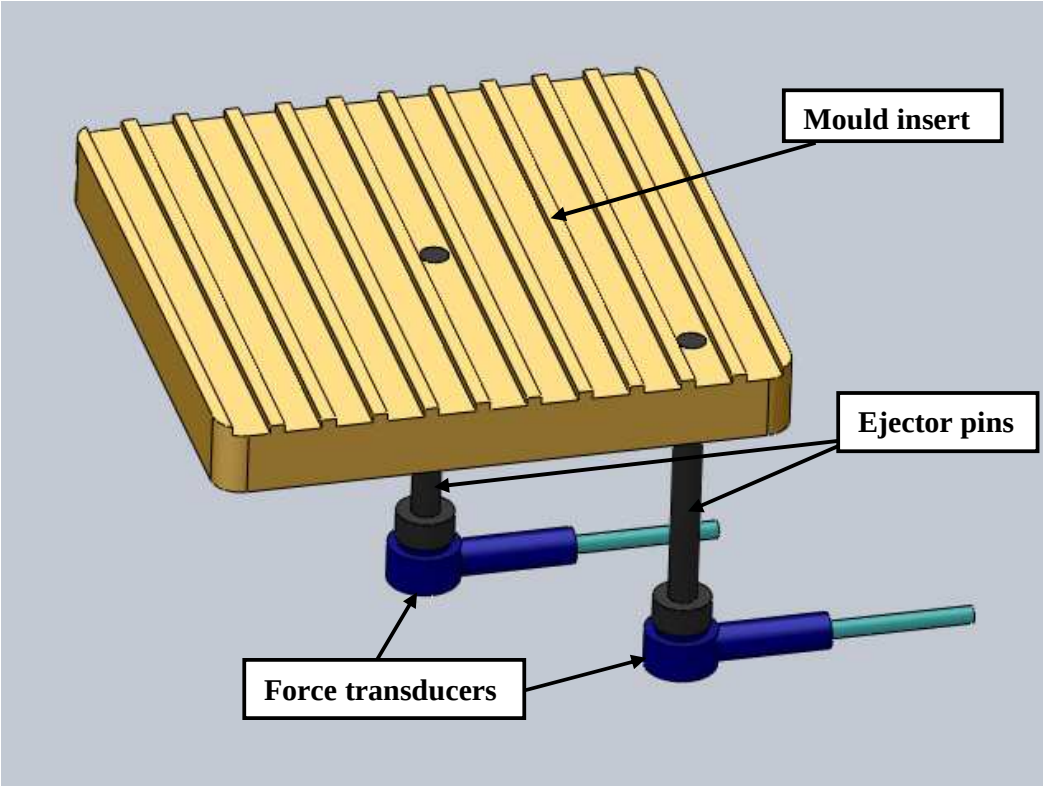

Figure 3.4 Design for indirect measurement of pressure

result of the applied compression force until it reaches a maximum value (P_{max}). Then, during the second stage, holding, initially P drops rapidly and then it decreases slowly due to the creeping behaviour of the melt under a constant load. Finally, the pressure reduction continues during the cooling stage until the end of the cycle. A typical pressure curve measured during HE is reported in Figure 3.5. It particular, the following pressure evolution can be observed along different stages:

- The start of the embossing cycle.
- Pressure occurring in the cavity due to the contact force.
- A sharp increase in pressure until it reaches to P_{max} during the velocity controlled moulding.
- A rapid drop in P due to polymer creeping during the force-controlled moulding stage.
- A slower reduction of P during the cooling stage.
- An eventual drop to atmospheric pressure due to the tool opening and part removal.

The investigation reported in this chapter focuses on the cavity pressure behaviour during the filling and holding stage of the hot embossing process. The process parameters influence on the cavity pressure during these two stages was quantified by using the above mentioned condition monitoring system.

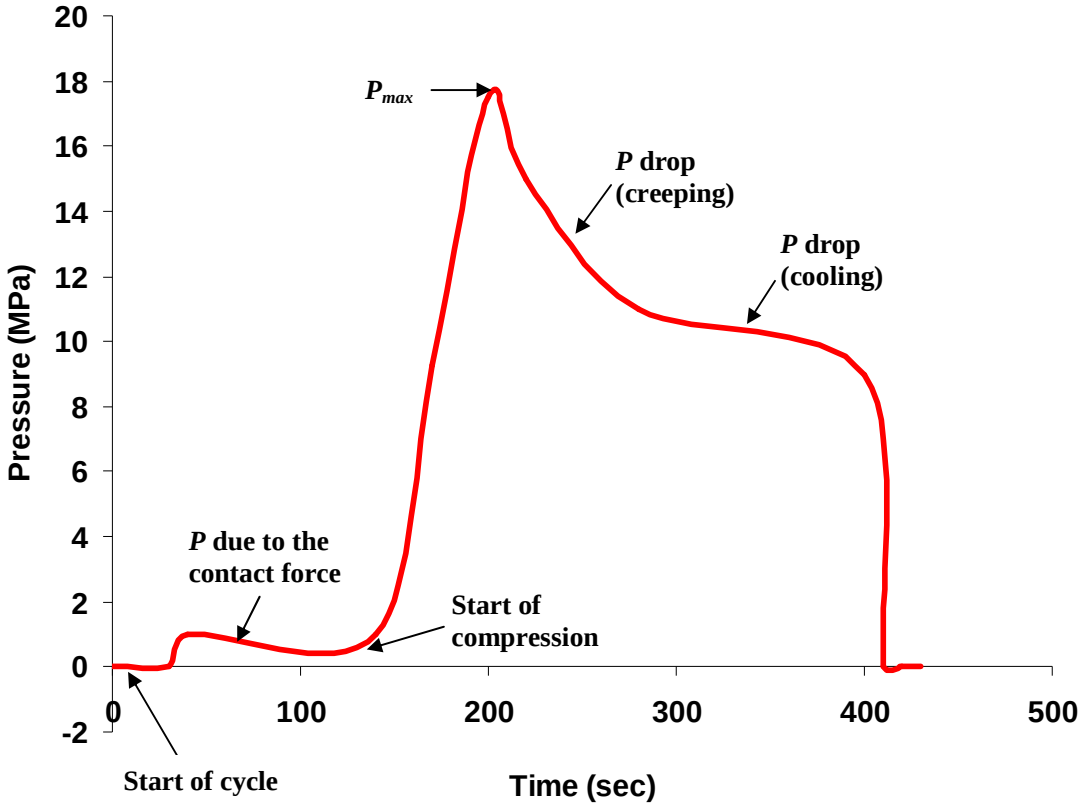

Figure 3.5 Typical cavity pressure evolution.

3.2.5 Planning of experiments

As mentioned in Chapter 2, the controllable process parameters in hot embossing are: the embossing temperature (T_m), the demoulding temperature (T_d), the embossing force (F), the holding time (t_h), the embossing velocity (V_m) and the demoulding velocity (V_d). This study focuses on the filling and holding stage where T_m, F, t_h and V_m can be varied and could affect the quality of the replicated structures. However, hot embossing is characterized by low flow velocities and short flow distances, which results in low shear stress in the replica and thus, it is well suited for applications where parts with low residual stress are required. For this reason, it is recommended to use low moulding velocities. Accordingly, V_m and V_d were fixed at the constant value of 1 $mm.min^{-1}$. In addition, the embossed parts were demoulded at 80^oC degrees in all experimental trials. Thus, the variable parameters considered in this study were the moulding temperature (T_m), the embossing force (F) and the holding time (t_h).

A comprehensive approach to condition monitoring was implemented by conducting a design of experiment (DOE) study. In this way, all investigated process parameters could be considered simultaneously, and their main effects analysed. This enables the systematic investigation of process related variables that influence the product and/or process quality. In particular, process conditions that affect the quality and cost of a replicated product should be identified in order to improve the production performance and throughput (Whiteside *et al.* 2005). Factorial design is commonly used for experiments involving a number of input factors for the purpose of studying the factors' effects on various responses. Two different approaches can be

distinguished when implementing DOE studies (Park and Ahn, 2004). More specifically, full-factorial design is widely used when it is required to conduct a comprehensive investigation of the joint effects of several factors on a response, and fractional factorial design is employed to reduce the experimental cost of large DOE studies and as a result, it is suitable for initial screening purposes.

In this research, a full-factorial design was applied for each investigated polymer material with the addition of a middle level. More specifically, two levels per factors were considered in the full factorial design and an addition middle level was included for which the value of each parameter was set between the values selected in the full factorial design. Thus, three levels were used for each of the selected three factors and 9 trials were designed. Table 3.3 shows the values adopted in this 2 level full factorial and middle level approach for the replication of PMMA and ABS. The chosen range of parameters levels was determined based on material properties, literature data (Ng *et al*. 2006a; Scheer and Schulz 2001; Schelb *et al*. 2011 and Luo *et al.* 2006), theoretical calculations described in the next section and preliminary experiments in order to ensure complete filling of the mould cavities and stable behaviour of the replication set-up throughout the experiments. The glass transition temperature of both materials is approximately 105 ^{o}C. Thus, T_g +15 ^{o}C = 120 ^{o}C was selected as the minimum embossing temperature for ABS and PMMA in order for the polymers to be in viscoelastic state. In addition, using theoretical calculations and initial experiments it was found that 10 kN was enough to make the polymers at this temperature fill the structures at zero holding time. Zero holding time corresponds to the end of the velocity-controlled moulding stage where the highest value of force and pressure are reached. The highest settings of the experiments, i.e. 180 ^{o}C, 40 kN and 5

Table 3.3 Process parameters design

Trial	T_m **(°C)**		F **(kN)**		t_h **(min)**	
N	***Level***	***value***	***Level***	***Value***	***Level***	***Value***
1	A1	120	B1	10	C1	0
2	A3	180	B1	10	C1	0
3	A1	120	B3	40	C1	0
4	A3	180	B3	40	C1	0
5	A1	120	B1	10	C3	5
6	A3	180	B1	10	C3	5
7	A1	120	B3	40	C3	5
8	A3	180	B3	40	C3	5
9	A2	150	B2	25	C2	2.5

mins. were chosen considering the fact that preliminary trials showed the filling of undesirable structures outside the mould insert. A further side effect could be that above these maximum levels, mould insert structures and plates can be deformed. For each of the designed trials, three repetitions were performed. The response variables considered were the pressure in the center (P_c) and in the edge (P_e) of the mould and their difference $\Delta P=P_c-P_e$. In addition, the minimum embossing force required to fill the cavities was calculated using a mathematical model, which is described in the next section.

3.2.6 Minimum required embossing force

This section focuses on calculating the minimum embossing force necessary for filling all the mould structures in order to feed the design of experiments. This is achieved by finding the theoretical minimum required pressure to fill the cavities. As it is discussed in Chapter 2, during the moulding of a polymer above its glass transition temperature, the compression force induced by pressing the mould plate onto the polymer sheet causes a non uniform pressure distribution in the melt. It is reported that this distribution is parabolic with the maximum pressure being generated in the centre of the mould. If insufficient embossing force is applied, non-uniform filling of the structures can occur. Therefore, it is important to describe a model for predicting the minimum required force that takes into account pressure distribution.

The polymer flow is analysed as being produced by the pressure difference in the radial direction of a disc material. It is assumed that no slip occurs between the mould insert and the polymer; the melt is incompressible and behaves like a

Newtonian fluid; the flow is steady and laminar. The analysed element is a portion of a cylinder of elementary thickness, *dr*, and height, *dz*, at some radius, *r*, from the center as shown in Figure 3.6. Based on Lin *et al.*'s (2003) work balancing the forces in the radial direction gives:

$$Pr\,d\theta dz - (P + dP)(r + dr)d\theta dz + 2P' drdz\,sin\left(\frac{d\theta}{2}\right) + \tau r d\theta dr - (\tau + d\tau)r d\theta dr = 0 \quad (3.1)$$

Where P and τ are pressure and shear stress, respectively. Here,

$$P' = P + \frac{dP}{2} \quad (3.2)$$

Simplifying equation (3.1) by approximating $\sin(d\theta/2)$ with $d\theta/2$ and neglecting higher order terms, it becomes:

$$-dPdz = d\tau dr \quad (3.3)$$

The viscous behaviour of the polymer material is assumed to correspond to that of a Newtonian fluid:

$$\tau = \eta\dot{\gamma} = \eta\left(-\frac{dv_r}{dz}\right) \quad (3.4)$$

where η is the viscosity, $\dot{\gamma}$ is the shear strain rate and v_r is the flow velocity in the

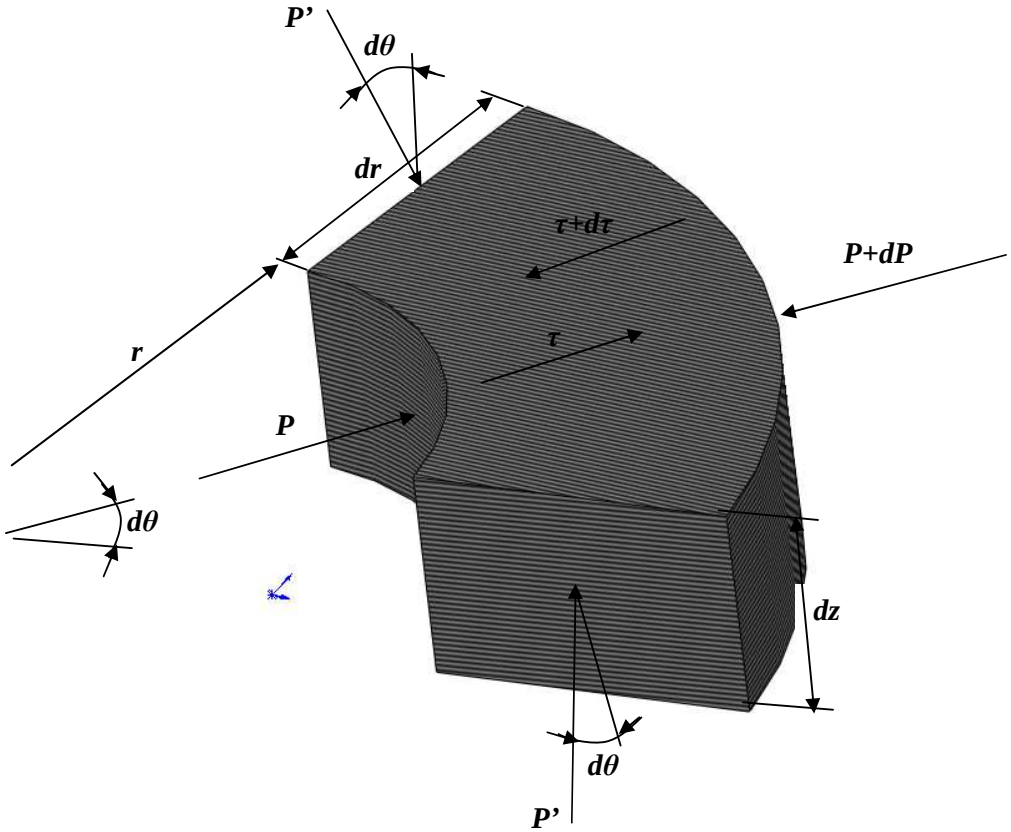

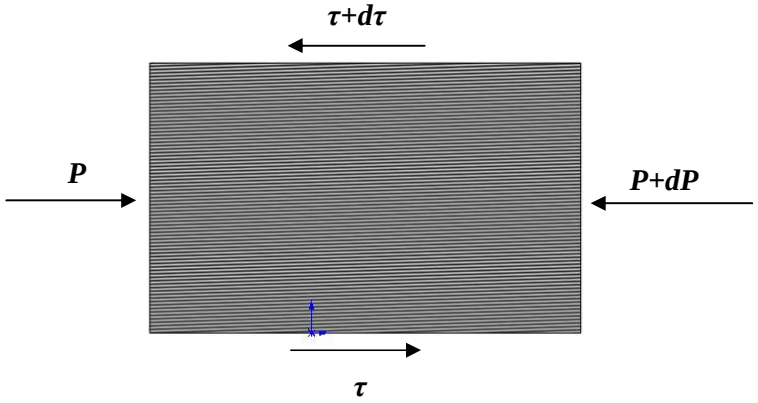

Figure 3.6 Force balance diagram.

radial direction. Substituting equation (3.4) into (3.3) gives:

$$\left(-\frac{dP}{dr}\right)dz = d\left[\eta\left(-\frac{dv_r}{dz}\right)\right] \tag{3.5}$$

after integrating equation (3.5) and considering $dv_r/dz = 0$ when z = 0, it results:

$$-\frac{dv_r}{dz} = \frac{1}{\eta}\left(-\frac{dP}{dr}\right)z \tag{3.6}$$

again, since $v_r = 0$ at $z = h/2$, the solution of equation (3.6) after integration is:

$$v_r = \frac{1}{2\eta}\left(-\frac{dP}{dr}\right)\times\left(\frac{h}{2}\right)^2 \times\left[1-\left(\frac{2z}{h}\right)^2\right] \tag{3.7}$$

During embossing the material continuous flow through a cylinder of radius *r* is expressed with:

$$q = 2\int_0^{2\pi}\int_0^{h/2} v_r r\,dz\,d\theta = 2\pi h v_r r \tag{3.8}$$

where *q* is the flow rate. As, shear strain rate is equal in *X* and *Y* direction, it can be assumed that:

$$\frac{V_m}{h} = \frac{2v_r}{r} \tag{3.9}$$

where V_m is the relative compression velocity of the upper and lower moulds of the embossing machine. So, substituting the equation (3.8) and (3.9) gives:

$$q = \pi r^2 V_m \tag{3.10}$$

Substituting the equation (3.7) into (3.10) and calculating the double integration yields:

$$-\frac{dP}{dz} = \frac{6\eta}{h^3} V_m r \tag{3.11}$$

since $P = 0$ when $r = R$, the solution of equation (3.11) following its integration is:

$$P = \frac{3\eta V_m}{h^3} \times \left(R^2 - r^2\right) \tag{3.12}$$

Balancing the forces of the compressive load of the embossing machine with that due to the pressure on the material in the z-direction gives:

$$F = \int_0^R \int_0^{2\pi} Pr \, d\theta dr \tag{3.13}$$

where F is the embossing force. Substituting equation (3.12) into (3.13) and performing the double integration in equation (3.13), gives the relationship between F and V_m:

$$F = \frac{3\pi}{2} \times \frac{\eta R^4}{h^3} V_m \tag{3.14}$$

Substituting this equation into (3.12) results in:

$$P = 2\left[1 - \left(\frac{r}{R}\right)^2\right] \times \frac{F}{A} \tag{3.15}$$

And the shear strain rate can be derived with the above equations:

$$\dot{\gamma} = -\frac{\mathrm{d}v_r}{\mathrm{d}z} = \frac{6rz}{h^3} V_m \tag{3.16}$$

or

$$\dot{\gamma} = \left(\frac{4}{\pi\eta}\right) \times \frac{rz}{R^4} \times F \tag{3.17}$$

The shear dependent behaviour can be described by the Cross-WLF model:

$$\eta(\gamma) = \frac{\eta_0}{1 + \left(\frac{\eta_0 \gamma}{\tau^*}\right)^{(1-n)}} \tag{3.18}$$

where η_0 is the viscosity at zero rate of shear, $\dot{\gamma}$ is the shear velocity, τ^* is the shear stress at the intersection of the two lines defining the change between Newtonian fluid and shear thinning behaviour, and n is the reciprocal flow exponent.

In case the cavities are considered to be channels the pressure drop in channels can be used to calculate the pressure. This model is only valid for Newtonian fluids, therefore the equations have to be adapted to describe the shear thinning and time-dependent behaviour of a polymer melt. Under the preconditions of laminar flow behaviour and homogeneous polymer melt, the model of the representative viscosity can be used (Worgull, 2009). The calculated pressure drop can be used as the minimum pressure needed to fill the cavity. The resulting pressure drop in the cavity can be estimated by:

$$P = \frac{8 V_m L \eta(\gamma)}{R^2} \tag{3.19}$$

The viscosity of the material according to the shear rate can be calculated from the equations (3.16) and (3.18). The calculated shear rate for 1 mm/min moulding speed is 0.2 1/sec and the related viscosity at the temperature of 120 ^{0}C is 9 x 10^7 Pa·s. Consequently, the minimum pressure required to fill the cavity can derived from equation (3.19) and it was found that the pressure to fill a hole with diameter of 2.55 mm is 1.2 MPa. Following this the minimum force required to feel the all structures in the centre and the edge can be estimated from equation (3.15). In this way, the minimum force necessary to fill the cavities was found to be approximately 5 kN.

Based on this model, preliminary experiments were conducted at 5 kN and the results showed that the embossing load was not enough to completely fill the sharp edges. This discrepancy compared to the theoretical result is due to the non-ideal experimental conditions where parallelism, flatness and material viscosity errors exist.

Additionally, this force was not enough to prevent cooling defects. Thus, 10 kN was used as the minimum force value at 120 ^{0}C in order to ensure a complete filling of the mould cavities and to avoid cooling and demoulding defects.

3.3 Analysis of the results

3.3.1 Process parameters effect on cavity pressure

Figure 3.7 shows the scanning electron microscope (SEM) images of a sample area of a replica. For each trial with each material, P_c, P_e and ΔP were measured and their mean values calculated based on the conducted three repetitions per trial. The results obtained are plotted in Figure 3.8.

From the results given in Figure 3.8 it can be seen that P_c is generally higher than $P_{e.}$ Furthermore, for PMMA and ABS, the highest pressure values for P_c and P_e were measured during trial 3. In particular the mean pressure in the center was 17.6 MPa and 24 MPa while in the edge it was 9.2 MPa and 8.4 MPa, respectively for PMMA and ABS. The lowest pressure was detected in trial 6 for both materials. The results also indicate that P_c has a higher standard deviation compared with P_e for both materials. More specifically the standard deviation for P_c and P_e is 5.4 MPa and 2.8 MPa, respectively, for PMMA while it is 7.2 MPa and 2.2 MPa, respectively, for ABS. This result indicates that the process factors have a greater influence on P_c for ABS compared to PMMA while the opposite is observed for P_e.

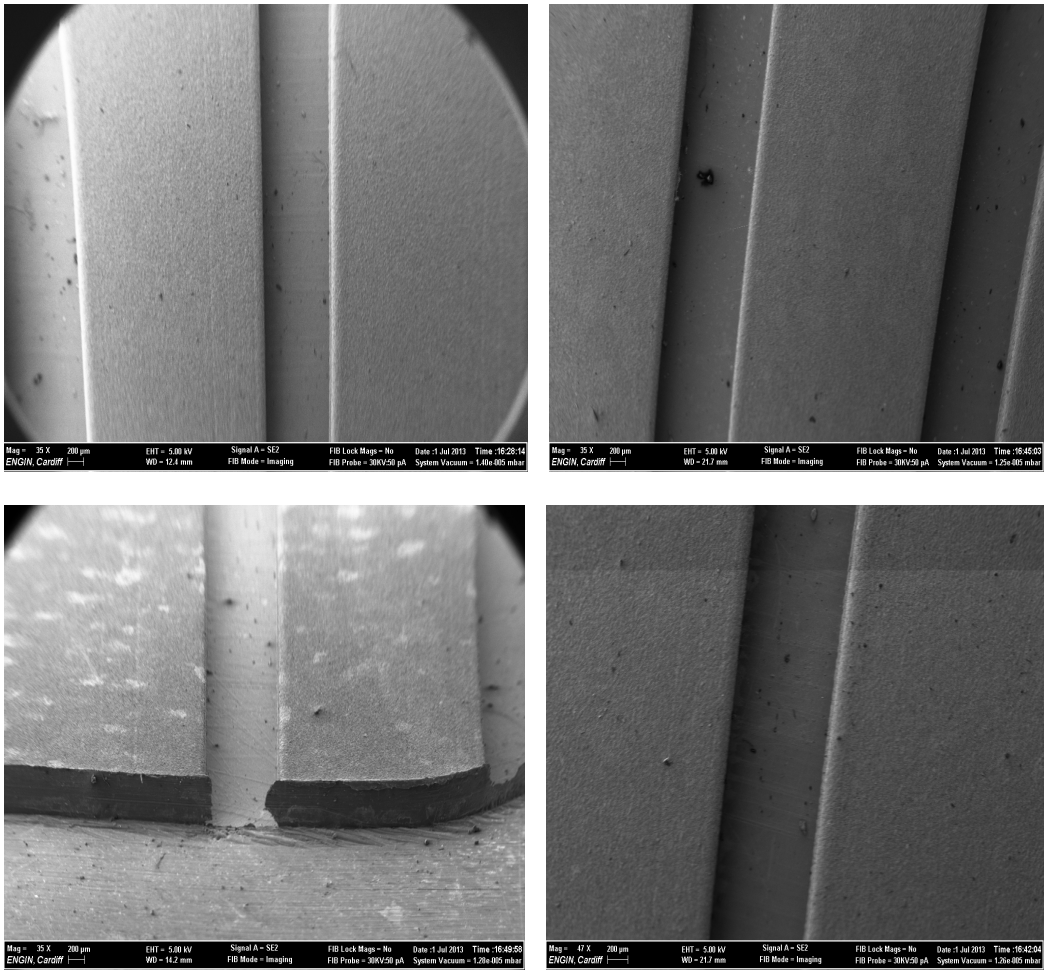

Figure 3.7 SEM images of embossed samples in PMMA.

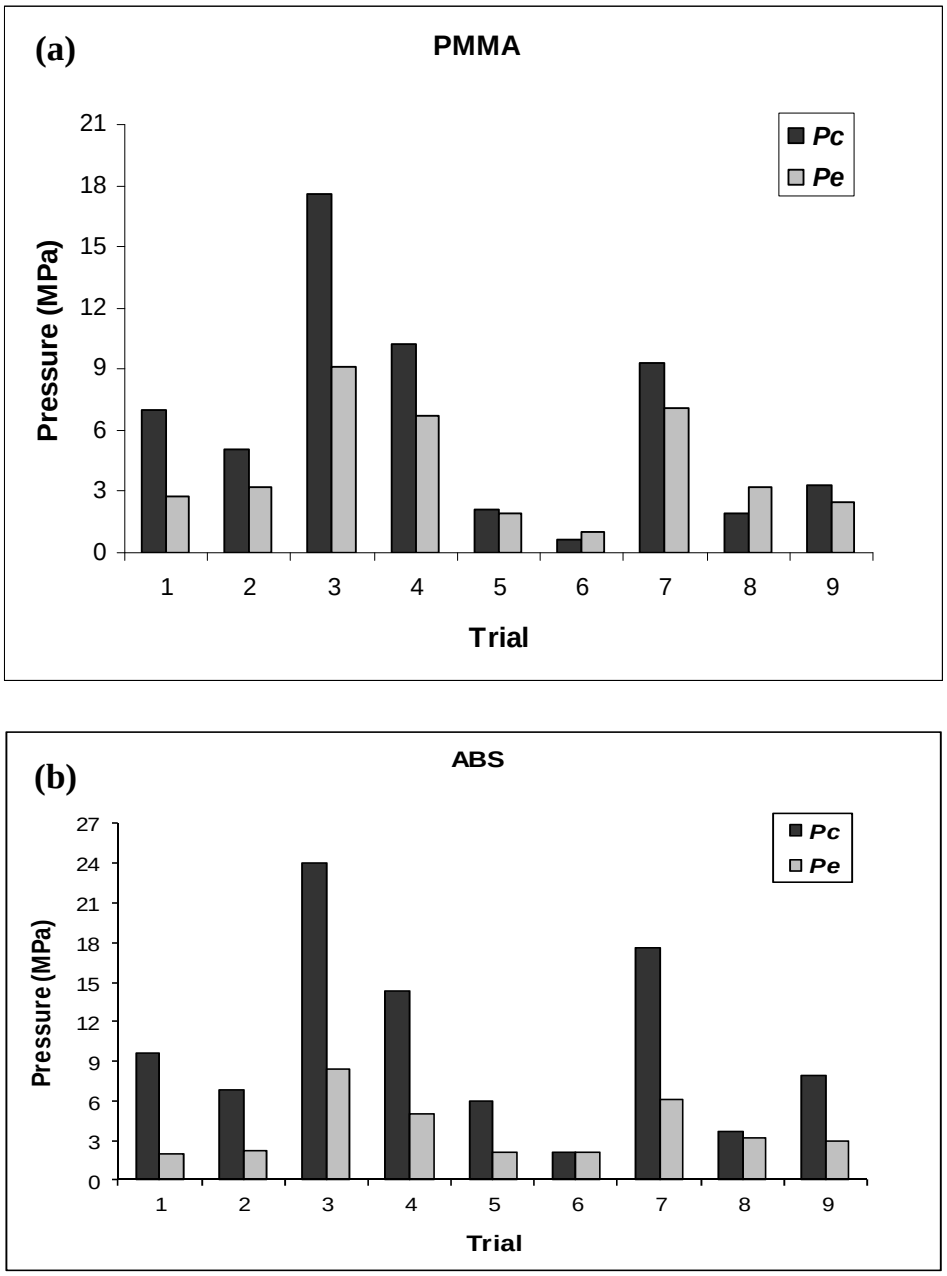

Figure 3.8 P_e and P_c results for (a) PMMA and (b) ABS

Based on the experimental results, an analysis of variance (ANOVA) was performed in order to assess the contribution of each processing parameter to the resulting P_c and P_e. Tables 3.4 and 3.5 and Figures 3.9 and 3.10 show the response of each parameter and the main effects plots, respectively. It is observed from these figures that, generally, an increase of F increases P, while an increase of T_m and t_h has the opposite effect. This observation for the effect of T_m was expected given that the viscosity of a polymer is directly dependent on its processing temperature. In particular, an increase of the temperature reduces the polymer internal stress and decreases its strength, which in turn eases the polymer flow during processing. The effect of t_h can be explained by the viscoelastic creeping behaviour of polymers, as creep is a time-dependent phenomenon and the pressure gradient will decrease when extending the time during which the embossing load is applied. Also, the above observations are in line with studies reported in Chapter 2. As it is obvious that an increase of F exerts higher pressure on the polymer to fill the cavities. On the other hand an increase in temperature under the same embossing force reduces the pressure but it does not mean that it also reduces filling capacity of the structures. In this case, the reduction of the pressure under the same embossing force is favourable for the polymer flow and it is also relevant to holding time.

From the response table provided for PMMA (Table 3.4), it is apparent that the most influential process parameter is different based on the levels considered. Particularly from Table 3.4(a), it can be seen that the temperature was the least important factor on P_c when it is increased from 120°C to 150°C, while it became the most influential parameter between 150°C to 180°C. The applied force was the second most influential factor in all cases. Finally, increasing the holding time from 0

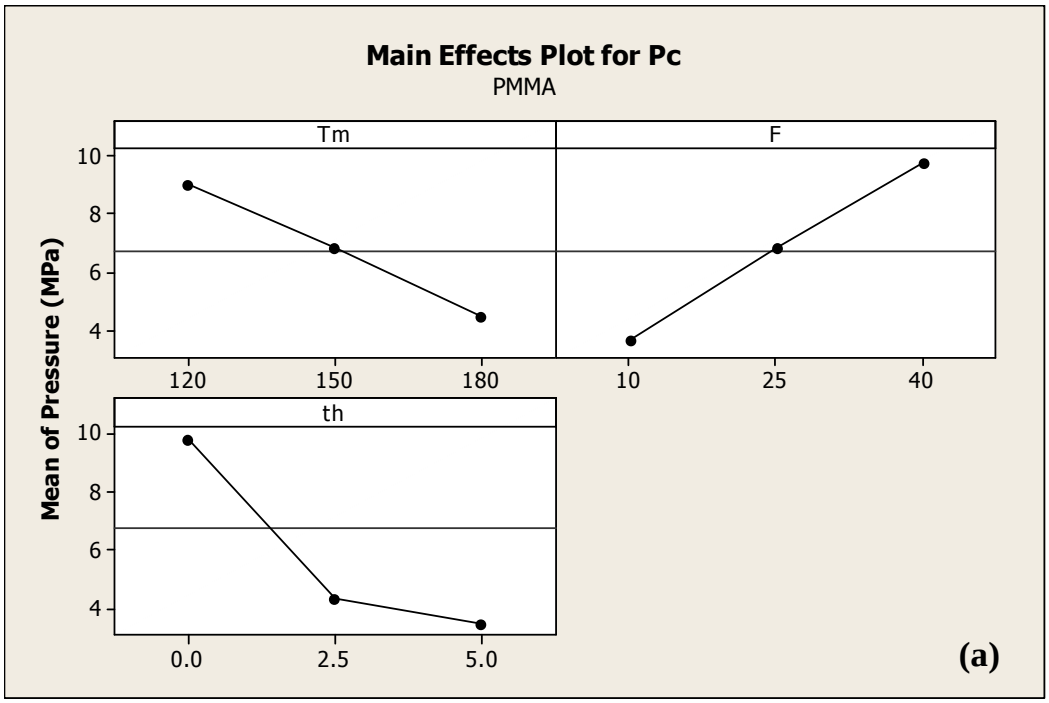

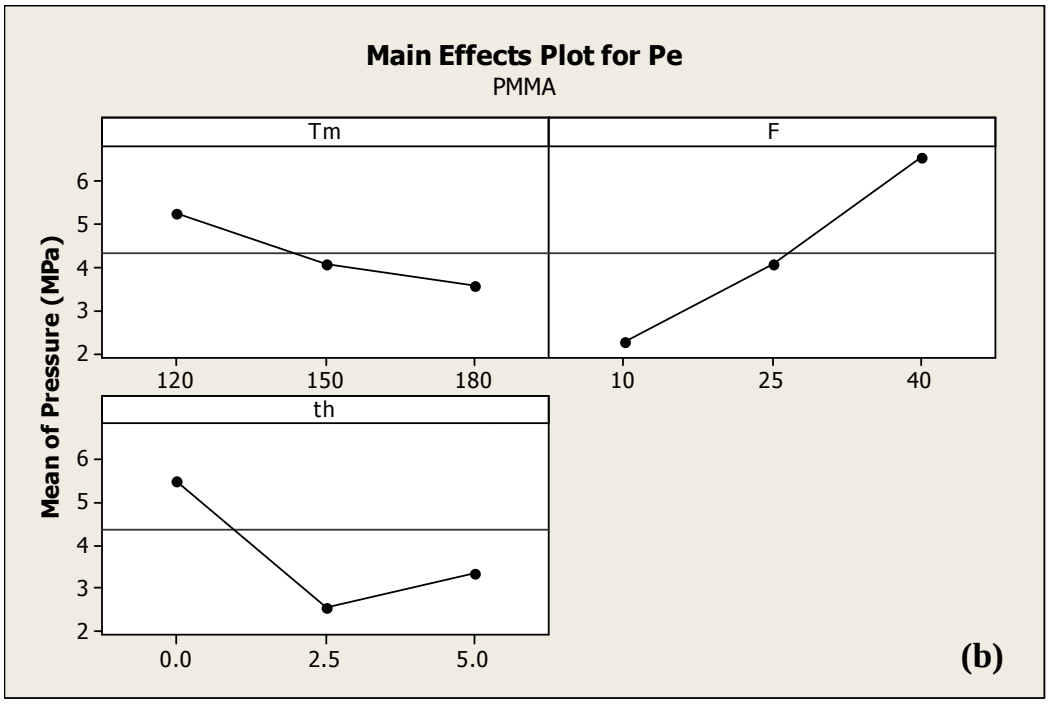

Figure 3.9 Main effect plots of (a) P_c and (b) P_e for PMMA

Table 3.4 Response table for (a) P_c and (b) P_e

(a)	PMMA	T_m	F	t_h
Levels	Level 1 (MPa)	9	3.7	9.9
	Level 2 (MPa)	6.9	6.9	4.4
	Level 3 (MPa)	4.5	9.8	3.5
Comparison between levels 1 and 2	Difference (MPa)	2.1	3.2	5.5
	Difference (%)	23.8	46.2	55.8
	Rank	**3**	**2**	**1**
Comparison between levels 2 and 3	Difference (MPa)	2.4	2.9	0.9
	Difference (%)	35	29.8	19.5
	Rank	**1**	**2**	**3**
Comparison between levels 1 and 3	Difference (MPa)	4.5	6.1	6.4
	Difference (%)	50.5	62.2	64.5
	Rank	**3**	**2**	**1**

(b)	PMMA	T_m	F	t_h
Levels	Level 1 (MPa)	5.3	2.3	5.5
	Level 2 (MPa)	4.1	4.1	2.5
	Level 3 (MPa)	3.6	6.6	3.3
Comparison between levels 1 and 2	Difference (MPa)	1.2	1.8	3
	Difference (%)	22.8	44.8	54
	Rank	**3**	**2**	**1**
Comparison between levels 2 and 3	Difference (MPa)	0.5	2.5	0.8
	Difference (%)	12.9	37.7	23.8
	Rank	**3**	**1**	**2**
Comparison between levels 1 and 3	Difference (MPa)	1.7	4.3	2.2
	Difference (%)	32.4	65.6	39.6
	Rank	**3**	**1**	**2**

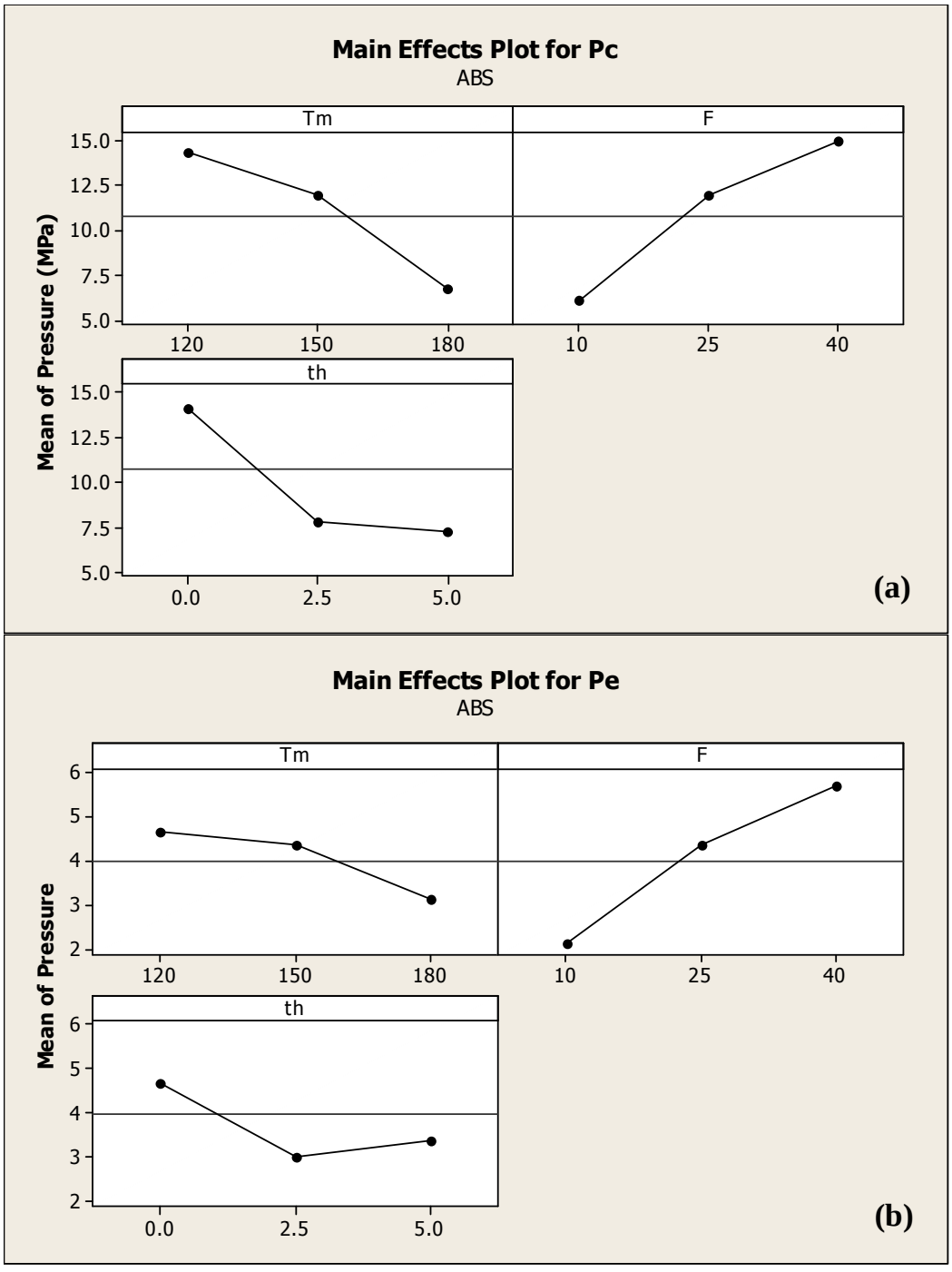

Figure 3.10 Main effect plots of (a) P_c and (b) P_e for ABS

Table 3.5 Response table for (a) P_c and (b) P_e

(a)	ABS	T_m	F	t_h
Levels	Level 1 (MPa)	14.3	6.1	14.2
	Level 2 (MPa)	11.9	11.9	7.9
	Level 3 (MPa)	6.7	14.9	7.4
Comparison between levels 1 and 2	Difference (MPa)	2.4	5.8	6.3
	Difference (%)	16.6	48.7	44.3
	Rank	**3**	**1**	**2**
Comparison between levels 2 and 3	Difference (MPa)	5.2	3	0.5
	Difference (%)	43.6	20.1	7
	Rank	**1**	**2**	**3**
Comparison between levels 1 and 3	Difference (MPa)	7.6	8.8	6.8
	Difference (%)	52.9	58.9	48
	Rank	**2**	**1**	**3**

(b)	ABS	T_m	F	t_h
Levels	Level 1 (MPa)	4.7	2.2	4.7
	Level 2 (MPa)	4.4	4.4	3
	Level 3 (MPa)	3.1	5.7	34
Comparison between levels 1 and 2	Difference (MPa)	0.3	2.2	1.6
	Difference (%)	6.2	49.8	35.2
	Rank	**3**	**1**	**2**
Comparison between levels 2 and 3	Difference (MPa)	1.2	1.3	0.4
	Difference (%)	28.4	23.1	10.4
	Rank	**1**	**2**	**3**
Comparison between levels 1 and 3	Difference (MPa)	1.5	3.5	1.3
	Difference (%)	32.9	61.4	27.7
	Rank	**2**	**1**	**3**

to 2.5 minutes had the highest impact on P_c when comparing parameters between levels 1 and 2, while this effect was not so pronounced when its value varied between 2.5 and 5 minutes. When comparing results between levels 1 and 3, i.e. across the whole range of processing values studied, it can be observed that the most influential process parameter on P_c was t_h. From the response analysis for P_e shown in Table 3.4(b), it is immediately apparent that T_m is least important parameter for all levels. Furthermore, t_h had the most influence between level 1 and 2 while between level 2 and 3 it was F. Overall, when embossing PMMA, it can be said that F was the most effective parameter on P_e, while it the case of P_c it was t_h, and T_m was the least influential parameter for both P_c and P_e.

Looking at the results for ABS in Table 3.5, it is observed that the rankings of the process parameters effect are the same for P_c and P_e. The temperature was the least important factor when it was increased from level 1 to 2 while the embossing force was detected as the most influential parameter in that case. On the other hand, temperature was the most significant parameter between levels 2 and 3 compared to F and t_h. Across all levels, it can be concluded that the embossing force had most impact on cavity pressure and holding time the least.

An interesting phenomenon is detected in the Tables 3.4(b) and 3.5(b), where an increase in holding time from 2.5 to 5 minutes increased P_e while the inverse effect initially takes place between 0 and 2.5 minutes. To explain this, it is assumed that the increase in pressure on the edge of the mould occurred due to a reduction in the thickness of the residual layer to a value smaller than the cavity depth where the flow of polymer in the radial direction was constrained by the mould structures. In this

situation, it becomes more difficult for the polymer to flow out of the cavity, hence the slight augmentation in pressure when the holding time is increased.

3.3.2 Process parameters effect on pressure distribution

According to Figure 3.11 and Table 3.6, it is evident that the increase in T_m and t_h reduces ΔP, while the opposite effect is occurring for F. However, the same phenomena is also observed for the P_c and P_e in previous section, it should be noted that increase in pressure by F is favourable due to its contribution to cavity filling. On the other hand an increase in ΔP is not desirable because this causes non-uniform filling. Consequently, it is noted that an increase in embossing force has a positive effect on cavity filling but a negative one for homogenous filling. Thus, it is worth selecting the optimum embossing load that takes into account P_c, P_e and ΔP.

Overall, the lowest ΔP value measured was obtained in trial 5 for PMMA and trial 6 for ABS and the highest one was in trial 3 for both materials. From the ΔP analysis, it is immediately apparent that there is not a unique selection of parameter levels that can be considered optimum for both polymers investigated in this research. In particular, across all levels, t_h had most significant effect on ΔP for PMMA while for ABS, it is T_m.

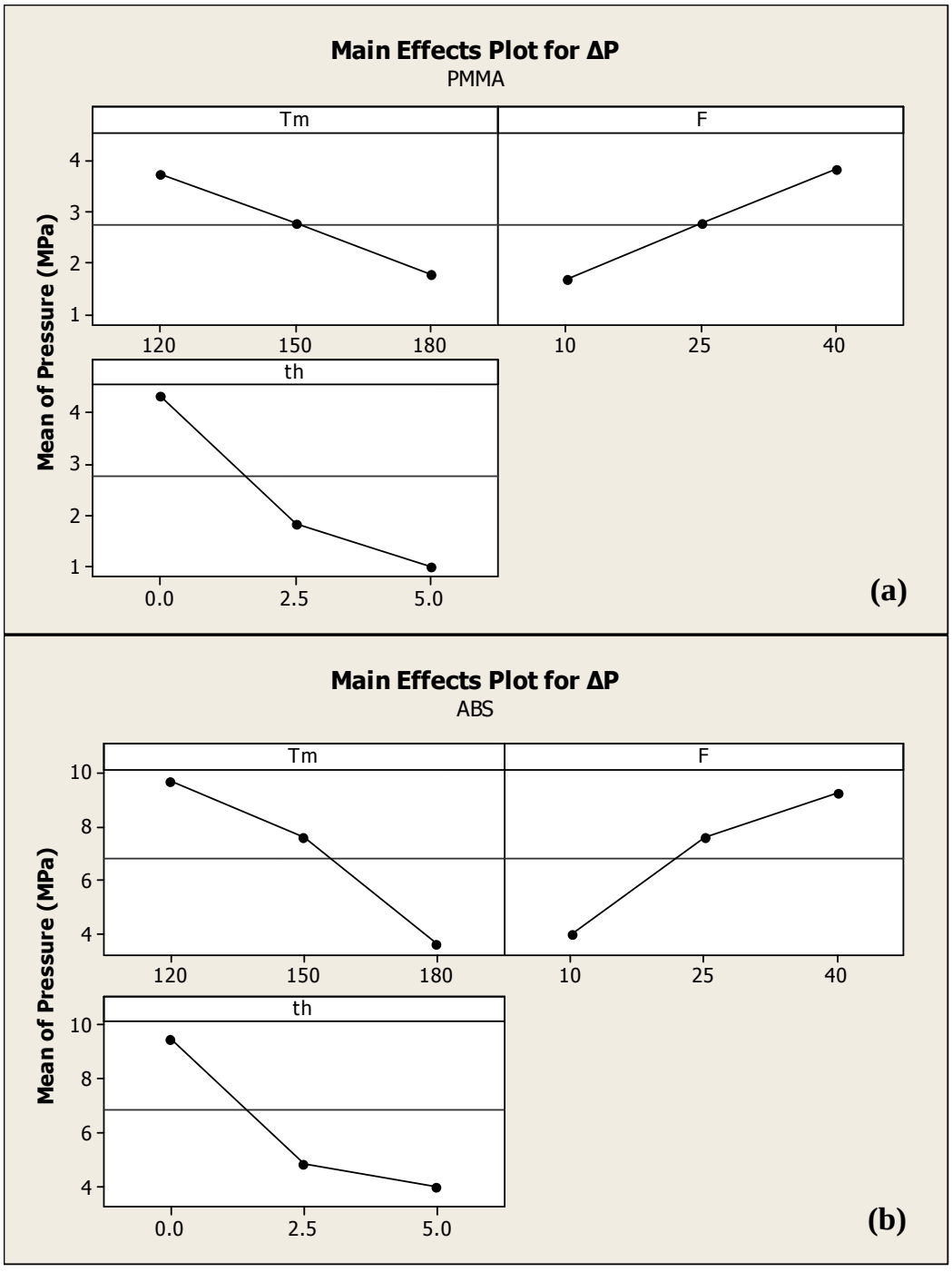

Figure 3.11 Main effect plots of Δ*P* for (a) PMMA and (b) ABS

Table 3.6 Response table of ΔP for (a) PMMA and (b) ABS

(a)	PMMA	T_m	F	t_h
Levels	Level 1 (MPa)	3.7	1.7	4.3
	Level 2 (MPa)	2.8	2.8	1.8
	Level 3 (MPa)	1.8	3.8	1
Comparison between levels 1 and 2	Difference (MPa)	0.9	1.1	2.5
	Difference (%)	25.9	40	58
	Rank	**3**	**2**	**1**
Comparison between levels 2 and 3	Difference (MPa)	1.01	1.1	0.8
	Difference (%)	36.5	27.9	45
	Rank	**2**	**3**	**1**
Comparison between levels 1 and 3	Difference (MPa)	1.9	2.2	3.3
	Difference (%)	52.9	56.8	76.9
	Rank	**3**	**2**	**1**

(b)	ABS	T_m	F	t_h
Levels	Level 1 (MPa)	9.7	4	9.5
	Level 2 (MPa)	7.6	7.6	4.9
	Level 3 (MPa)	3.6	9.3	4
Comparison between levels 1 and 2	Difference (MPa)	2.1	3.6	4.6
	Difference (%)	21.6	47	49.1
	Rank	**3**	**2**	**1**
Comparison between levels 2 and 3	Difference (MPa)	4	1.7	0.9
	Difference (%)	52.4	18.2	18.1
	Rank	**1**	**2**	**3**
Comparison between levels 1 and 3	Difference (MPa)	6.1	5.3	5.6
	Difference (%)	62.7	56.7	58.3
	Rank	**1**	**3**	**2**

3.4 Summary

This chapter reported an experimental study on the effects of process parameters on pressure conditions in cavities when replicating parts in PMMA and ABS. To measure the pressure state of a polymer inside mould cavities, a condition monitoring system was implemented. Then, by employing a design of experiment approach, the pressure behaviour was studied as a function of different process conditions. In particular, the effects of three process parameters T_m, F and t_h on the cavity pressure and the pressure distribution were investigated. It was shown that cavity pressure and pressure distribution were dependent on both materials and processing conditions. The obtained results indicate that an increase in T_m and t_h reduced P_c, P_e, and ΔP while the opposite effect takes place for F. Also, it was observed that the increase of the embossing force has a positive effect on cavity filling but does not promote for homogenous filling. In addition, using a simple analytical model, the minimum required embossing force to fill the cavities across the mould surface was calculated. The theoretical value obtained was then used to inform the design of the experiments.

CHAPTER 4

MODELLING, SIMULATION AND VALIDATION OF DEMOULDING FORCE IN HOT EMBOSSING

4.1 Overview

One of the most challenging issues to overcome when implementing polymer micro and nano replication techniques is to prevent the formation of structural defects that can occur during demoulding. From the literature review presented in Chapter 2, it is clear that, while FE models enable a better understanding of the demoulding process mechanisms in hot embossing in comparison to experimental approaches, there is still a need to develop more advanced simulation models for investigating the combined effects of material properties, demoulding temperature, pressure, mould design, sidewall geometry and adhesion on the demoulding force. In this context, the motivation for the research presented in this chapter is to develop and validate an analytical model for predicting the demoulding force in hot embossing of polymer materials by taking into account these process factors. An analytical approach was favoured over the development of an FE solution in order to reduce the computational complexity generally associated with FE models. In addition, the ultimate aim of the developed model is to enable the optimisation of the demoulding step of the hot embossing process and thus, the reduction of structural defects in replicated parts.

The remainder of the chapter is organised as follows. First, the developed model is presented taking into account the contribution from the adhesion, deformation and friction forces. Next, the test material, mould design, plan of experiments and the method used to measure the demoulding force for validating the proposed model are explained. Finally, the comparison between the simulation and the experimental results is discussed focusing on the effect of the demoulding temperature, applied embossing force and structure layout on the achieved demoulding force.

4.2 Model development

The model was developed to consider the combined effects of friction, deformation and adhesion phenomena. Thus, the demoulding force, F_d, is constituted of the following three components: (1) the adhesion force between the mould and the polymer, F_{ad}, (2) the deformation force, F_{def}, due to the presence of undercuts on the sidewalls of the mould structures, which are inherent to master making processes and (3), the friction force on the structure sidewalls, F_{fr}:

$$F_d = F_{ad} + F_{def} + F_{fr} \tag{4.1}$$

4.2.1 Adhesion force

The detailed calculation of the adhesion force is difficult because adhesion is a function of the material pair properties and interface conditions such as crystal

structure, crystallographic orientation, solubility of one material into another, chemical activity, surface cleanliness, normal load, temperature, duration of contact and separation rate (Bhushan, 2003). A simplified approach for modelling adhesion uses the concept of surface energy. In particular, this energy contributes to the work of adhesion, W_{ad}, or the energy of adhesion per unit area, which is defined as follows:

$$W_{ad} = \gamma_{\alpha} + \gamma_{\beta} - \gamma_{\alpha\beta} \tag{4.2}$$

where γ_a and γ_β are the surface energies of the two solids, separately, and $\gamma_{\alpha\beta}$ is the interfacial energy between the two materials in contact. Fundamental adhesion models such as the JKR (Johnson *et al.* 1971) or DMT (Derjaguin *et al.* 1975) models incorporate W_{ad} to predict the adhesion force between two solids. A recent review provides a comprehensive description of different adhesion models available to date (Prokopovich and Starov, 2011). The application of fundamental adhesion models in the context of this study requires the calculation of the work of adhesion between the mould and the polymer for different demoulding temperatures. However, this task is hampered by the lack of theoretical and experimental data in the temperature range of interest. For this reason, a model proposed by Kendall (1973) which describes the adhesion strength change of a material with temperature variations is applied to predict the adhesion force at different demoulding temperatures for the HE process. This model considers that the residual stress due to the shrinkage of the material contributes to the strain energy of the system, which in turn reduces the initial adhesive energy required to fracture a unit area interface at zero shrinkage, γ:

$$\sigma_{ad} = \left[\frac{2K}{t_p} \left(\gamma - \frac{t_p . K\varepsilon^2}{2} \right) \right]^{1/2} \tag{4.3}$$

where σ_{ad} is the adhesion strength, K is the bulk modulus, ε is the thermal shrinkage strain and t_p is the thickness of the polymer. Thus, the expression of the adhesion force adopted in this study is as follows:

$$F_{ad} = \sigma_{ad} \times A \tag{4.4}$$

where A is the total surface area of contact between the polymer and the mould.

4.2.2 Deformation force

Metal replication masters are often structured by mechanical processes. Thus, the machined surfaces have a specific roughness that can cause interlocking on the sidewalls of the mould features leading to demoulding issues. In particular, the polymer replica and the master have to deform to slide over each other during demoulding at locations where interlocking occurs. Thus, the friction between the two materials increases as a result of this deformation. Colton *et al.* (2001) proposed a model to predict the ejection force in injection moulding, which takes into account the roughness of periodic surfaces and implemented it for moulds fabricated with the stereolithography process (Pham and Colton, 2002). This model was also recently adapted by Delaney *et al.* (2010) and applied to surfaces machined by turning. Colton's model introduces an "equivalent" coefficient of friction, which is the sum of the coefficient of friction and a contribution from the elastic deformations of the

mould and the polymer parts that are necessary to overcome the interlocking between them due to the periodic surface roughness on the sidewalls of the mould structures.

In this study, the mould cavities are created with micro drilling and thus, the generated surface on the sidewalls of such features is also periodic (Figure 4.1). For this reason, the model from Colton *et al.* (2001) was adapted to describe the deformation force F_{def} as follows (Figure 4.2):

$$F_{def} = \frac{\delta^2}{L \times r_c} \cdot \frac{E}{1-\nu} \cdot A_w \tag{4.5}$$

where δ represents the maximum peak to valley distance generated with the micro drill, L and r_c are the tooth load and the tool nose radius respectively, E and ν are the Young's modulus and the Poisson ratio of the polymer and A_w is the area of contact on the sidewalls of the cavities. Given that the feed rate, f, spindle speed, v, and tool nose radius used during the micro drilling process are known parameters, it is possible to calculate δ as follows (Elkaseer *et al.* 2012):

$$\delta = r_c - \sqrt{r_c^2 - \left(\frac{f}{2}\right)^2} \tag{4.6}$$

In addition, L can also be expressed as:

$$L = \frac{f}{N \times v} \tag{4.7}$$

where N is the number of teeth of the micro drill.

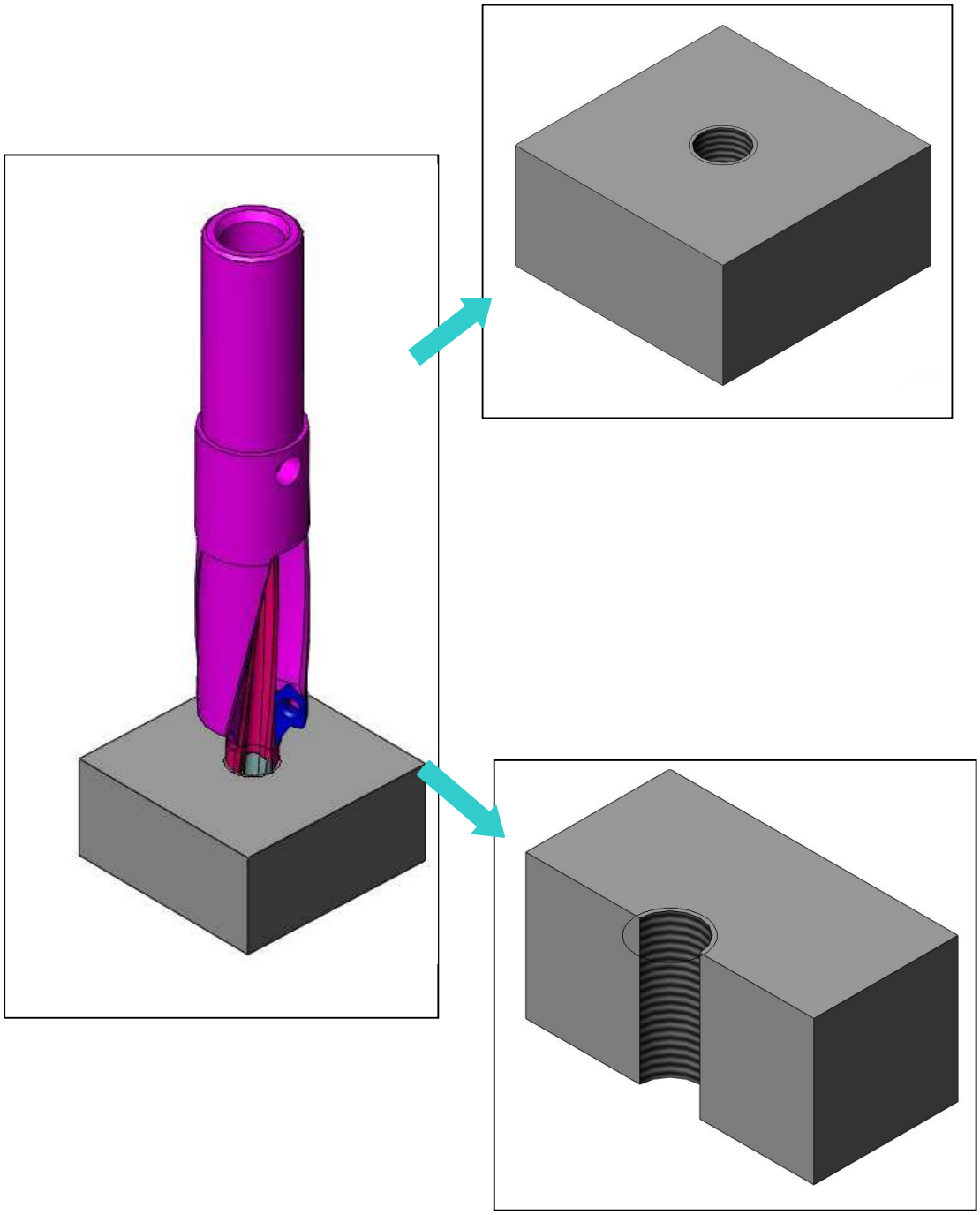

Figure 4.1 Micro Drilling Process.

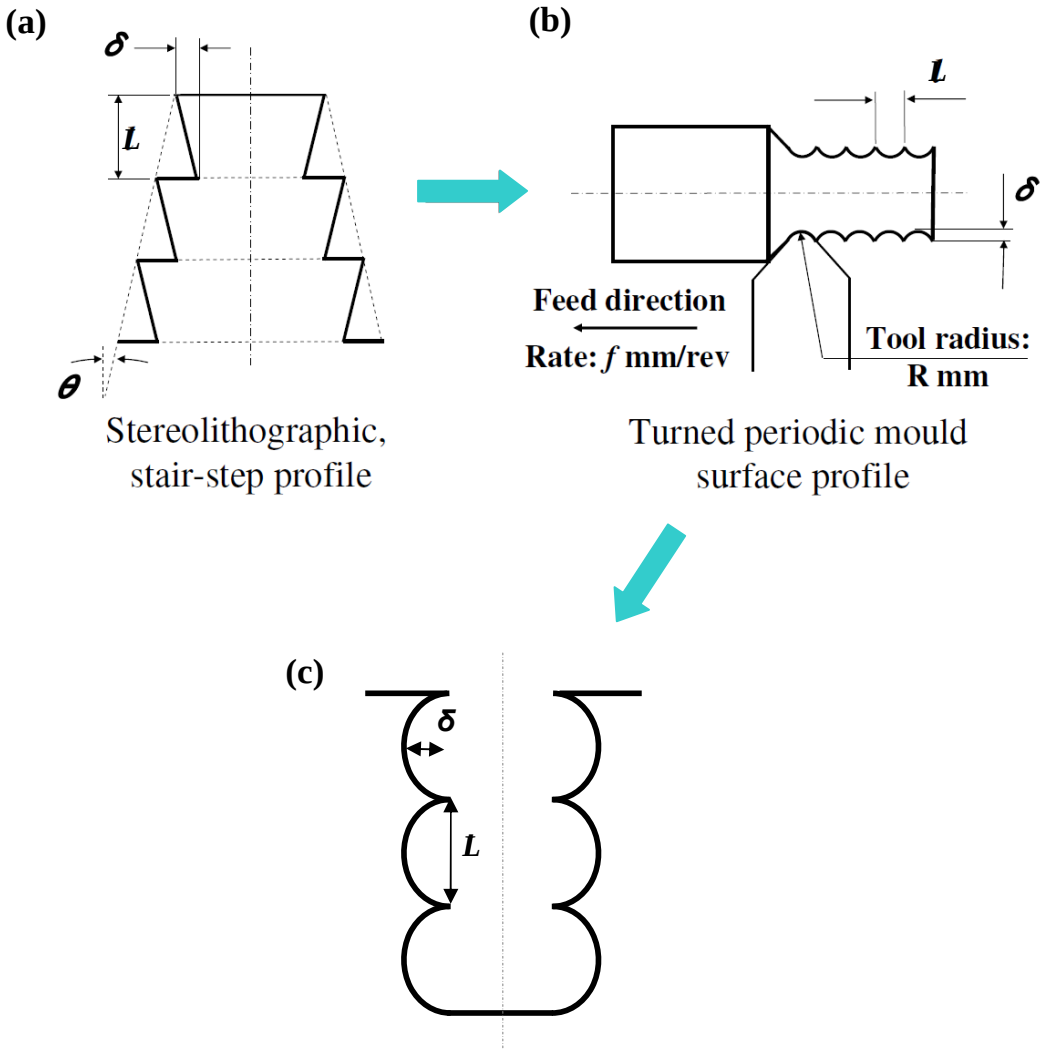

Figure 4.2 Analogy between (a) stereolithographic surfaces (Pham and Colton, 2002), (b) turned periodic surfaces (Delaney *et al.* 2010) and (c) drilled periodic surfaces.

4.2.3 Friction force

The force required during demoulding must overcome the effect of the normal force on the sidewall of the micro structures present in the mould. Most mathematical models developed to quantify the demoulding process simply derive the expression of the friction force based on the empirical Coulomb's law of friction (Menges and Mohren, 1986). Thus, in this study the friction force, F_{fr}, is described by:

$$F_{fr} = \mu \cdot \sigma_d \cdot A_w \tag{4.8}$$

where μ is the coefficient of friction, σ_d is the contact stress on the sidewalls of the mould structures upon demoulding and A_w is the area of contact between the polymer and the mould on the sidewalls. The contact stress, σ_d, should be considered based on two different HE processing stages, namely during cooling and upon demoulding, in order to take into account the polymer pressure history.

To achieve this, the contact stress upon demoulding is examined first. In particular, when demoulding begins, the mould does not exert any pressure on the polymer and thus, the stress that results from the shrinkage behaviour of the polymer as it is cooled down, tends to move towards the centre of the replica. In this case, the stress condition within the polymer is illustrated in Figure 4.3 and the contact stress upon demoulding is expressed as:

$$\sigma_d = \sigma_f + \sigma_{ad} + \sigma_{bd} - \mu\sigma_{ad} \tag{4.9}$$

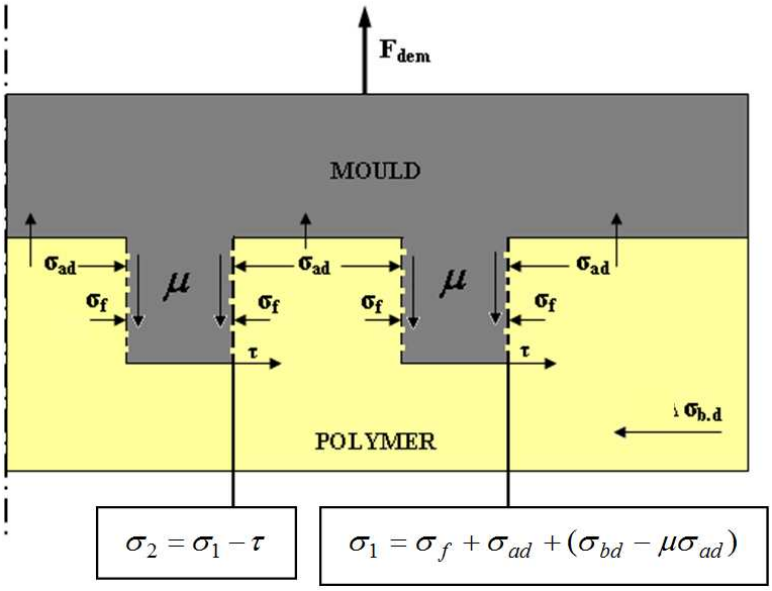

Figure 4.3 Contact stress upon demoulding.

where σ_{ad} is described by equation (4.3) and manifests itself on the vertical walls as illustrated in Figure 4.3, while $\mu\sigma_{ad}$ is acting on the lateral surfaces, σ_{bd} is the contact stress before demoulding and σ_f is the flow-induced residual stress. As shown in Figure 4.3, the above equation takes into account the fact that, the adhesion between the polymer and the horizontal surface of the mould tends to oppose the thermal shrinkage towards the centre of the replica. The flow-induced residual stress, σ_f, can be explained as follows. When a polymer is in a molten state, its molecules are unstressed and they tend to reach an equilibrium state. During HE, the polymer is sheared and elongated and as a result, the molecules are oriented in the flow direction. If the polymer solidification occurs before the molecules can fully relax back to their state of equilibrium, the molecular orientation is locked within the embossed replica and this creates such type of stress. However, due to the typically slow cooling in hot embossing, σ_f is considered very low and thus, it can be neglected.

As shown in Figure 4.3, the contact stress on a given mould structure is also dependent on its location. This is due to the fact that the polymer is also subjected to shear stress, τ, which occurs as the polymer shrinkage towards the center of the replica is prevented by the mould surface features. This is the reason why outside structures are sometimes incorporated on HE plates in order to absorb most of the stress and thus, to reduce the risk of damage to some functional features during the replication process. This shear stress can be expressed as follows:

$$\tau = \frac{F_{bd}}{A_s} \tag{4.10}$$

where F_{bd} is the force generated by σ_{bd}, and A_s is the area of a given mould structure

that is perpendicular to the shrinkage direction. In Figure 4.3, σ_1 represents the contact stress upon demoulding on the mould feature which is further away from the centre of the replica and it is calculated using equation (4.9). Then, the contact stress, σ_2, acting on the adjacent structure in the lateral direction towards the core of the polymer is derived from σ_1 by taking into account the influence of the shear stress, τ, and is given by:

$$\sigma_2 = \sigma_1 - \tau \tag{4.11}$$

In this way, the contact stress upon demoulding can be calculated as a function of the mould design, in particular by considering the location of the mould structures. However, in order to express σ_d using equation (4.9) above, the contact stress before demoulding, σ_{bd}, should be calculated. For this, the distribution of σ_{bd} when the polymer is cooled down to the demoulding temperature while it is still subjected to the embossing load is illustrated with Figure 4.4. From the figure, it can be seen that the friction, adhesion and pressure within the replica tend to oppose shrinkage. Thus, to account for the reduced shrinkage effect due to these factors, σ_{bd} is expressed with the following equation:

$$\sigma_{bd} = P + \mu(P + \sigma_{ad}) - \sigma_T \tag{4.12}$$

where σ_T is the thermally-induced residual stress and P is the pressure generated due to the applied embossing force. P shows a parabolic distribution in open die embossing due to the polymer flow and can be calculated with (Lin *et al.* 2003):

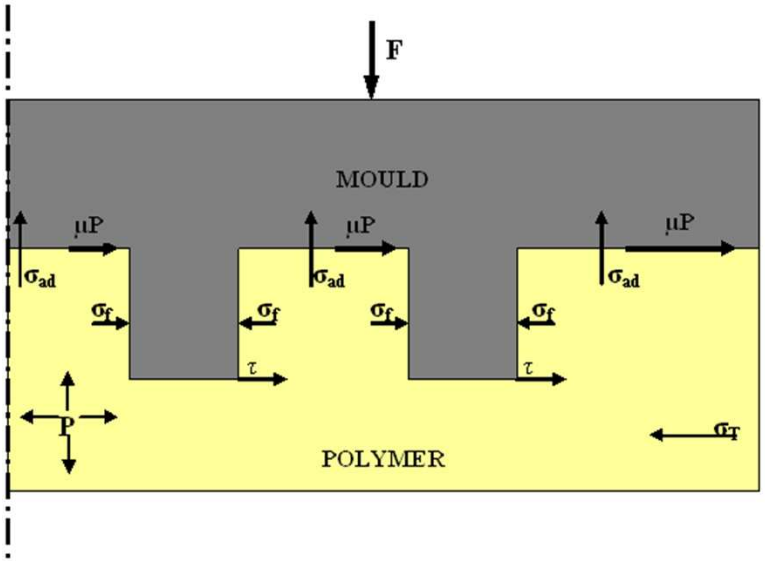

Figure 4.4 Contact stress before demoulding.

$$P = \frac{n+3}{n+1}\left[1-\left(\frac{r}{R}\right)^{n+1}\right]\frac{F}{A} \tag{4.13}$$

where F is the applied force, n is the material constant and in the case of PMMA, n = 0.25 (Lin *et al.* 2003). It should be noted that this pressure distribution is not valid when the lateral flow of the polymer melt is prevented using special fixtures.

The thermally-induced residual stress, σ_T, arises during the cooling stage and is a consequence of polymer shrinkage. In particular, the thermal expansion of polymers is significantly higher than that of metals. Thus, this difference in thermal shrinkage during cooling results in high contact stress between a replica and a metallic master which, in turn, contributes to the demoulding force. The influence of this phenomenon is therefore important for all replication processes, especially when the feature size decreases. The thermally-induced residual stress is expressed as follows:

$$\sigma_T = (\alpha_p - \alpha_m)(T_g - T_d)\frac{E}{1-\nu} \tag{4.14}$$

where: α_p and α_m are the coefficients of thermal expansion for the polymer and the mould material respectively, T_d is the demoulding temperature for the replica and T_g denotes the solidification temperature which corresponds to the glass transition temperature for amorphous thermoplastics or the melting temperature for semi crystalline polymers.

4.3 Experimental set-up

In this study, experiments were conducted with an HEX03 HE machine from Jenoptik Mikrotechnik to validate the proposed model. The following sub-sections describe the design and the manufacture of the mould used along with the properties of the polymer material processed, the experimental design adopted and the measurement technique employed to assess the demoulding force. The mould design, the polymer properties and the experimental plan were also used as an input for the conducted simulation study in order to compare the theoretical and experimental results.

4.3.1 Test materials and mould design

Two millimeter thick PMMA sheets were used in the experiments. The PMMA mechanical and thermal properties are shown in Table 4.1 (Matbase, 2012 and Dirckx, 2010).

The embossing mould was made from a 5 mm thick aluminium workpiece with overall lateral dimensions of 40 mm x 40 mm. The material properties of the aluminium used to produce the test plate are given in Table 4.1. The structured area of the mould included four arrays of 3 x 4 micro drilled holes. The depth of each hole was 400 µm and the diameter 200 µm. To assess the effect of the holes' location on the demoulding force, two designs were implemented. For the first design, the four arrays of holes were positioned in the central area of the mould while, for the second design, an array of holes was located at each corner of the workpiece (Figure 4.5).

Table 4.1 Material Properties

PMMA	
Properties	**Values**
Young Modulus (25 ^{0}C)	3.1 GPa
Young Modulus (50 ^{0}C)	2.4 GPa
Young Modulus (90 ^{0}C)	1.34 GPa
Young Modulus (150 ^{0}C)	4 MPa
Compressive Strength	83-124 MPa
Poisson's Ratio	0.39
Glass Transition Temperature	105 ^{0}C
Coeff. of Thermal Expansion	8.4 x $10^{-5}/^0$C
Aluminum	
Properties	**Values**
Young Modulus	70 GPa
Poisson's Ratio	0.33
Coeff. of Thermal Expansion	2.44 x $10^{-5}/^0$C

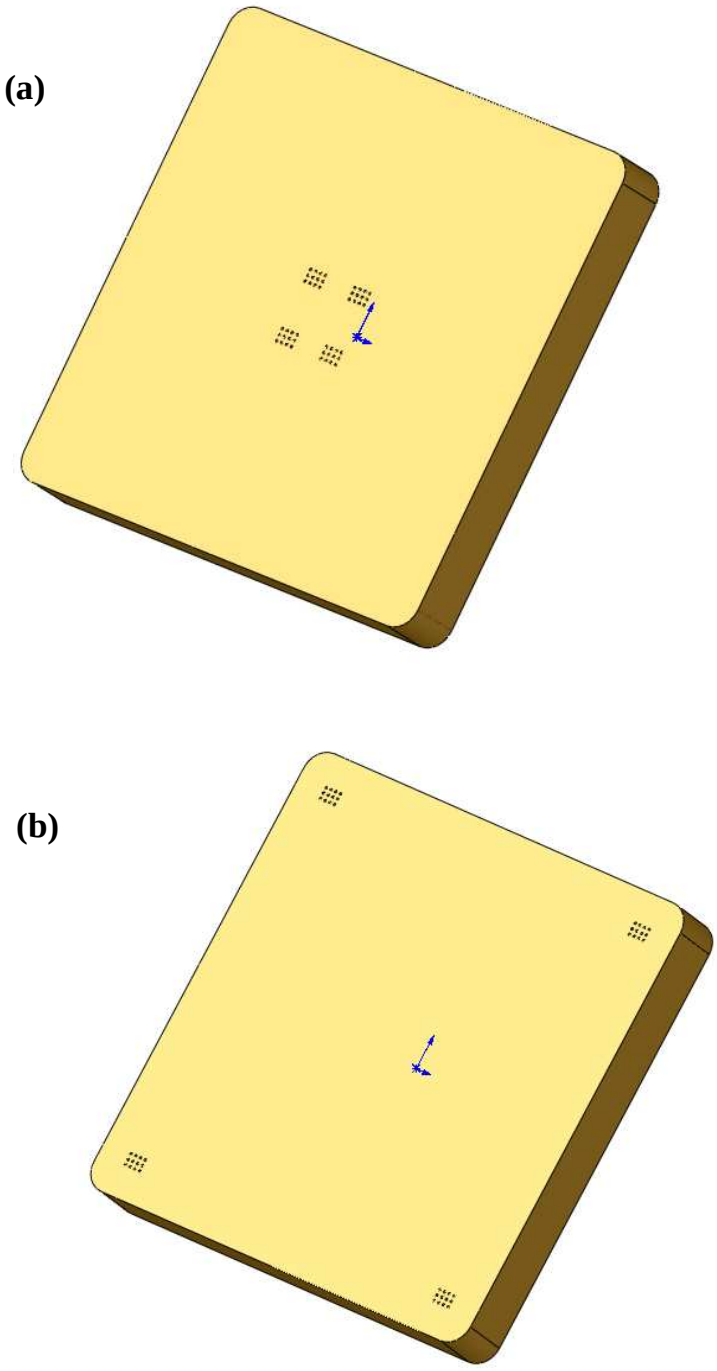

Figure 4.5 Mould design: structures located in the (a) central area and (b) corners.

The fabrication of the mould structures was carried out with micro drilling by employing a Kern HSPC 2216 micro-machining centre. In particular, 200 μm diameter end-mill cutters with two teeth, having 6° rake and 25° helix angles, were utilised in the experiments. Prior to the cutting tests, each cutter was imaged using a SEM to measure the approximate radii of the cutting edges as shown in Figure 4.6. It was found that these were in the range 2 to 2.5 μm. The parameters and values of the drilling process are given in Table 4.2.

4.3.3 Planning of experiments and force measurements

In these experiments, the demoulding force was measured as a function of the demoulding temperature, T_{dem}, when varying it in the range from 50°C to 90°C. In addition, measurements were also conducted when varying the applied embossing force, F, at the maximum and minimum values considered for T_{dem}. For all trials, the embossing temperature was kept at 150°C, while the holding time was 5 minutes and the demoulding velocity applied was 1 mm.min^{-1}. Each of the trials was repeated three times. The combinations of the parameters' values utilised for F and T_{dem} are provided in Table 4.3. The chosen range of parameters levels was determined based on material properties and preliminary experiments in order to ensure complete filling of the mould cavities during the embossing stage of the process and also to study an extended range of demoulding temperatures.

The demoulding force required in each experiment was measured with the force sensor built in the hot embossing machine. The output of the sensor is collected every second and provides online force curves in which the demoulding force

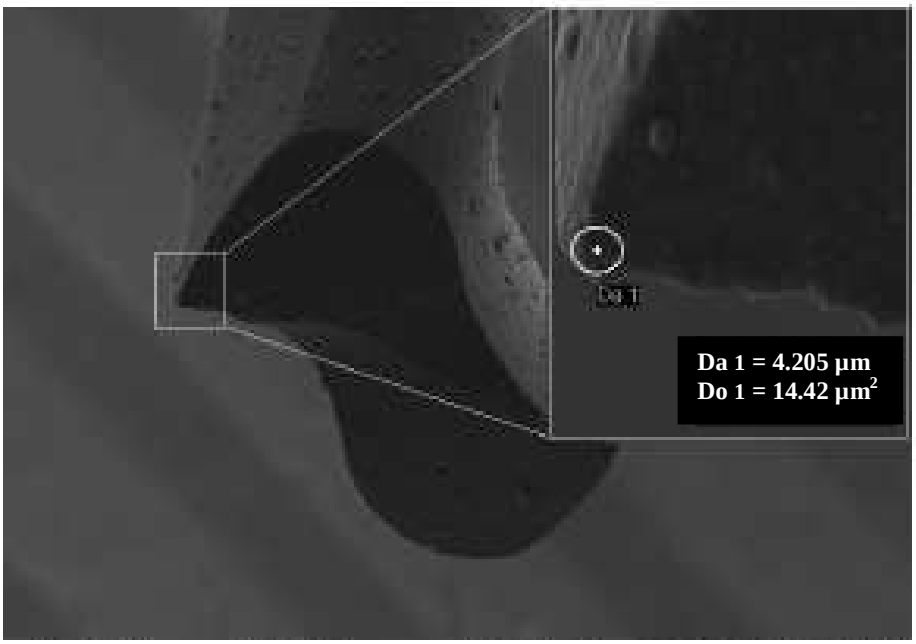

Figure 4.6 SEM image of cutting tool edge.

Table 4.2 Micro Drilling Process parameters and values

Micro Drilling Process	
Parameters	**Values**
Feed rate	77 mm/min
Spindle Speed	18000 rev/min
Tool radius	200 µm
Tool nose radius	5 µm

Table 4.3 Process Parameters Design

Trial	F (kN)	T_{dem} (^{0}C)
1	15	90
2	15	80
3	15	70
4	15	60
5	15	50
6	5	90
7	5	50
8	25	90
9	25	50

is characterized by a sudden release of the stamp from the polymer leading to characteristic ‘‘jumps” due to overcoming the static forces as illustrated in Figure 4.7 and 4.8. The robustness of the system in terms of achieving repeatable demoulding force results was checked with initial trials. The mould was screwed to the top plate and in order to have an automatic demoulding the bottom plate was sand blasted. The image of the sand blasted plate is presented in Figure 4.9. As explained in Chapter 2, during moulding the rough surface generates a high adhesion between the residual layer and the plate, and then during cooling the shrinkage of the polymer onto the surface roughness features ensures that the replica and the bottom plate will stay in contact while demoulding. The required roughness of the sand blasted plate was selected by a trial and error approach.

4.4 Model Implementation and Validation

The analytical model presented earlier to predict the demoulding force, F_d, was implemented employing the Matlab software. The following sub-sections describe initial experiments conducted to obtain the necessary data to calculate the demoulding force with the proposed model as well as the experimental demoulding force measurements achieved to test its validity.

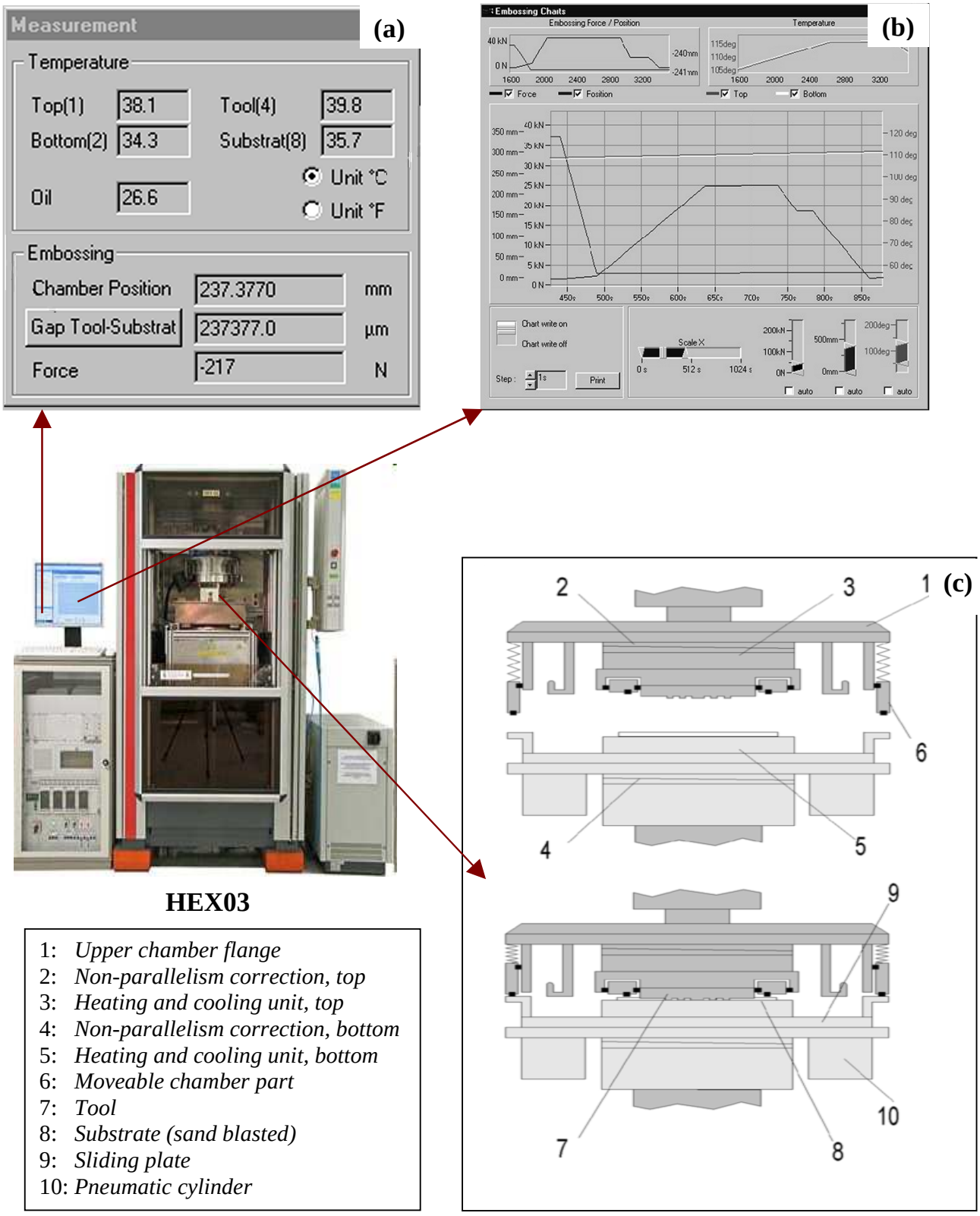

HEX03

1: *Upper chamber flange*
2: *Non-parallelism correction, top*
3: *Heating and cooling unit, top*
4: *Non-parallelism correction, bottom*
5: *Heating and cooling unit, bottom*
6: *Moveable chamber part*
7: *Tool*
8: *Substrate (sand blasted)*
9: *Sliding plate*
10: *Pneumatic cylinder*

Figure 4.7 HEX03 set-up (a) Parameter readings, (b) HE process chart and (c) HE machine parts.

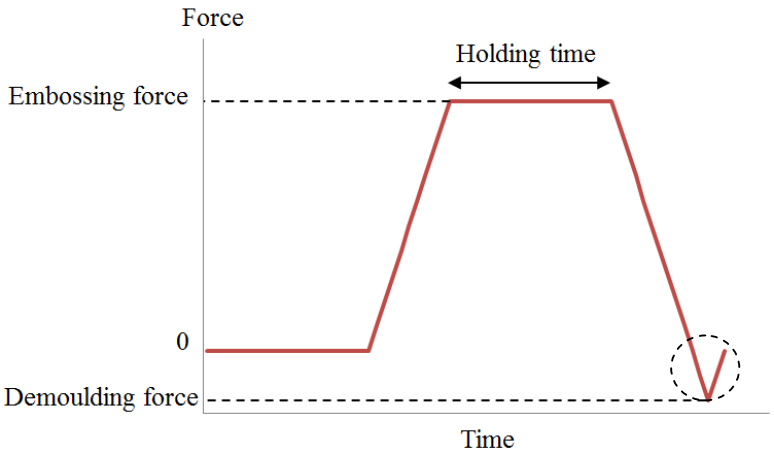

Figure 4.8 Typical force evolution during the HE process.

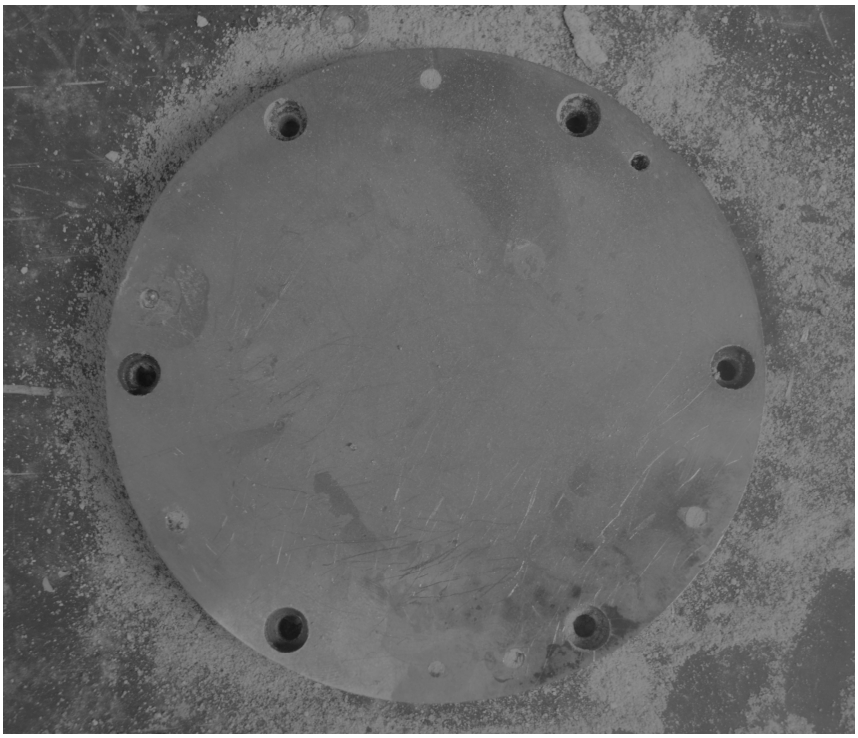

Figure 4.9 Sand blasted bottom plate.

4.4.1 Adhesion and stress-strain tests

The adhesive energy at zero shrinkage strain, γ, defined by Kendall (1973) and that is required in equation (4.3) was assessed by embossing a flat mould with no structures onto a circular PMMA sheet. In particular, the demoulding force required was measured without cooling and thus, for a T_{dem} value of 150°C. This force was assumed to include only the adhesion force component without any contributions from friction and deformation. Thus, based on equation (4.3) and by using 4 MPa and 0.49 for the Young modulus and Poisson's ratio values, respectively as well as by measuring the the thickness of the obtained replica, which was found to be 0.6 mm, γ was calculated to be equal to 13×10^{-3} J.m^{-2}.

Stress-strain tests were also conducted for different embossing loads at 150°C as shown in Figure 4.10. These tests were important to measure the final thickness and diameter of the embossed PMMA sheets that are required for the proposed model. The strain rate of the material was calculated by measuring the cross bar movement of the embossing machine.

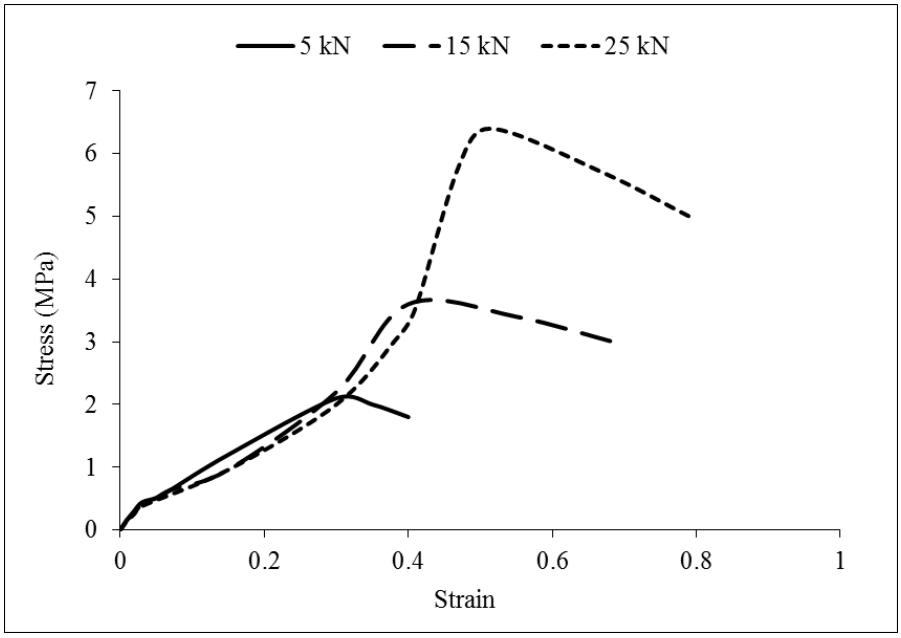

Figure 4.10 Stress strain curve for different embossing forces.

4.4.2 Effect of the embossing temperature on the demoulding force

The relationship between the demoulding temperature and the demoulding force is shown in Figure 4.11. More specifically, this figure provides a comparison between the results obtained experimentally and those predicted by the analytical model for a range of demoulding temperatures. From this figure, it can be observed that the predicted values agree well with the experimental results with an average error of 13%. The demoulding force decreases initially as the demoulding temperature is reduced until it reaches a minimum value, and then it increases, which is in-line with studies reported earlier. The initial force reduction is due to the decrease in the adhesion force with the reduction of the demoulding temperature. However, the further reduction of the temperature leads to an increase of the friction and deformation force components as they become more dominant.

It can also be seen from this figure that the analytical results underestimate the experimental demoulding force across the range of demoulding temperatures studied. This should be due to the fact that the model considers the pressure to be constant within the polymer during embossing while, in reality, it decreases during the holding stage of the process due to the creep time effect of the material. As a result, the pressure value used in the model is larger than the experimental one, which in turn, leads to the underestimation of the friction force. In addition, it is noticed that the larger difference between the analytical and the experimental results occur for the higher demoulding temperature of 90°C. This suggests that the calculated contribution of the adhesion force is less accurate at higher temperature. This result could be

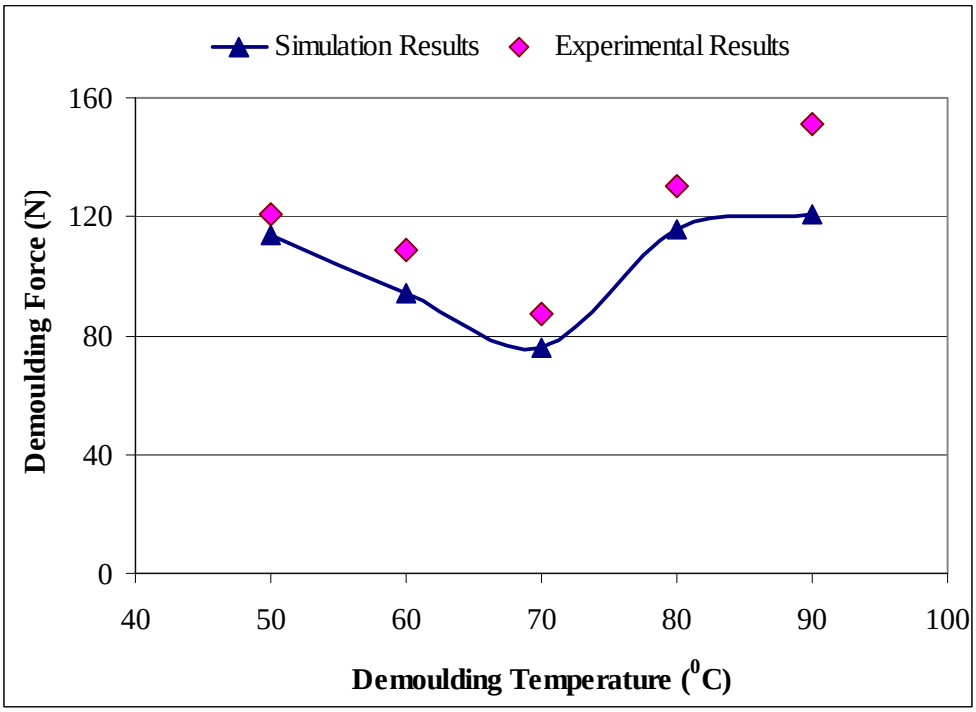

Figure 4.11 Comparison of experimental and analytical results as a function of the demoulding temperature.

explained by the fact that, as described earlier, the implementation of the adhesion force model relies on initial experimental data to assess the thickness and diameter of embossed replicas without any contributions from the friction and deformation phenomena. However, such data were obtained by measuring the displacement of the cross bar of the HE machine and thus, there could be a larger degree of uncertainty associated with these measurements.

4.5.3 Effect of the embossing load on the demoulding force

The comparison of the experimental and analytical results obtained to study the effect of the embossing force on the demoulding process is given in Figure 4.12. The applied force generates different flow stresses and, the higher the applied pressure is, in regards to the yield point of the polymer, the less strain recovery is taking place. Also, a higher pressure within the polymer, caused by a higher embossing force, reduces the shrinkage effect, which in turn leads to a reduced contact stress on the sidewalls of the structures. At the same time, a high embossing load also reduces the final thickness of the replica and enlarges its area, which consequently leads to an increase of the adhesion force. These phenomena can be observed in Figure 4.12. In particular, within the adhesion-dominated demoulding regime, i.e. at 90°C, the lowest demoulding force is achieved with the lowest embossing load of 5kN. This is due to the resulting smaller contact area and the reduced polymer shrinkage at this temperature. In contrast, in the friction-dominated regime, i.e. at 50°C, a higher embossing load of 25kN is required to achieve the lowest demoulding force. This can be explained with the fact that the higher pressure generated in the replica opposes the shrinkage effect. Again, a good agreement was achieved between the analytical and

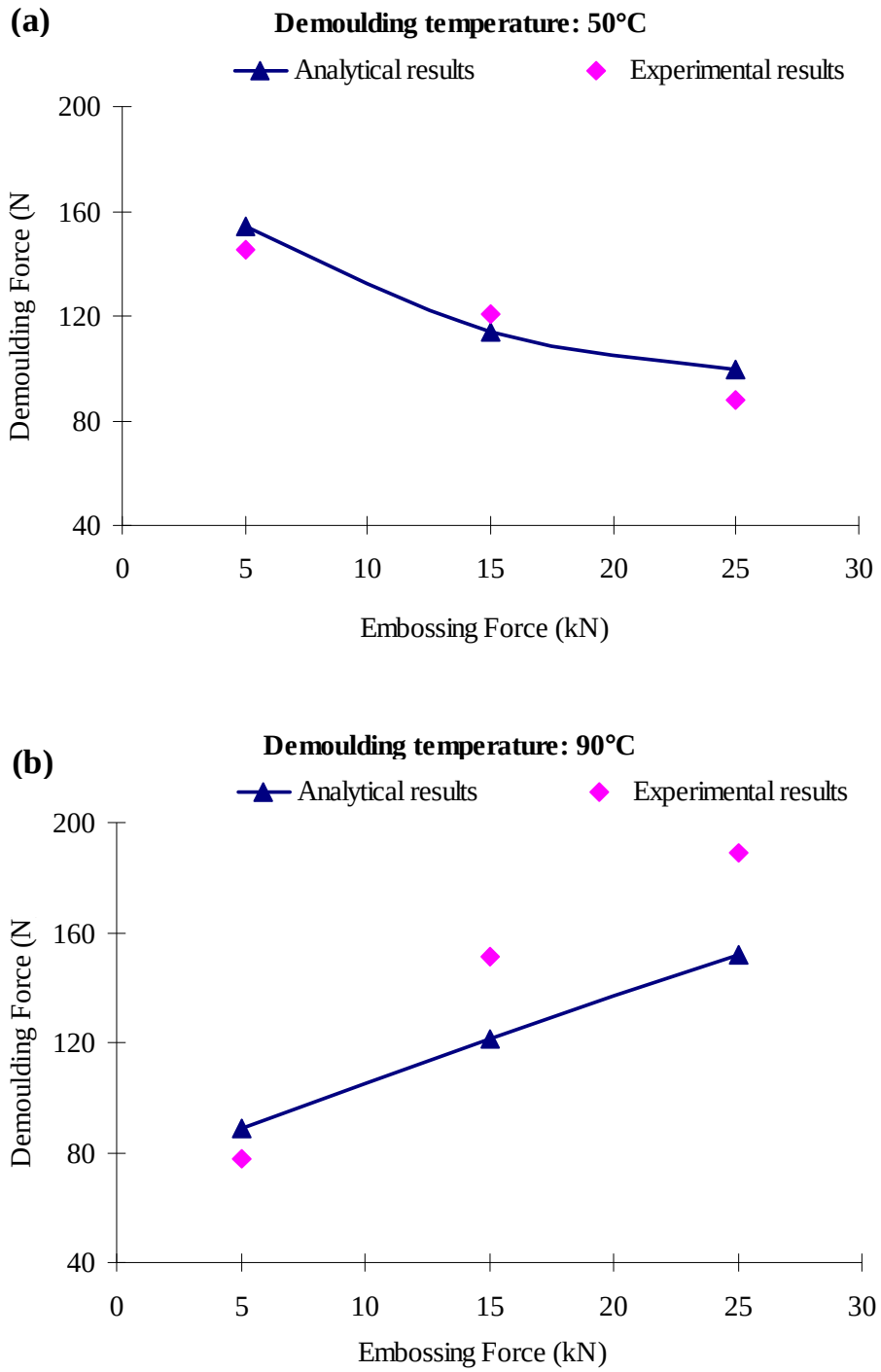

Figure 4.12 Comparison of experimental and analytical results for different embossing loads when demoulding at (a) 50°C and (b) 90°C.

experimental results with a combined average prediction error of 15%. The larger error between the analytical and experimental results observed in the adhesion-dominated regime at higher embossing loads (see Figure 4.12(b)) further supports the assumption put forward earlier that such discrepancies should be due to the less accurate experimental implementation of the adhesion force model adopted.

4.4.4 Effect of structure layout

As mentioned previously, two designs were considered in this study in order to assess the effect of structure layout on the demoulding force. The first design consisted of arrays of holes located in the middle and the second one had one array of holes located in the corner. The relationship between these designs and the demoulding force is presented in Figure 4.13. It can be seen from this figure that the demoulding force is higher at both adhesion and friction dominant temperatures for the design that incorporate structure located near the edge of the mould. The main reason for this difference is due to the fact that the thermal stress is higher at the edges. In addition, the difference in demoulding force between the designs was more pronounced more at 50 ^{0}C rather than at 90 ^{0}C because the friction force was higher at a lower temperature.

4.4.5 Comparison of simulation and experimental results

The differences between the simulation and experimental results can be explained with the idealised embossing conditions used to simplify the model. In practice, the following factors also contribute to the demoulding force:

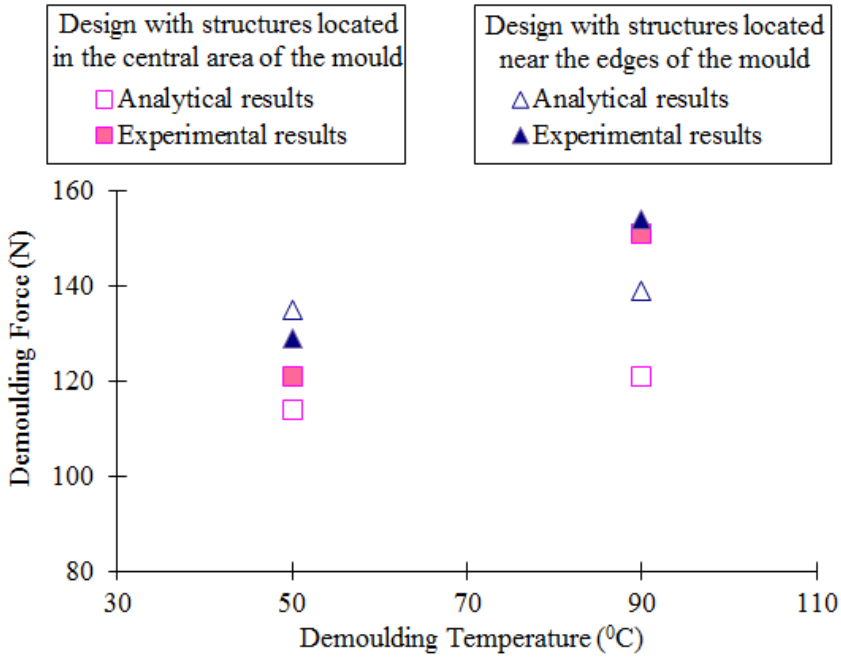

Figure 4.13 Comparison of experimental and simulation results for the structures located in the centre and edges of the mould.

- Embossing temperature: The moulding temperature influences the friction in particular via the viscosity of the polymer. A higher embossing temperature, contributes to a better filling of intricate surface features, which results in increased interlocking. This interlocking is reflected by an increased demoulding force. Initial experiments conducted by the author at different temperatures (120 ^{0}C, 150 ^{0}C and 180 ^{0}C) indicated that extremely high demoulding forces could be observed at high embossing temperatures while poor filling was detected at low temperatures.

- Holding time: During the velocity-controlled moulding step, the pressure gradient increases and reaches the maximum at the end of this moulding step. After switching to force-controlled moulding, the pressure gradient decreases with time, as the moulded area increases due to the creeping of the melt under a constant load. It is reported that at the end of a holding time of 280 seconds, the maximum pressure decreases by about 57% (Worgull *et al*. 2008). The model used for the prediction of the demoulding force does not consider the creep time effect; therefore the calculated pressure is much higher than the actual one. Consequently, the resulting lower pressure means that friction force should increase.

- Demoulding speed: Initial experiments carried out by the author revealed that the demoulding speed has an influence on the demoulding force. Three different velocities 0.5 mm/min, 1 mm/min and 5 mm/min were selected for trials. It was not possible to record any demoulding force at 5 mm/min due to high tensile velocity. At lower velocity of 0.5 mm/min it was also difficult to

detect any “jumps” in the force curve history, which is an indication that demoulding happens in a peeling movement. Tin this case the substrate can bend upwards and subsequently demoulds from the borders of the mould towards its centre.

4.4.6 Part Failure Analysis

As discussed in Chapter 2, the failures can be classified into three types: 1) filling defects, 2) cooling defects and 3) demoulding defects. The most critical failures occur during the demoulding step and can lead to overstretched structures, damaged edges and broken features. The reasons of these failures are high adhesion and friction force and undercuts between structure and mould during demoulding. During the movement of the crossbar the mentioned forces have to transfer over the cross section of the structures and this will result in stress inside these structures. It should be noted that this force is 2-4 times higher than the demoulding force detected. In the case of higher stress inside the structure compared to the yield point of the material at demoulding temperature, the structures will be deformed.

The above model could be improved to predict what failures can occur and taking this into account the mould design can be optimised. Overall, it would be better to demould at minimum demoulding force and to design larger structures in order to avoid the risk of failure. However, other factors should be considered such as very low demoulding temperatures which can induce bulges (Dirckx *et al.* 2010) and very high temperatures which can result in warpage due to high adhesion forces. The high demoulding temperatures should be still under T_g. Above T_g, amorphous polymers

enter a rubbery state in which they can support large deformations and still recover to nearly their original shape.

To characterise the quality and type of failure of embossed samples, an optical coordinate measuring machine was employed. The results for different demoulding temperatures from trial 1 to trial 5 are shown in Table 4.4. The optical coordinate measuring machine (OCMM) images are presented in Figure 4.14.

4.5 Summary

This chapter proposed a theoretical model to predict demoulding forces in hot embossing which provides a unified treatment of adhesion, friction and deformation phenomena that take place during demoulding of polymer microstructures. The close agreement between the predicted results and those measured experimentally suggests that the model successfully captures the relationship between mould design, feature sidewall, applied pressure, material properties, demoulding temperature and the resulting demoulding force. The model was implemented employing the Matlab software. The theoretical results have been confirmed through comparisons with the demoulding experiments using a HEX03 embossing machine. The temperature at which the demoulding force is minimised depends on the geometry of the mould features along with the material properties of the mould and replica. The applied embossing load has an important influence on the demoulding force as the increase in pressure augments the adhesion force due to changes in material dimensions and reduces the friction force due to resulting decrease in the thermal stress.

Table 4.4 Failure analysis of embossed samples

Demoulding Temperature	Overstretched structures	Damaged Edges	Broken structures
50 ^{0}C	**X**	**O**	**X***
60 ^{0}C	**O**	**O**	**3**
70 ^{0}C	**O**	**X**	**X**
80 ^{0}C	**O**	**X**	**15**
90 ^{0}C	**X**	**X**	**48**

X - Not detected

O - Detected

***** High stress was concentrated in the bond area of the structures and thus, the structures were bended. Simple tests by sliding the structures in contact with a flat surface showed that the structures were very fragile and easily broken. Thus, it was assumed that these were broken following demoulding.

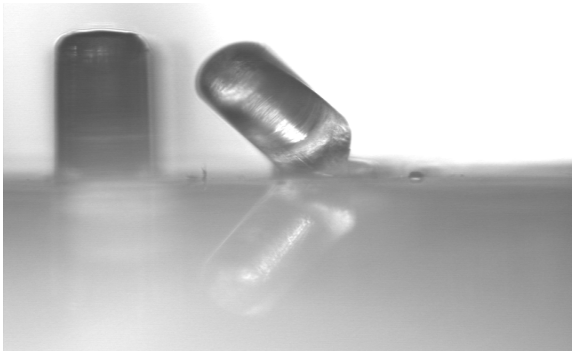

Broken structures

Overstretched

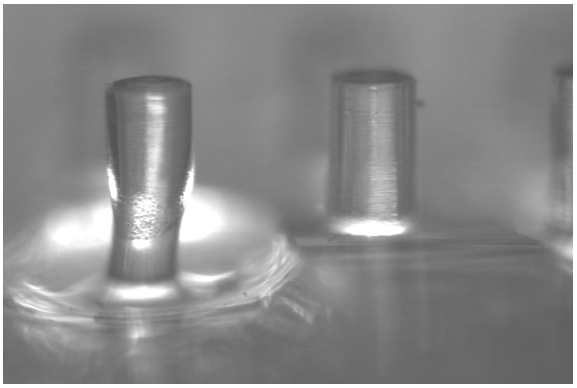

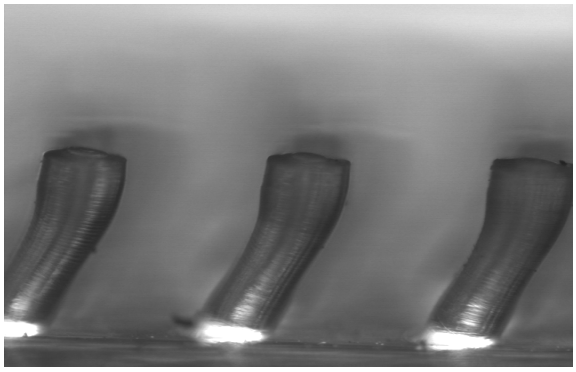

Bended structures

Damaged edges

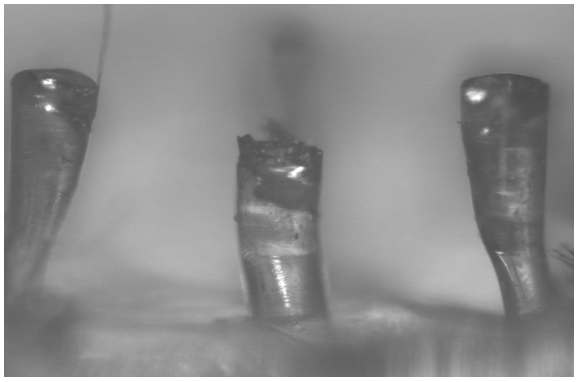

Figure 4.14 OCMM images of failed structures

CHAPTER 5

Simulation and Experimental Study of the Effects of Process Factors on the Uniformity of the Residual Layer Thickness in Hot Embossing

5.1 Overview

Hot embossing replica are characterised by the quality of the moulded structures and the uniformity of the residual layer. In particular, the even distribution of the residual layer thickness (RLT) is an important issue in HE and the related process of thermal nanoimprint lithography as variations in the RLT may affect the functionality or further processing of replicated parts. The influence of the machine, the mould, the polymer and the process parameters on the uniformity of the RLT is complex and has to be investigated systematically. In this context, the chapter presents an experimental and simulation study on the influence of three process factors, namely the moulding temperature, the embossing force and the holding time, on the residual layer homogeneity achieved when processing 2 mm thick PMMA sheets with HE. Using a design of experiments approach performed on both experimental and simulation data, the relation between process parameters and the resulting residual layer thickness is established.

The chapter is organised as follows. In the following section, the experimental

and simulation set-up, the mould, the selected material and the RLT measurement technique used in this research are described. The design of experiments together with the approach adopted to perform the trials and analyse the data are also presented. Finally, the results obtained are reported and the relationship between the process settings and the RLT achieved in HE are discussed.

5.2 Experimental set-up

In this study, the experiments were conducted with the HEX03 hot embossing machine from Jenoptik Mikrotechnik. The mould design, the polymer properties and the planning of the experiments were also used as input for the conducted simulation study in order to compare theoretical and experimental results. The particular simulation tool utilised in this research was the Simprint Core simulation software (Simprint Nanotechnologies Ltd 2012).

5.2.1 Mould design and fabrication

The structured area of the mould used was 28 mm x 28 mm and consisted of 16x16 arrays of transistor gate electrodes with different sizes. The depth of the gates was 500 nm and the width varied between 500 nm, 1μm and 2μm. The material used for the mould was nickel. An areal protrusion density of the stamp used with the Simprint Core Simulation software is shown in Figure 5.1.

The fabrication of the nickel mould was carried out using a process chain developed previously (Velkova *et al.* 2010; Hirshy *et al.* 2011 and Lalev *et al.* 2009).

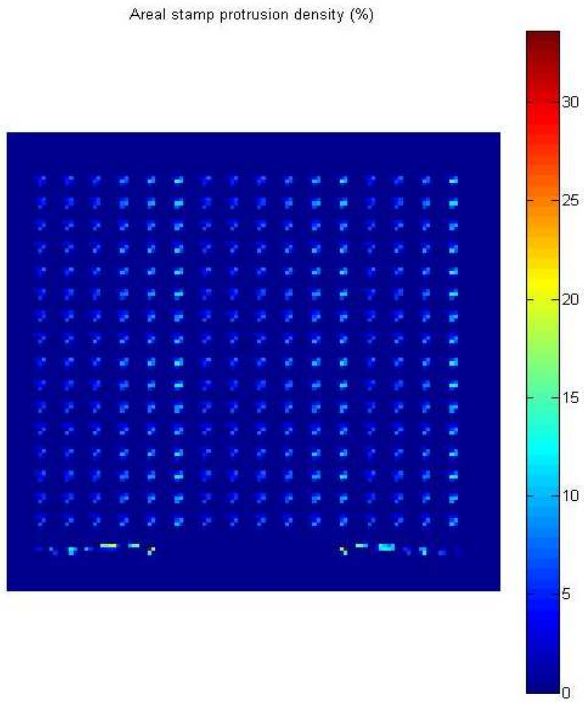

Figure 5.1 Areal stamp protrusion densities

This approach proved to be cost-effective for micro and nano structuring relatively large areas on nickel substrates with high dimensional accuracy and surface roughness. This process chain consists of three main steps: 1) template fabrication, 2) replication with UV imprint lithography using a step and repeat approach and 3) electroforming as illustrated in Figure 5.2.

Initially, a fused silica template was prepared to be utilised as a master for the UV- nanoimprint lithography step. After cutting a silica plate into a 65 mm x 65 mm square, mechanical grinding was used to produce a mesa with lateral dimensions of 30 mm x 30 mm and a height of 40 µm. The fabrication of the 28 mm x 28 mm structured area on the surface of the mesa was done in two stages: 1) micro structuring with photolithography and 2) nano-patterning with focused ion beam (FIB). Using conventional photolithography, a Microposit S1813 resist was spin-coated on the template at 4000 rpm and then baked at 97 °C for 2 min to achieve a thickness of ~1.8 µm. A Karl Suss mask aligner with a UV light wavelength of 365 nm was then used to expose the resist for 3s. The template was then dipped in the Microposit MF319 developer solution for 15s to remove unwanted resist. Next, the template was rinsed in deionised (DI) water and dried with N2 gas. The following step was to transfer the pattern into the fused surface by dry etching using an Oxford Instrument PlasmaPlus 80 Reactive Ion etcher (RIE). For this, a mixture of Trifluoromethane (CHF3 12sccm) and Argon (Ar 38sccm) at a pressure of 30 mTorr and a power of 200 W was used as the etching gas. An exemple of created microstructures following this photolithography process is given in Figure 5.3.

The nano structuring step was then performed with a Carl Zeiss XB 1540

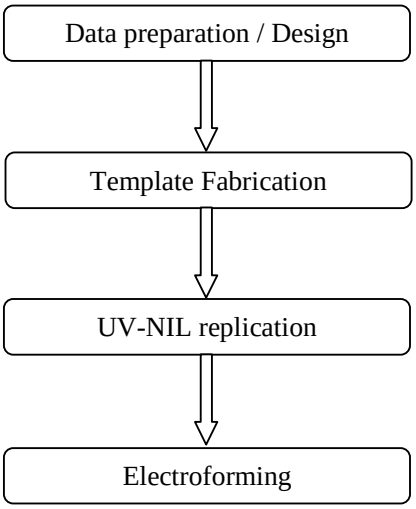

Figure 5.2 Process chain used to manufacture the hot embossing Ni mould.

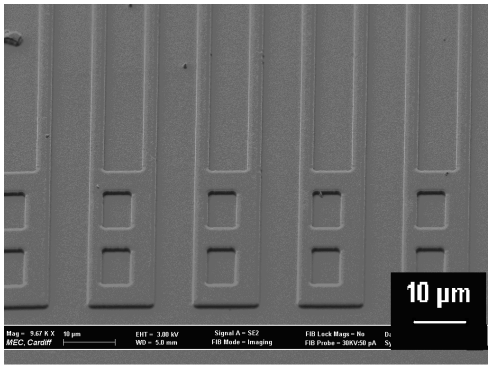

Figure 5.3 Microstructures produced by photolithography.

FIB/SEM cross beam system to add the features on the mesa which had widths comprised between 1 µm and 500 nm as shown in Figure 5.4. A 20 nm thick chromium layer was first sputter coated on the template surface to avoid any charging effects during the FIB machining. A range of FIB probe currents comprised bewteen 200pA and 2nA were used depending on the targeted feature size. Despite the low removal rates and consequently the long machining time associated with FIB milling, the process exhibits high resolution and high surface quality which are important characteristics when producing nano scale features on master moulds/templates (Li *et al.* 2007).

Following the completion of the FIB nano patterning step, the chromium layer was etched away and the fused silica template was loaded into the UV-imprint system for replication. A Molecular Imprints Imprio 55 S-FIL system was employed to imprint the template topography on an 8" wafer. Figure 5.5 shows a selected area of imprinted structures. The imprinting was performed on a double-sided polished silicon wafer spin-coated with a 60 nm thick layer of Transpin, which served as a planarization layer and a bottom anti-reflective coating.

Finally, a commercial electroforming system, Digital Matrix SA/1m, was utilised to produce the nickel mould. The micro and nano features were replicated by growing Ni on top of the imprinted wafer. This processing step allows the precise replication of micro and nano features in Ni-shim form (McGeough *et al.* 2001). The parameters used to carry out the electro chemical deposition are provided in Table 5.1. Figure 5.6 shows an example of some of the features replicated in Ni.

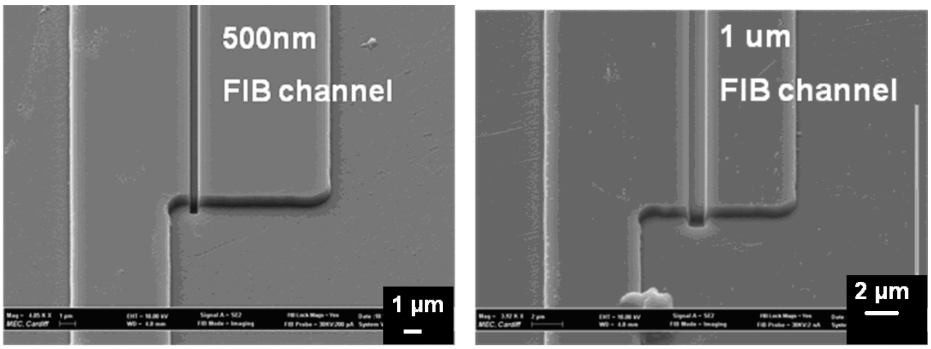

Figure 5.4 Sub-micron structures produced by FIB

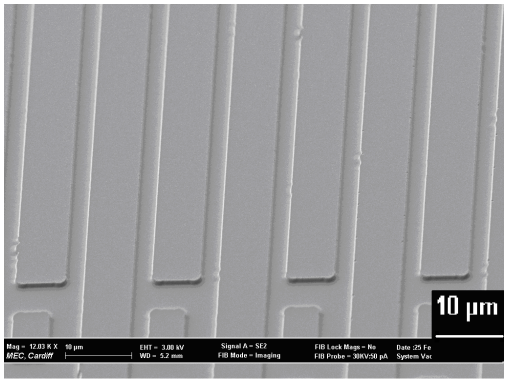

Figure 5.5 Structures replicated by UV-imprinting

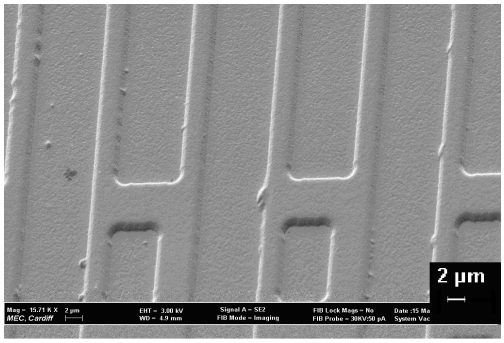

Figure 5.6 Replication of structures in Ni by electroforming

Table 5.1 Electroforming process parameters

Parameter	Value
Electrolyte	Nickel Sulfamate
Bath temperature	50 °C
Heat rotation speed	30 rpm
pH	3.96
Baume	37.8
Current density	0.1/0.5 A/dm^2
Waveform	Skipped down/ ramp down
Shim thickness	120 µm
Cycle time	10 ms

A Carl-Zeiss XB 1540 cross beam system was used to take SEM images of the features at each stage of the process chain to investigate the deviation in dimensions occurring after each step. To minimize the measurement errors all images were taken at the same magnification, 3 KV EHT, and at the same SEM aperture. The measured widths were found to be within 5% deviation of the targeted dimensions, revealing good compatibility between the steps within the process chain. Due to resolution it was not possible to employ the stamp design to NIL software. So, it was minimised to one square to achieve a desired resolution.

5.2.2 Test material

Two millimetre thick PMMA sheets were used for the HE experiments. The mechanical properties of PMMA are shown in Chapter 3 in Table 3.2.

5.2.3 Planning of experiments

The parameters considered in this study were the moulding temperature (T_m), the embossing force (F) and the holding time (t_h). Three levels were used for each of the selected three factors. Table 5.2 shows the 11 trials that were designed where a full factorial approach was employed for T_m and t_h. Two additional experiments were also conducted in which F was varied to provide an indication of its influence. The chosen range of parameters levels was determined based on material properties, initial simulation results, literature data and preliminary experiments in order to ensure complete filling of the mould cavities and stable behaviour of the replication set-up throughout the experiments. The rationale behind the selection of levels for the

temperature is provided in Chapter 3. In addition, preliminary tests showed that 5 kN could be used as the minimum force due to the shallow structures and also it was enough to avoid cooling and demoulding defects. Initial trials revealed that embossing loads more than 15 kN causes a bending on a the edges of the stamps. For each of the designed trials, three repetitions were performed. The combinations of the parameters' values for the selected three factors are provided in Table 5.2.

5.2.4 Residual layer thickness measurement

An optical coordinate measuring machine was employed to measure the residual layer thickness of the embossed samples. In particular, this was achieved by auto-focusing the optical head of the OCMM on the top and the bottom surface of the samples to record the height difference between two corresponding measured points on these surfaces. The accuracy of the OCMM when performing height measurements is stated to be 3 µm by the manufacturer of the system (Mitutoyo, 2004). For each embossed sample, 13 thickness values were obtained in this way from points distributed equally all over the surface of the PMMA replica including the edges and the middle area as shown in Figure 5.7. In order to ensure that the thickness values were consistently obtained from the same locations on each replica, measurement marks were engraved by laser machining on the nickel mould. To minimise measurement errors, the maximum magnification allowed by the instrument (x 212) was used to assess the height of the selected points.

Table 5.2 Process parameters design

Trial	T_m (°C)		F (kN)		t_h (min)	
1	A1	120	B2	10	C1	1
2	A1	120	B2	10	C2	5
3	A1	120	B2	10	C3	10
4	A2	150	B2	10	C1	1
5	A2	150	B2	10	C2	5
6	A2	150	B2	10	C3	10
7	A3	180	B2	10	C1	1
8	A3	180	B2	10	C2	5
9	A3	180	B2	10	C3	10
10	A2	150	B1	5	C2	5
11	A2	150	B3	15	C2	5

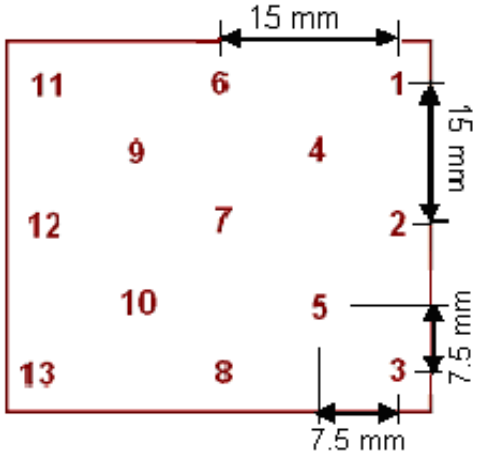

Figure 5.7 Selected measurement points

5.2.5 Simulation Software

During the last decade, the simulation of the thermal imprinting process gathered some interests. Different approaches have been used to simulate the embossing process. Efficient numerical simulations of the deformations of elastic and elastic-plastic bodies (Johnson, 1985 and Nogi and Kato, 1997) such as in contact mechanics have been widely used by researchers in tribology. These simulations rely on a description of the deformation of the material's surface in response to a point-load, together with, in the elastic-plastic cases, a criterion for yielding of the material. The Simprint Core software used for the simulation study was developed by Taylor and is based on the contact mechanics theory (Taylor *et al.* 2009). The stamp and substrate are modelled as linear-elastic and distinguished between local stamp/substrate indentation and stamp bending (Figure 5.8). The software is capable of modelling linear viscoelastic resists as well as simply Newtonian ones. It enables the prediction of elastic stamp deflections, pressure distribution and the formation of arbitrarily thin residual layers (see Figure 5.9). The accuracy of the simulation in HE is critically dependent on the viscosity of the polymer material studied. In this research, the typical viscosity values of PMMA depending on the shear rate and the temperature are taken from those given in Worgull (2009) and illustrated in Figure 5.10.

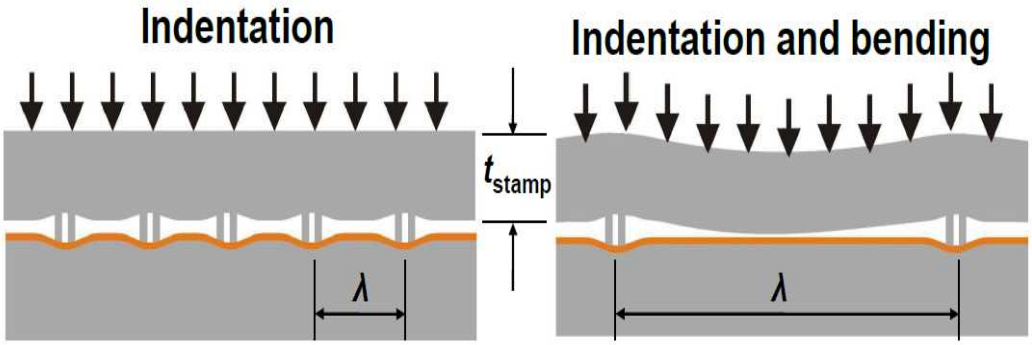

Figure 5.8 Stamp indentations and bending (Merino *et al.* 2008).

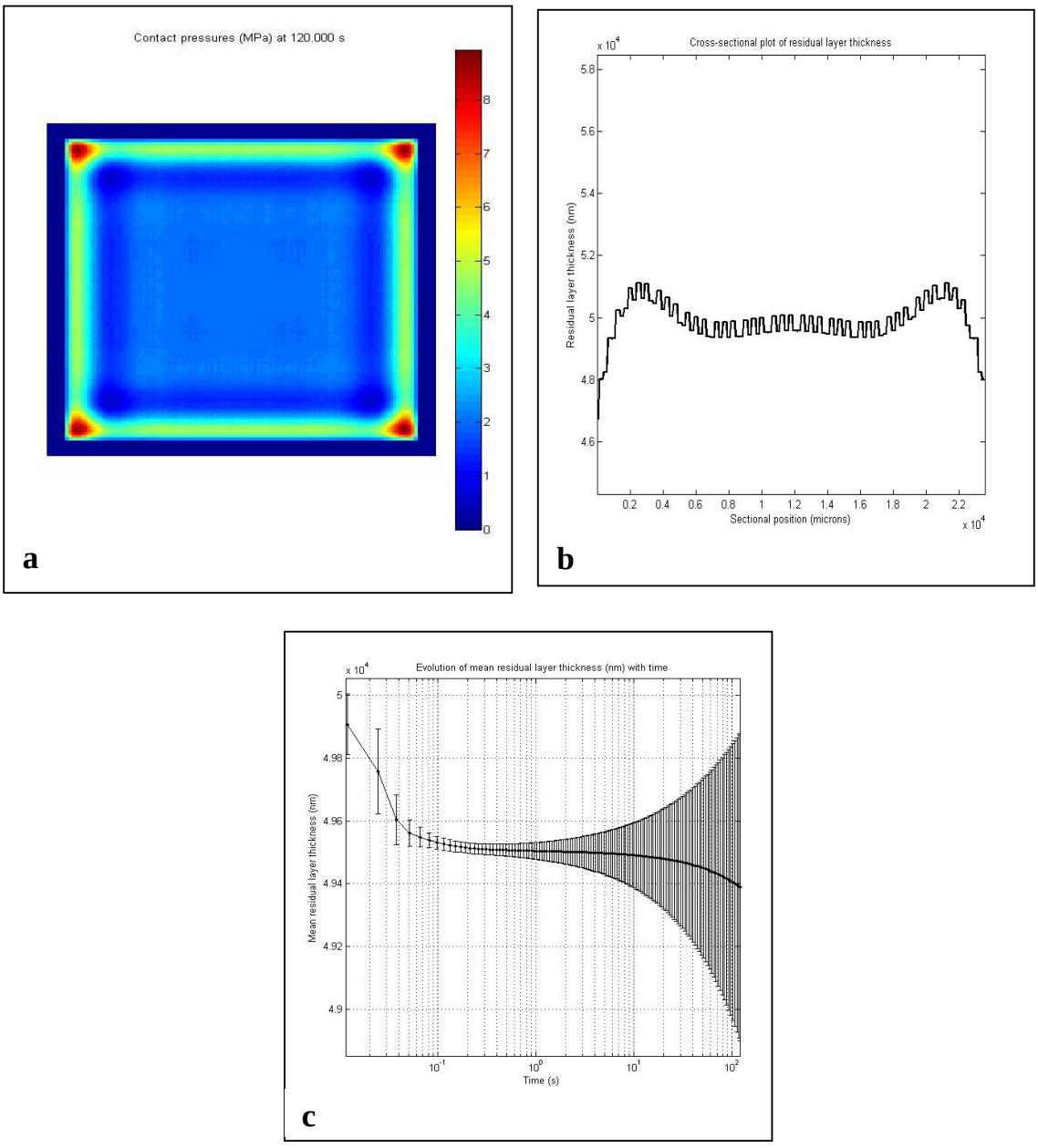

Figure 5.9 Simulation software results or a) pressure distribution b) cross section of residual layer c) mean residual layer thickness and deviation

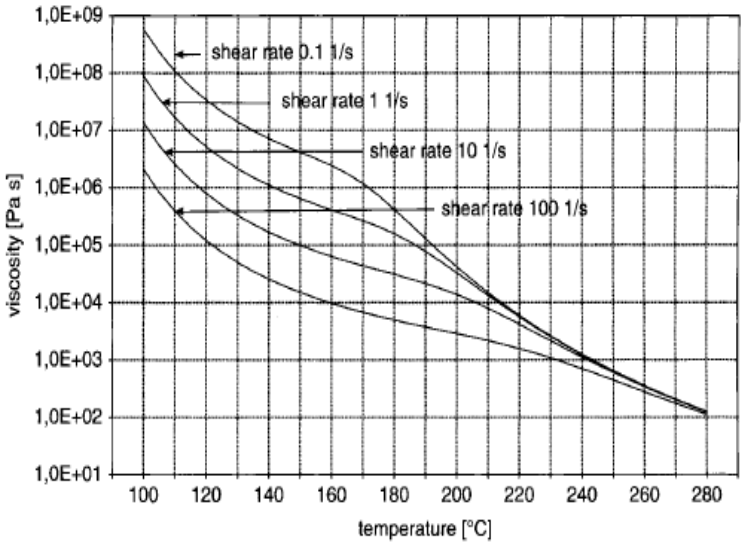

Figure 5.10 Viscosity model of PMMA (Worgull 2009).

5.3 Results and Discussion

5.3.1 Residual layer uniformity

Figure 5.11 shows an SEM image of a sample area of a replica. All the experimental trials exhibited a complete embossing of the mould structures. The RLT values obtained from the simulation and experiments are presented in Table 5.3. The uniformity of the RLT was assessed by calculating the ± one standard deviation of the measured data for each trial. Thus, an increased standard deviation value from one experimental trial to another implies a larger non-uniformity. By comparing the experimental results shown in Table 5.3, it can be observed that the selected values of the studied parameters have an effect on the resulting RLT of the embossed samples. In particular, the difference between the largest and lowest RLT standard deviation is 18 µm, which is higher than the accuracy of the OCMM used to carry out the measurements. The experimental results show that the highest measured RLT standard deviation was for trial 1, while the lowest was for trial 9, which respectively correspond to the trials with the lower and higher settings for T_m and t_h.

The experimental and simulation data show a relatively good agreement for the mean RLT as the average percentage difference between both sets of results is 14%. However, the simulation results do not predict an important RLT non-uniformity as the difference between the largest and lowest simulated RLT standard deviation is 2.2 µm, which is only 12% of its experimental counterpart, 18 µm. The highest and smallest simulated standard deviations occur for trials 10 and 11 respectively. These correspond to the experiments with the lower (trial 10) and higher

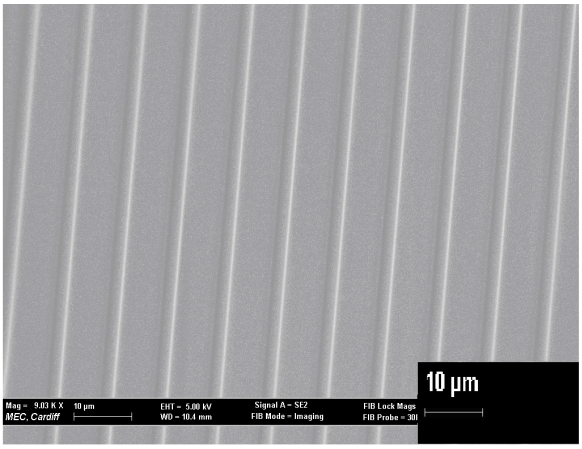

Figure 5.11 Example area on a hot embossed PMMA replica.

Table 5.3 Experimental and simulation results for the mean RLT and the RLT standard deviation

Trial	Experiments		Simulation	
	Mean RLT (µm)	RLT standard deviation (µm)	Mean RLT (µm)	RLT standard deviation (µm)
1	859	32	991	2.3
2	613	24	629	2.2
3	601	22	454	2.1
4	472	30	547	2.2
5	312	23	324	2.2
6	271	20	231	2.1
7	246	23	252	2.2
8	112	16	146	2.1
9	70	14	103	2.0
10	345	18	452	1.1
11	263	27	265	3.3

(trial 11) settings for the embossing force, F. This important difference between the predicted and experimental data can be explained with the fact that the simulated results reflect only local mould deflections. In practice, the following factors also contribute to the non-uniformity of the RLT:

- The roughness and flatness errors of the mould insert, the top plate and the bottom plate. In this study, through the application of grinding and lapping, the achieved values of roughness and flatness of the plates used were 0.5 µm Ra and 4 µm, respectively.

- The parallelism errors between the plates due to the machine set-up.

- The elastic deformation of the polymer during demoulding due to the release of the compression force applied by the mould. In particular, given the non-uniformity of the pressure distribution during embossing, this deformation can be inhomogeneous across the surface of the moulded polymer.

The experimental RLT standard deviation results for the different considered values of temperature (T_m) and embossing time (t_h) are presented in Figure 5.12. This figure clearly shows that an increase of T_m results in an improved RLT uniformity. This is an expected result given that the viscosity of a polymer is directly dependent on its processing temperature and thus reducing its viscosity value through an increase of its temperature will improve its flow behaviour. In particular, an increase in the temperature reduces the polymer internal stress and decreases its strength, which in turn eases the polymer flow during processing. This will lead to a reduced filling time

of the mould cavities and also will be beneficial to achieve a better uniformity of the RLT.

For both the predicted and experimental data obtained, the comparison between the results for the trials 5, 10 and 11, in which the moulding temperature and the holding time are constant parameters, show that the RLT uniformity reduces when the embossing force becomes larger. This can be explained by the fact that an increased embossing force results in a higher pressure gradient in the polymer and also in a larger deformation of the mould. The simulation results reported in Figure 5.13 show the increase in contact pressure distribution from an embossing force of 5 kN to 15 kN at a fixed processing temperature of 150°C and for an embossing time of 5 min, which are the conditions corresponding to trials 5, 10 and 11. Some initial simulation tests also showed that augmenting the embossing force always resulted in an increase of the RLT non-uniformity regardless of the different temperature or holding time values considered.

As mentioned earlier, due to its elastic behaviour, a polymer under compression tends to expand after releasing the load to which it is subjected at demoulding temperature. This results in variations in the RLT after demoulding which will be more pronounced in the central area of the processed polymer sheet where the applied pressure is the highest and negligible at the edges where the pressure is very low. In this work, the contribution of this shape change after demoulding is also assessed. To achieve this, the compression modulus, K, of the polymer can be calculated at demoulding temperature taking into account its temperature-dependent Poisson's ratio value, v, and Young's modulus, E (Worgull, 2009):

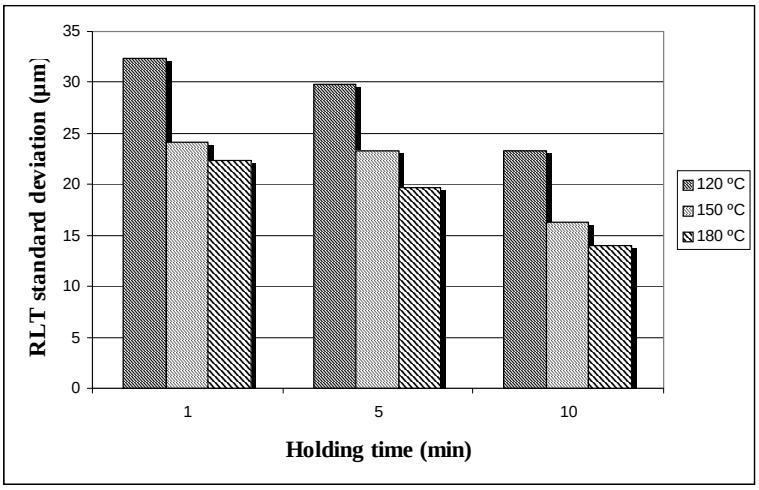

Figure 5.12 RLT uniformity plot for different values of temperature and holding time

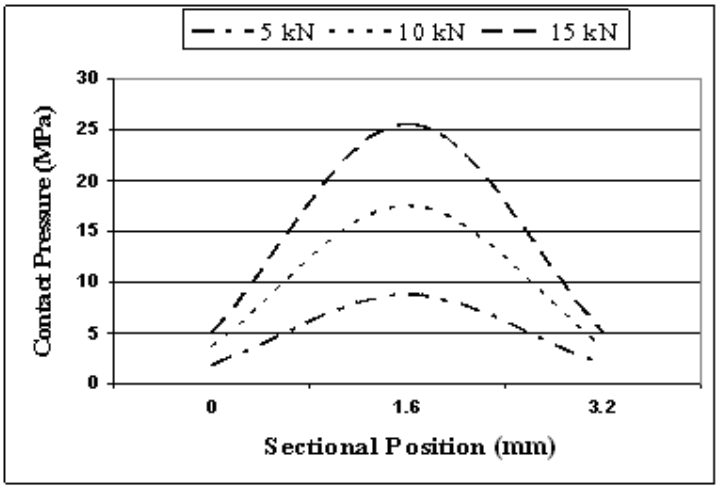

Figure 5.13 Cross sectional views of the simulated pressure distribution at applied embossing forces of 5 kN, 10 kN and 15 kN

$$K(t,T) = \frac{E(t,T)}{3(1 - 2\nu(T))} \tag{5.1}$$

In the conducted experiments, demoulding was carried out at 90ºC and in this case, the Young's modulus of PMMA is E = 2.4 GPa and its Poisson's ratio value is ν = 0.33. Thus, the compression modulus the processed polymer is calculated to be K = 2.35 GPa during demoulding. Given that demoulding takes place below the glass transistion temperature, T_g, of the polymer and that the range of embossing force considered in this work is too low to induce plastic deformation below T_g, it is assumed that a full elastic recovery will take place following release of the embossing load. The change of the thickness *dl* for an isotropic material can be determined as a function of the pressure variation to which it is subjected (Spetzler and Meyer, 1975):

$$K = V - \frac{dP}{dV} = \frac{-l}{dl/dP} \tag{5.2}$$

where *dl* is the value of the RLT variation due to compression. In this case, it is taken as the difference in the RLT before and after the release of the embossing force. *dP* is the difference between the pressure just before demoulding and the atmospheric pressure and *l* is considered to be the RLT after demoulding. The experimental and simulated results across the surface of the polymer and the simulated pressure distribution were employed to calculate *dl*. In this way, it was possible to estimate that the maximum percentage contribution of *dl* to the RLT standard deviation is 8% for the experiments and 45% for the simulation. The simulated pressure and RLT distributions at the end of embossing for the trial number 2 are shown in Figure 5.14 (a) and (b) respectively. In addition, based on equation (5.2) above, the calculated

RLT distribution taking into account polymer expansion after demoulding is provided in Figure 5.14 (c) and in this case, the predicted RLT standard deviation increases from 2.2 µm to 4 µm.

To assess the impact of the holding time on the RLT uniformity, 3 different values (1, 5 and 10 mins) were used for each temperature range. From the results shown in Figure 5.12, it can be said that increasing the holding time improved the RLT uniformity. This can be explained by the viscoelastic creeping behaviour of polymers. In particular, as creep is a time-dependent phenomenon, the polymer deformation will increase and the pressure gradient will decrease when extending the time during which the embossing load is applied (see Figure 5.12).

5.3.2 Main effects and response table

Figure 5.15 and Table 5.4 present respectively the main effect plot and the response table of the process parameters on the RLT standard deviation. It is observed from this figure that an increase of T_m *and* t_h improves the RLT uniformity, while an increase of F has the opposite effect. From the response table provided, it is apparent that the most influential process parameter is different based on the levels considered. In particular, the temperature was the least important factor when it is increased from 120°C to 150°C, while it became the most influential parameter between 150°C to 180°C. The applied force was the second most influential factor in all cases. Finally, increasing the holding time from 1 to 5 mins had the highest impact on the RLT uniformity when comparing parameters between levels 1 and 2, while this effect was not so pronounced when its value varied between 5 and 10 mins. When comparing

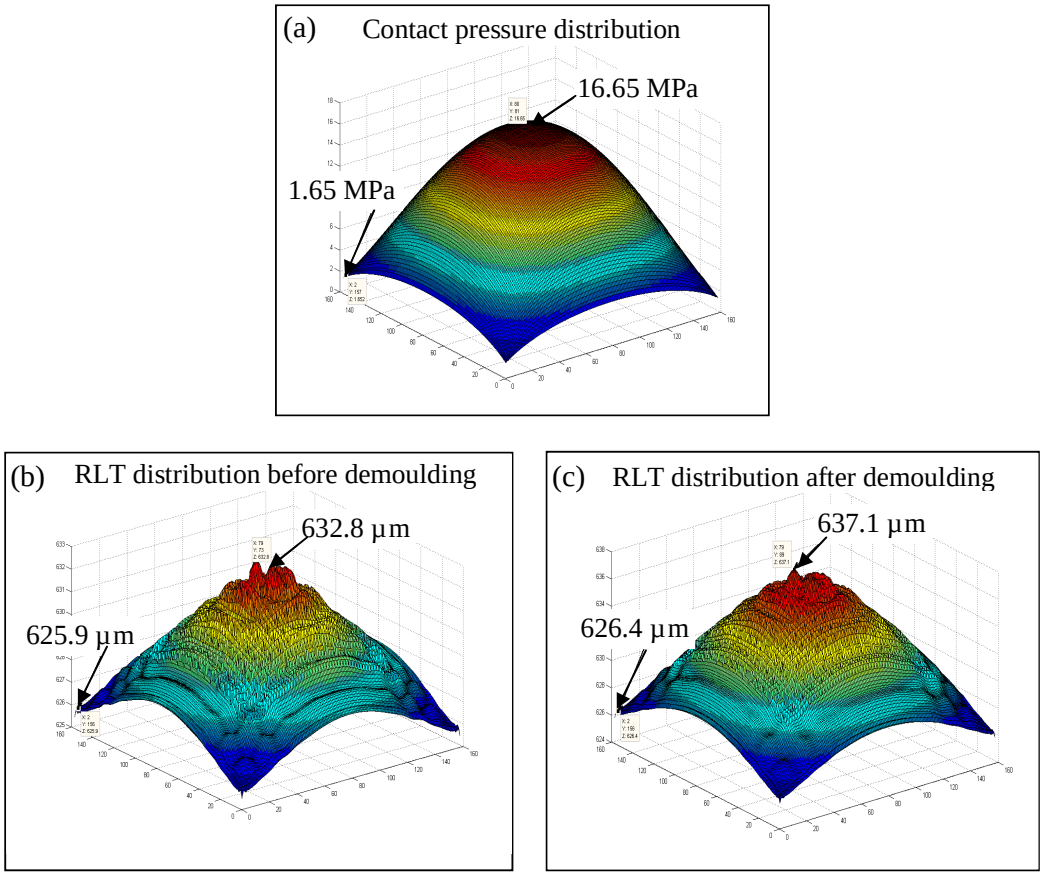

Figure 5.14 (a) Pressure distribution, (b) RLT distribution under load and (c) RLT distribution after the release of the embossing force.

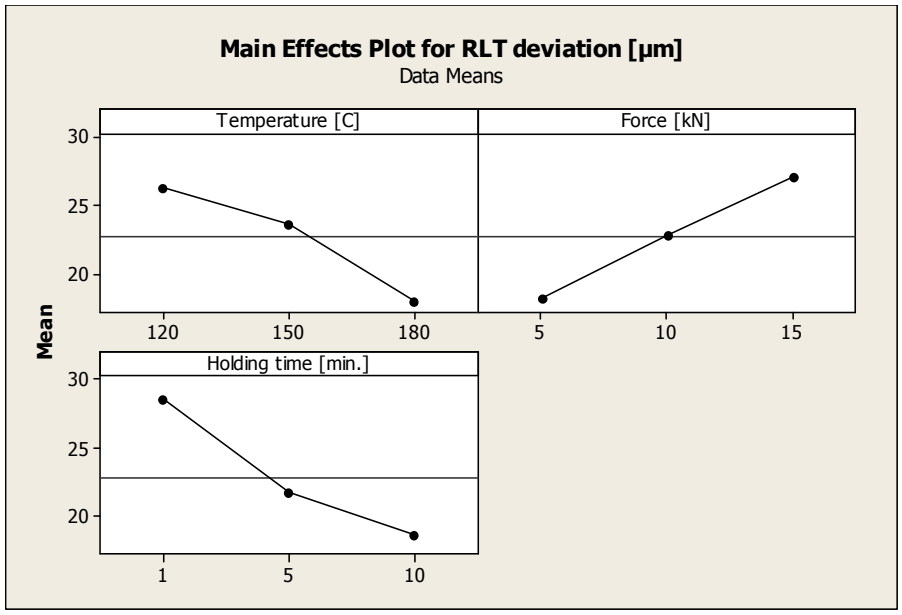

Figure 5.15 Main effect plots for the RLT standard deviation

Table 5.4 Response table for the RLT standard deviation

		T_m	F	t_h
Levels	Level 1 (µm)	26.3	18.2	28.5
	Level 2 (µm)	23.6	22.8	21.8
	Level 3 (µm)	17.9	27.0	18.7
Comparison between levels 1 and 2	Difference (µm)	2.7	4.6	6.7
	Difference (%)	10	20	24
	Rank	**3**	**2**	**1**
Comparison between levels 2 and 3	Difference (µm)	5.7	4.2	3.1
	Difference (%)	24	16	14
	Rank	**1**	**2**	**3**
Comparison between levels 1 and 3	Difference (µm)	8.4	8.9	9.8
	Difference (%)	32	33	35
	Rank	**3**	**2**	**1**

results between levels 1 and 3, i.e. across the whole range of processing values studied, it can be observed that the considered three parameters have a relatively equal influence on the RLT distribution.

Finally, the theoretical optimum set of parameter levels to achieve the lowest RLT standard deviation for this experimental set-up was determined based on the results provided in Figure 5.15 and corresponds to 180°C, 5 kN and 10 mins for T_m, F and t_h respectively. A verification experiment was further conducted with this theoretical best combination of parameters and resulted in a RLT standard deviation of 10.6 µm. By comparing this result with those reported in Table 5.4, in which the lowest standard deviation is 14 µm, this experiment confimed that the identified parameters were the optimum combination with respect to the RLT uniformity.

5.4 Summary

In addition to the quality of the moulded structures, the achieved RLT uniformity is an important process output in hot embossing. The analysis of the literature on this subject revealed that the influence of the process parameters on the homogeneity of the RLT has not been systematically studied. In this context, using simulation and experimental studies, this work investigated the relationship between the residual layer uniformity and three process parameters when processing PMMA sheets. In particular, the characteristics of the RLT of embossed parts were analysed as a function of the moulding temperature, the embossing force and the holding time. Increasing the moulding temperature resulted in a reduction on the average residual layer thickness and on its non-uniformity. An increase in the embossing force led to a decrease in the homogeneity of the residual layer. Also, an improvement of the RLT uniformity was observed when embossing with a longer holding time. The results of the conducted experimental and simulation studies were analysed to identify potential ways for optimising the HE process.

CHAPTER 6

CONCLUSIONS

This chapter summarises the main contributions and the conclusions reached in this study. It also provides suggestions for future work.

6.1 Contributions

This research is an original contribution to the field of hot embossing. The effects of process parameters on specific issues of cavity pressure, demoulding force and residual layer thickness were examined and the following contributions were made to the current state-of-the-art:

Process Factors Influence on Cavity Pressure Behaviour in Hot Embossing

a. **Addressing the relationship between the process parameters, namely embossing force, embossing temperature and holding time, and the resulting pressure conditions.** A thorough investigation of he influence of process parameters on cavity pressure and pressure distribution was carried out. In particular, an experimental study was conducted to investigate the

response of pressure conditions in cavities when replicating parts in PMMA and ABS.

b. **Developing a specially designed condition monitoring system that offers a comparative assessment of pressure distribution during embossing.** An indirect measurement method was conducted to assess pressure variations in the centre and the edge of the mould. The set-up on the HEX03 machine was modified to accommodate an ejector assembly system previously used in a micro injection moulding machine and enabled the integration of the condition monitoring system.

c. **Proposing a new simple model to calculate the minimum required force to fill all cavities over the mould surface.** Using a simple analytical model and considering the pressure distribution, the minimum embossing force to fill the cavities across the mould surface was calculated. The theoretical value obtained was then used to feed the design of the experiments.

Modelling, Simulation and Validation of Demoulding Force in Hot Embossing

d. **Developing a new analytical model to simulate the demoulding force in hot embossing.** The distinguishing characteristic of the proposed model lies in integrating the contributions from the adhesion, friction and deformation phenomena that take place when demoulding microstructures. The advanced simulation model was constructed to predict the combined effects of material properties, demoulding temperature, pressure, mould design, sidewall

geometry and adhesion on the demoulding force. The model was implemented employing the Matlab software. The theoretical results have been confirmed through comparisons with demoulding experiments using a HEX03 embossing machine. The close agreement between the predicted results and those measured experimentally suggests that the model successfully captures the relationship between the mentioned factors and the resulting demoulding force.

Simulation and Experimental Study of the Effects of Process Factors on the Uniformity of the Residual Layer Thickness in Hot Embossing

e. **Conducting a simulation and experimental study of the effect of process factors on the residual layer uniformity of embossed parts.** By utilising a simulation and experimental approach, this work investigated the relationship between the residual layer uniformity and three process parameters when processing PMMA sheets. In particular, the characteristics of the RLT of embossed parts were analysed as a function of the moulding temperature, the embossing force and the holding time. The results of the conducted experimental and simulation studies were compared and analysed also to investigate the influences of the mould local deflections and polymer spring back effects. Consequently, potential ways were identified for improving the hot embossing process with respect to the RLT uniformity.

6.2 Conclusions

The following conclusions can be drawn based on the work in the areas of:

Process Factors Influence on Cavity Pressure Behaviour in Hot Embossing

- It is possible to assess cavity pressure conditions during part filling by employing a specially designed condition monitoring set-up.

- The obtained results show that an increase in T_m and t_h reduced P_c, P_e, and ΔP while the opposite effect takes place for F.

- The standard deviation of the measured data indicates that the process parameters have a greater influence on P_c for ABS and on P_e for PMMA.

- With respect to the cavity pressure in the centre of the mould, across all levels, the embossing force appears to be the most influential parameter for ABS while for PMMA, the holding time is found to have slightly more effect than the embossing force.

- For the cavity pressure on the edge of the mould, the embossing force was observed to be the most effective parameter for both materials.

- The measured results to characterise the difference between the cavity pressure in the centre and in the edge of the mould showed that the embossing

temperature dominates as the most influential parameter for ABS, while for PMMA, it is the holding time.

- Consequently, an increase in P_c and P_e by F is favourable due to its contribution to cavity filling. On the other hand, an increase in ΔP is not desirable because of the resulting in non-uniform filling. Thus, it can be concluded that an increase in the embossing force has a positive effect on cavity filling but a negative influence for homogenous filling. That is why it is important to select the optimum embossing load that takes into account P_c, P_e and ΔP.

This study can help users to understand the pressure behaviour during the embossing which in turn provides a better insight into the dynamics of the process. Pressure can be used as an output parameter which depends on force, temperature and time together for optimising the process for different polymers. As it can be seen from the above conclusions, different materials react differently to the embossing conditions. The results of this research show that it is possible to achieve a complete and uniform filling over the moulding area; these can be especially helpful while replicating large area moulds with high aspect ratio structures.

Modelling, Simulation and Validation of Demoulding Force in Hot Embossing

- The proposed model has proven its feasibility to predict demoulding forces in hot embossing by providing a unified treatment of adhesion, friction and deformation phenomena.

- The study showed that the predicted values agree well with the experimental results with an average error of 14%.

- The theoretical results show that the demoulding force decreases initially as the demoulding temperature is reduced until it reaches a minimum value, and then it increases with the further reduction of the temperature, which is in-line with studies reported earlier.

- The results confirm also that the design of the mould affects the resulting demoulding force. In particular, it is was observed that the demoulding force is higher, at both adhesion and friction dominant temperatures, for the design that incorporate structures located near the edge of the mould compared to the design having the structures located in the central area

- Additionally, the applied embossing load was observed to have a significant effect on demoulding. More specifically, the increase in pressure within the polymer raises the adhesion force while it also reduces the friction force due to the consequent decrease in the thermal stress.

- Another important point is that the temperature at which the demoulding force is minimised depends on the geometry of the mould features along with the material properties of the mould and replica.

- Overall, it can be concluded that the developed model can provide useful information on the mechanisms that influence the demoulding force required in hot embossing by considering the effects of mould design, feature sidewall, applied pressure, material properties and demoulding temperature.

This study expands that state-of-the-art on the modeling of the demoulding force by considering the different complicated phenomena which have an important effect on the final results. The developed model shows a potential for predicting demoulding force with a low error and this can be applied to optimize the input parameters and material properties in order to avoid demoulding defects. Demoulding force is an output of different factors and by implementing this model users can obtain a clear indication of the effects of these factors separately.

Simulation and Experimental Study of the Effects of Process Factors on the Uniformity of the Residual Layer Thickness in Hot Embossing

- Increasing the moulding temperature resulted in a reduction on the average residual layer thickness and on its non-uniformity. This is directly related to the fact that polymer flow is improved at elevated temperature.

- An increase in the embossing force led to a decrease in the homogeneity of the residual layer. It is expected that this is caused by the increased pressure gradient at higher compression forces which can result in mould deformation and a more pronounced polymer recovery between the central and boundary area of the processed sheet.

- An improvement of the RLT uniformity was also observed when embossing with a longer holding time. This should be the result of the polymer creep effect under load.

- The comparison between the obtained experimental and simulation results suggest that approximately 12% of the RLT uniformity is affected by the local deflections of the mould.

- For the studied set-up, it was calculated that polymer expansion after release of the embossing load contributes to 8% of the RLT non uniformity. This value is calculated to be 45% for the ideal conditions where the plates and the mould are completely flat, parallel and uniform.

- Generally, it can be concluded that a better uniformity of the RLT could be achieved by using the highest selected settings for the temperature and holding time and the lowest value of embossing force.

- Finally, the analysis of the obtained results also shows that, across the range of processing values studied, the considered three parameters have a relatively equal influence on the RLT distribution. However, when examining narrower ranges of processing values, it is apparent that the most influential process parameter depends on the levels considered. In particular, the holding time had the most effect on the RLT uniformity when embossing with the lower values

of process parameters while, with higher processing settings, the moulding temperature became the most influential factor.

This study further develops the research carried out on the geometric accuracy of the replicated parts in hot embossing. It can be seen from the results obtained that the RLT is very sensitive to the above mentioned factors and important variations can occurr which can be detrimental for the replica specifically for optical devices. The research study shows a systematic analysis of the results which can be applied to optimise the process parameters in order to achieve highly uniform residual layers and improve the functionality of the products.

6.3 Recommendations for Future Work

Based on the work presented in this thesis, some ideas for future research work have been identified as follows:

- Investigating the cavity pressure behaviour during the cooling and demoulding stage in order to further understand the process dynamics.

- Developing the proposed simple analytical model for predicting the minimum required force to fill the cavities to a more advanced level by considering the material following a power law relationship.

- Expanding the demoulding force model for capturing the effects of embossing temperature, flow stress and demoulding.

- Developing the proposed demoulding force model to be employed as a tool to help optimising the hot embossing process by predicting the occurrence of polymer part defects, damages and failures.

- Investigating the effect of additional factors such as the flatness error of the mould and plates on the influence of the RLT process parameters studied.

- Developing a RLT simulation model that takes into account the spring back phenomena for predicting the residual layer uniformity

REFERENCES

Adithyavairavan M. and Subbiah S., 2011, "A morphological study on direct polymer cast micro-textured hydrophobic surfaces", *Surface & Coatings Technology,* 205, pp. 4764-4770.

Austin M. D., Ge H., Wu W., Li M., Yu Z., Wasserman D., Lyon S. A. and Chou S. Y., 2004, "Fabrication of 5 nm linewidth and 14 nm pitch features by nanoimprint lithography", *Applied Physics Letters,* 84, pp. 5299-5302.

Becker H. and Heim U., 2000, "Hot embossing as a method for the fabrication of polymer high aspect ratio structures", *Sensors and Actuators,* A 83, pp. 130-135.

Bharat Bushan, 2003, "Adhesion and stiction: Mechanisms, measurement techniques, and methods for reduction", *Journal of Vacuum Science & Technology,* B 21, pp. 2262-2296.

Bogdanski N., Schulz H., Wissen M., Scheer H.-C., Zajadacz J. and Zimmer K., 2004, "3D-Hot embossing of undercut structures – an approach to micro-zippers", *Journal of Microelectronic Engineering,* 73–74, pp. 190-195.

Cao D. M., Meng W. J., and Kelly K. W., 2004, "High-temperature instrumented microscale compression molding of Pb", *Microsystem Technologies,* 10, pp. 323-328.

Chang J.-H. and Yang S.-Y., 2003, “Gas pressurized hot embossing for transcription of micro-features”, *Microsystem Technologies*, 10, pp. 76-80.

Chien R.-D., 2006, “Hot embossing of microfluidic platform”, *International Communications in Heat and Mass Transfer*, 33, pp. 645-653.

Chou S. Y., Krauss P. R. and Renstrom P. J., 1995, “Imprint of sub 25 nm vias and trenches in polymers” *Applied Physics Letters*, 67, pp. 3114-3117.

Colton J. S., Crawford J., Pham G., Rodet V. and Wang K. K., 2001, “Failure of rapid prototype molds during injection molding”, *CIRP Annals*, 50, pp. 129-132.

Cui B. and Veres T., 2006, “Pattern replication of 100 nm to millimeter-scale features by thermal nanoimprint lithography”, *Microelectronic Engineering*, 83, pp. 902-905.

Datta P. and Goettert J., 2006, “Method for polymer hot embossing process development”, *Microsystem Technologies*, 13, pp. 265-270.

Delaney K., Bisacco G. and Kennedy D., 2010, “A study of demoulding force prediction applied to periodic mould surface profiles” *Society of Plastics Engineers Annual Technical Conference ANTEC 2010, Orlando, Florida*, pp. 1279-1284.

Derjaguin B. V., Muller V. M. and Toporov Y. P., 1975, “Effect of contact deformations on the adhesion of particles”, *Journal of Colloid and Interface Science*, 53, pp. 314-326.

Dirckx M. and Hardt D. E., 2011, “Analysis and characterization of demolding of hot embossed polymer microstructures”, *Journal of Micromechanics and Microengineering*, 21, pp. 1-10.

Dirckx M., 2010, “Demolding of hot embossed polymer microstructures”, *PhD Thesis Mechanical Engineering*, Massachusetts Institute of Technology, Cambridge, MA.

Dirckx M., Taylor H. K. and Hardt D. E., 2007, “High-temperature de-molding for cycle time reduction in hot embossing”, So*ciety of Plastics Engineers Annual Technical Conference ANTEC 2007, Cincinnati, Ohio*, pp. 2926-2930.

Elkaseer A. M., Dimov S. S., Popov K. B., Negm M. and Minev R., 2012, “Modeling the material microstructure effects on the surface generation process in microendmilling of dual-phase materials”, *Journal of Manufacturing Science and Engineering*, 134, 044501, (10 pages).

Elkaseer A., 2011, “Modelling, Simulation and Experimental Investigation of the Effects of Material Microstructure on the Micro-Endmilling Process”, *PhD thesis*, Institute of Mechanical and Manufacturing Engineering, Cardiff University.

Esch M. B., Kapur S., Irizarry G. and Genova V., 2003, “Influence of master fabrication techniques on the characteristics of embossed microfluidic channels”, *Lab on a Chip*, 3, pp. 121-127.

Focke M., Kosse D., Al-Bamerni D., Lutz S., Muller C., Reinecke H., Zengerle R. and

Stetten F., 2011, “Microthermoforming of microfluidic substrates by soft lithography (μTSL): optimization using design of experiments”, *Journal of Micromechanics and Microengineering*, 21, pp. 1-11.

Gao H., Tan H., Zhang W., Morton K. and Chou S. Y., 2006, “Air Cushion Press for Excellent Uniformity, High Yield, and Fast Nanoimprint Across a 100 mm Field”, *Nano Letters*, 6, pp. 2438-2441.

Gerberich W. W. and Cordill M. J., 2006, “Physics of Adhesion”, *Reports on Progress in Physics*, 69, pp. 2157-2203.

Giboz J., Copponnex T. and Mcle P., 2007, “Microinjection molding of thermoplastic polymers: a review”, *Journal of Micromechanics and Microengineering*, 17, pp. 96-109.

Griffiths C. A., Dimov S. S., Scholz S., Hirshy H. and Tosello G., 2011, “Process factors influence on cavity pressure behaviour on microinjection moulding” *Journal of Manufacturing Science and Engineering*, 133, 031007 (10 pages).

Guan W.-S., Huang H.-X. and Wu Z., 2012, “Manipulation and online monitoring of micro-replication quality during injection-compression molding”, *Journal of Micromechanics and Microengineering*, 22, pp.1-10.

Tosello G., 2008, “Precision moulding of polymer micro components”, *PhD Thesis*, DTU department of Mechanical Engineering, Denmark.

Guo J. L., 2007, “Nanoimprint Lithography: Methods and Material Requirements”, *Journal of Advanced Materials*, 19, pp. 495-513.

Guo Y., Liu G., Xiong Y. and Tian Y., 2007a, “Study of the demolding process - implications for thermal stress, adhesion and friction control”, *Journal of Micromechanics and Microengineering*, 17, pp. 9-19.

Guo Y., Liu G., Xiong Y., Jun W., Xilong H. and Tian Y., 2007b, “Study of hot embossing using nickel and Ni-PTFE LIGA mold inserts”, *Journal of Microelectromechanical Systems*, 16, pp. 589-597.

Guo Y., Liu G., Zhu X. and Tian Y., 2007c, "Analysis of the demolding forces during hot embossing," *Microsystem Technologies*, 13, pp. 411-15.

Hansen H. N., Hocken R. J. and Tosello G., 2011, “Replication of micro and nano surface geometries”, *CIRP Annals - Manufacturing Technology*, 60, pp. 695-714.

Hardt D. E., Anthony B. W. and Tor S. B., 2010, “A teaching factory for polymer micro-fabrication - µFAC”, *Journal of Nanomanufacturing*, 6, pp.137-151.

He Y., Fu J.-Z. and Chen Z.-C., 2005, “Research on modeling of hot embossing polymeric microfluidic chip”, *Journal of Zhejiang University (Engineering Science)*, 39, pp.1911-1914.

He Y., Fu J.-Z. and Chen Z.-C., 2007, “Research on optimization of the hot

embossing process", *Journal of Micmmechanics and Microengineering*, 17, pp. 2420-2425.

He Y., Fu J.-Z.. and Chen Z.-C., 2008, "Optimization of control parameters in micro hot embossing", *Microsystem Technologies*, 14, pp. 325-329.

Heckele M. and Schomburg W. K., 2004, "Review on micro molding of thermoplastic polymers", *Journal of Micromechanics and Microengineering*, 14, pp. R1-R14.

Heckele M., Andreas G. and Thomas S., 2001, "Large area polymer replication for microstructured fluidic devices", *Proceedings of SPIE* 4408, pp. 469-476.

Heyderman L. J., Schift H., David C., Gobrecht J. and Schweizerb T., 2000, "Flow behaviour of thin polymer films used for hot embossing lithography", *Microelectronic Engineering*, 54, pp. 229–245.

Hirai Y., Konishi T., Yoshikawa T. and Yoshida S., 2004, "Simulation and experimental study of polymer deformation in nanoimprint lithography", *Journal of Vacuum Science & Technology*, B 22, pp. 3288-3294.

Hirai Y., Yoshida S. and Takagi N., 2003, "Defect analysis in thermal nanoimprint lithography", *Journal of Vacuum Science and Technology*, B 21, pp. 2765-2770.

Hirshy H., Lalev G., Velkova V. L., Popov K., Scholz S. and Dimov S. S., 2011, "Master tool fabrication for the replication of micro and nano features", Eighth

International Conference on Multi-Material Micro Manufacture, 4M2011, Stuttgart, Germany, November 8-10, pp. 317-320.

Hocheng H. and Wen T. T., 2008, “Innovative approach to uniform imprint of micron and submicron features”, *Journal of Achievements in Materials and Manufacturing Engineering*, 28, pp. 79-82.

Hocheng H. and Wen T. T., 2010, “Submicron imprint of trench structures by external and intrinsic electromagnetic force”, *CIRP Annals - Manufacturing Technology*, 59, pp. 263-266.

Hsueh C.-H., Lee S., Lin H.-Y., Chen L.-S. and Wang W.-H., 2006, “Analyses of mechanical failure in nanoimprint processes”, *Materials Science and Engineering*, A 433, pp. 316-322.

Jaszewski R. W., Schift H., Schnyder B., Schneuwly A. and Gröning P., 1999, "Deposition of anti-adhesive ultra-thin teflon- like films and their interaction with polymers during hot embossing", *Applied Surface Science*,143,pp. 301-308.

Jenoptik Mikrotechnik, 2002, Datasheet of HEX03 hot embossing system.

Johnson K. L., Kendall K. and Roberts A. D., 1971, “Surface energy and the contact of elastic solids” *Proceedings of Royal Society*, A 324, pp. 301-313.

Johnson K.L., 1985, “Contact Mechanics”, Cambridge University Press, Cambridge

and New York.

Kendall K, 1973, “Shrinkage and peel strength of adhesive joints”, *Applied Physics*, 6, pp. 1782-1787.

Koc M. and Ozel T., 2011, “Micro-Manufacturing”, John Willey and Sons, INC., Publication.

Lalev G., Petkov P., Sykes N., Hirshy H., Velkova V., Dimov S.S. and Barrow D. A., 2009, “Fabrication and validation of fused silica NIL templates incorporating different length scale features”, *Micorelectronic Engineering*, 86, pp. 705-708.

Lan S., Lee H.-J., Kim E. H., Ni J., Lee S.-H., Lai X., Song J.-H., Lee N. K. and Lee M. G., 2009, “A parameter study on the micro hot-embossing process of glassy polymer for pattern replication”, *Microelectronic Engineering*, 86, pp. 2369–2374.

Lazzarino F., Gourgon C., Schiavone P. and Perret C., 2004, “Mold deformation in nano imprint lithography”, *Journal of Vacuum Science and Technology*, B 22, pp. 3318-3323.

Li J. M., Liua C. and Penga J., 2008, “Effect of hot embossing process parameters on polymer flow and microchannel accuracy produced without vacuum”, *Journal of Materials Processing Technology*, 207, pp. 163-171.

Li W., Dimov S. and Lalev G., 2007, “Focused-ion-beam direct structuring of fused

silica for fabrication of nano-imprinting templates", *Microelectronic Engineering*, 84, pp. 829-832.

Lin C.-R., Chen R.-H. and Hung C., 2003, "Preventing non-uniform shrinkage in open-die hot embossing of PMMA microstructures", *Journal of Materials Processing Technology*, 140, pp. 173-178.

Lin C.-R., Chen R.-H. and Hung C., 2002, "The Characterisation and Finite-Element Analysis of a Polymer under Hot Pressing", *International Journal of Advanced Manufacturing Technologies*, 20, pp. 230–235.

Luo Y., Xu M., Wang X. D. and Liu C., 2006, "Finite Element Analysis of PMMA Microfluidic Chip Based on Hot Embossing Technique", *Journal of Physics: Conference Series*, 48, pp. 1102-1106.

Macintyre D.S. and Thomas S., 2005, "A study of resist flow during nanoimprint lithography. *Microelectronic Engineering*, 78–79, pp. 670-675.

Malek C. K., Thuillier G., Duffait R. and Guyout L., 2008, "Double hot-embossing with polymeric intermediate mould", *Mulit-Material Micro Manufacturing Conference 2008*, Cardiff, UK, pp. 1-10.

Matbase VOF, Material Properties Database, Delft; http://www.matbase.com/material/polymers/commodity/pmma/properties

Mathur A., Roy S.S., Tweedie M., Mukhopadhyay S., Mitra S.K. and McLaughlin J.A., 2009, "Characterisation of PMMA microfluidic channels and devices fabricated by hot embossing and sealed by direct bonding", *Current Applied Physics*, 9, pp. 1199-1202.

McGeough J. A., Leu M. C., Rajurkar K. P., De Silva A. K. M. and Liu Q., 2001, "Electroforming Process and Application to Micro/Macro Manufacturing", *CIRP Annals*, 50, pp. 499-514.

McGeough J., 2002, "Micromachining of Engineering Materials", Marcel Dekker, Chapter 4.

Menges G. and Mohren P., 1986, "How to Make Injection Moulds", Hanser, New York.

Merino S., Retolaza A., Juarros A. and Schift H., 2008, "The influence of stamp deformation on residual layer homogeneity in thermal nanoimprint lithography", *Microelectronic Engineering*, 85, pp. 1892-1896.

Mitutoyo, 2004, "Quick Vision Accel – CNC Vision Measuring System", http://www.mitutoyo.com/pdf/QV%20Accel%201759.pdf

Narasimhan J. and Papautsky I., 2003, "Polymer embossing tools for rapid prototyping of plastic microfluidic devices", *Journal of Micromechanics and Microengineering*, 14, pp. 96-103.

Ng S. H., Wang Z. F., Tjeung R. T. and de Rooij N. F., 2006a, “Process Issues for a Multi-Layer Microelectrofluidic Platform”, *Symposium on Design, Test, Integration and Packaging of MEMS/MOEMS, DTIP 2006, Stresa, Italy*.

Ng. S. H., Tjeung R. T. and Wang Z., 2006b, “Hot Embossing on Polymethyl Methacrylate”, *Eight IEEE Electronics Packaging Technology Conference, EPTC’06, Singapore, December 6-8,* pp. 615-621.

Nogi T. and Kato T., 1997, ““Influence of a hard surface layer on the limit of elastic contact Part I: Analysis using a real surface model,” *Journal of Tribology, Transactions of the ASME,* 119, pp. 493-500.

Pan C. T., Wu T. T., Chang Y. C., and Huang J. C., 2008, “Experiment and simulation of hot embossing of a bulk metallic glass with low pressure and temperature”. *Journal of Micromechanics and Microengineering,* 18, pp. 1-12.

Park K., and Ahn J. H., 2004, “Design of Experiment Considering Two-Way Interactions and its Application to Injection Molding Processes with Numerical Analysis,” *Journal of Material Processing Technologies,* 146, pp.221–227.

Park S., Schift H., Padeste C., Schnyder B., Kötz R. and Gobrecht J., 2004, "Anti-adhesive layers on nickel stamps for nanoimprint lithography," *Microelectronic Engineering,* 73-74, pp. 196-201.

Park S., Song Z., Brumfield L., Amirsadeghi A. and Lee J., 2009, “Demolding

temperature in thermal nanoimprint lithography", *Applied Physics,* A 97, pp. 395-402.

Pham G. T. and Colton J. S., 2002, "Ejection force modeling for stereolithography injection molding tools", *Polymer Engineering and Science,* 42, pp. 681-693.

Piotter V., Mueller K., Plewa K., Ruprecht R. and Hausselt J., 2002, "Performance and simulation of thermoplastic micro injection molding", *Microsystem Technologies,* 8, pp. 387-390.

Prokopovich P. and Starov V., 2011, "Adhesion models: from single to multiple asperity contacts", *Advances in Colloid and Interface Science,* 168, pp. 210-222.

Prokopovich P., Theodossiades S., Rahnejat H. and Hodson D., 2010, "Nano- and component level scale friction of rubber seals in dispensing devices", *Wear,* 268, pp. 845-852.

Ramani K.-R.-T. and Yao D., 2009, "Hot Embossing of Discrete Microparts", *Polymer Engineering and Science 2009*, pp. 1894-1901.

Ressier L., Martin C. and Peyrade J. P., 2004, "Atomic force microscopy study of micrometric pattern replica by hot embossing lithography", *Microelectronic Engineering,* 71, pp. 272-276.

Rowland H. D. and King W. P., 2004, "Polymer deformation and filling modes during microembossing", *Journal of Micromechanics and Microengineering,* 14, pp. 1625-

1632.

Rowland H. D., King W. P., Sun A. C., and P. R. Schunk, 2007, “Simulations of non-uniform embossing: the effect of asymmetric neighbour cavities on polymer flow during nanoimprint lithography”, *Sandia report SAND2007-4121*.

Saha B., Liu E., Tor S. B., Khun N. W., Hardt D. E. and Chun J. H., 2010, "Replication performance of Si-N-DLC-coated Si micro-molds in micro-hot-embossing," *Journal of Micromechanics and Microengineering*, 20, 045007.

Scheer H.-C. and Schulz H., 2001, “A contribution to the flow behaviour of thin polymer films during hot embossing lithography”, *Microelectronic Engineering*, 56, pp. 311-332.

Scheer H.-C., Bogdanski N., Wissen M., Konishi T. and Hirai Y., 2006, “Profile evolution during thermal nanoimprint”, *Microelectronic Engineering*, 83, pp. 843-846.

Schelb M., Vannahme C., Kolew A. and Mappes T., 2011, “Hot Embossing of Photonic Crystal Polymer Structures with a High Aspect Ratio”, *Journal of Micromechanics and Microengineering*, 21, pp. 1-5.

Schift H., Heyderman L. J., Auf der Maur M. and Gobrecht J., 2001, “Pattern formation in hot embossing of thin polymer films”, *Nanotechnology*, 12, pp. 173-177.

Schubert A., Edelmann J. and Burkhardt T., 2006, “Micro structuring of borosilicate glass by high temperature micro-forming”, *Microsystem Technologies*, 12, pp. 790-795.

Schulz H., Wissen M., Bogdanski N., Scheer H.-C., Mattes K. and Friedrich Ch., 2006, “Impact of molecular weight of polymers and shear rate effects for nanoimprint lithography”, *Microelectronic Engineering*, 83, pp. 259-280.

Schulz H., Wissen M., Bogdanski N., Scheer H.-C., Mattes K. and Friedrich Ch., 2005, “Choice of the molecular weight of an imprint polymer for hot embossing lithography”, *Microelectronic Engineering*, 78–79, pp. 625-632.

Shan X. C., Liu Y. C., and Lam Y. C., 2008, “Studies of polymer deformation and recovery in micro hot embossing”, *Microsystem Technologies*, 14, pp. 1055-1060.

Shen X.-J., Pan L.-W. and Lin L., 2002, “Microplastic embossing process: experimental and theoretical characterisation”, *Sensors and Actuators*, 97-98, pp. 428-433.

Simprint Nanotechnologies Ltd, Bristol; http://simprintnanotech.com

Sirotkin V., Svintsov A., Schift H. and Zaitsev S., 2007, “Coarse-grain method for modelling of stamp and substrate deformation in nanoimprint”, *Microelectronic Engineering*, 84, pp. 868-871.

Song Z., Choi J., You B. H., Lee J. and Park S., 2008, “Simulation study on stress and

deformation of polymeric patterns during the demolding process in thermal imprint lithography", *Journal of Vacuum Science and Technology*, B 26, pp. 598-605.

Spetzler H. A. and Meyer M. D., 1974, "Precise length measurement technique under hydrostatic pressure: Isothermal bulk modulus of PMMA", *Review of Scientific Instruments*, 45, pp. 911-915.

Taylor H., Lam Y. C. and Boning D., 2009, "A computationally simple method for simulating the micro-embossing of thermoplastic layers", *Journal of Micromechanics and Microengineering*, 19, 075007 (16 pages).

Titomanlio G. and Jansen K. M. B.,1996, "In-mold shrinkage and stress prediction in injection molding", *Polymer Engineering and Science*, 36, pp. 2041-2049.

Toh A. G., Wang Z. F. and Wang Z. P., 2009, "Ambient hot embossing of Polycarbonate, Poly-Methyl Methacrylate and Cyclic Olefin Copolymer for microfluidic applications", *IEEE Symposium on Design, Test, Integration & Packaging of MEMS/MOEMS, Singapore, April 01-03*, pp. 359-362.

Trabadelo V., Schift H., Merino S., Bellini S. and Gobrecht J., 2008, "Measurement of demolding forces in full wafer thermal nanoimprint", *Microelectronic Engineering*, 85, pp. 907-909.

Velkova V., Lalev G., Hirshy H., Scholz S., Hiitola-Keinänen J., Gold H., Haase A., Hast J., Stadlober B. and Dimov S., 2010, "Design and validation of a novel master-

making process chain for organic and large area electronics on flexible substrates", *Microelectronic Engineering*, 87, pp. 2139-2145.

Veres T., Jakeway S. C., Crabtree H. J., Cameron N. S. and Roberge H., 2006, "High fidelity, high yield production of microfluidic devices by hot embossing lithography: rheology and stiction", *Lab on a Chip*, 6, pp. 936-941.

Whiteside, B. R., Martyn, M. T., and Coates, P. D., 2005, "In-Process Monitoring of Micromoulding—Assessment of Process Variation," *International Journal of Polymer Processing*, 21, pp.162-169.

Worgull M. and Heckele M., 2004, "New aspects of simulation in hot embossing", *Microsystem Technologies*,10, pp. 432-437.

Worgull M., 2009, "Hot Embossing: theory and technology of microreplication", *Elsevier Oxford.*

Worgull M., Heckele M. and Schomburg W. K., 2005, "Large-scale hot embossing", *Microsystem Technologies*, 12, pp. 110-115.

Worgull M., Hétu J.-F., Kabanemi K. K. and Heckele M., 2008a, "Hot embossing of microstructures: characterization of friction during demoulding", *Microsystem Technologies*, 14, pp. 767-773.

Worgull M., Kabanemi K. K., Marcotte J.-P., Hétu J.-F. and Heckele M., 2008b,

"Modelling of large area hot embossing", *Microsystem Technologies,* 14, pp. 1061-1066.

Worgull M., Kolew A., Heilig M., Schneider M., Dinglreiter H. and Rapp B., 2011, "Hot embossing of high performance polymers", *Microsystem Technologies,* 17, pp. 585-592.

Yao D. and Ramani K.-R.-T., 2008, "An enlarged process window for hot embossing", *Journal of Micmmechanics and Microengineering,* 18 045023 (7pp).

Yeo L. P., Ng S. H., Wang Z. F., Xia H. M., Wang Z. P., Thang V. S., Zhong Z. W. and Rooij N. F., 2010, "Investigation of hot roller embossing for microfluidic devices", *Journal of Micromechanics and Microengineering,* 20, pp. 1-10.